INFORMATION TO USERS

This manuscript has been reproduced from the microfilm master. UMI films the text directly from the original or copy submitted. Thus, some thesis and dissertation copies are in typewriter face, while others may be from any type of computer printer.

The quality of this reproduction is dependent upon the quality of the copy submitted. Broken or indistinct print, colored or poor quality illustrations and photographs, print bleedthrough, substandard margins, and improper alignment can adversely affect reproduction.

In the unlikely event that the author did not send UMI a complete manuscript and there are missing pages, these will be noted. Also, if unauthorized copyright material had to be removed, a note will indicate the deletion.

Oversize materials (e.g., maps, drawings, charts) are reproduced by sectioning the original, beginning at the upper left-hand corner and continuing from left to right in equal sections with small overlaps.

Photographs included in the original manuscript have been reproduced xerographically in this copy. Higher quality 6" x 9" black and white photographic prints are available for any photographs or illustrations appearing in this copy for an additional charge. Contact UMI directly to order.

Bell & Howell Information and Learning
300 North Zeeb Road, Ann Arbor, MI 48106-1346 USA

UMI®
800-521-0600

Flux Enhancement and Fouling Reduction in a Centrifugal Membrane Process

by

David Steven Lycon
B.Sc., Saint Mary's University, 1986
B.Eng., Technical University of Nova Scotia, 1990
M.A.Sc., Technical University of Nova Scotia, 1993

A Dissertation Submitted in Partial Fulfillment of the
Requirements for the Degree of

DOCTOR OF PHILOSOPHY

in the Faculty of Graduate Studies

We accept this dissertation as conforming
to the required standard

Dr. T.M. Fyles, Co-Supervisor (Department of Chemistry)

Dr. G.W. Vickers, Co-Supervisor (Department of Mechanical Engineering)

Dr. N. Djilali, Member (Department of Mechanical Engineering)

Dr. M.B. Hocking, Member (Department of Chemistry)

Dr. K.J. Smith, External Examiner (Department of Chemical & Bio-Resource Engineering, University of British Columbia)

Co-Supervisors: Dr. Thomas M. Fyles
Dr. Geoff W. Vickers

ABSTRACT

The Centrifugal Membrane and Density Separation (CMDS) process is a novel type of membrane process that exploits the action of a centrifuge to generate process pressure for reverse osmosis and nanofiltration. The centrifuge could potentially enhance flux and alleviate fouling of the membrane as a result of the hydrodynamic environment of the centrifuge. All experimental work has been conducted on a prototype model of the CMDS process. The apparatus allows a membrane module to be fixed in space at a specified orientation, with respect to the rotation. This orientation in space is denoted by the terms "pitch, roll and yaw" (p,r,y).

Experiments have been done using brine feed solutions at various concentrations to determine if the CMDS process minimizes the effects of concentration polarization. An example of this was illustrated with a 54% flux enhancement relative to a conventional membrane process using a 35000 ppm NaCl feed solution. Colloidal feed solutions were also used to examine how the CMDS process enhances flux in a fouling environment. These feed solutions include 21 g/L silica and 300 mg/L humic acid, with typical relative flux enhancement factors (κ) found to be 0.59 and 0.14, respectively. The final group of experiments examined the use of 50 g/L whey feed solutions with nanofiltration membranes. Results obtained here indicate that the centrifugal action enhanced the flux with an absolute flux enhancement factor (κ') of 17.5 L/m^2 hr. These experiments have shown that a given orientation (90,270,0) best enhances the flux of a membrane with respect to colloidal fouling, while showing that another orientation (90,180,0) best reduces the effects of concentration polarization.

Scanning electron microscopy (SEM) and an energy dispersive x-ray (EDX) detector have helped to examine the nature of the fouling layers and determine how well the layers adhere to the surface of the membrane. It was determined that in some cases, the

fouling layer adhered better to the surface of a membrane used in the CMDS process. However, as the fluxes were typically higher in the dynamic process, it leads to the conclusion that the fouling layer on the CMDS membranes is more permeable.

From the experimental work it has been concluded that the forces at work in the CMDS process create sufficient secondary flow instabilities to reduce the effects of fouling and concentration polarization on the membrane surface. The significance of this process with respect to industrial applications is considered, and the process is deemed feasible for such applications.

Examiners:

Dr. T.M. Fyles, Co-Supervisor (Department of Chemistry)

Dr. G.W. Vickers, Co-Supervisor (Department of Mechanical Engineering)

Dr. N. Djilali, Member (Department of Mechanical Engineering)

Dr. M.B. Hocking, Member (Department of Chemistry)

Dr. K.J. Smith, External Examiner (Department of Chemical & Bio-Resource Engineering, University of British Columbia)

TABLE OF CONTENTS

Abstract.....ii

Table of Contents.....iv

List of Tables.....vi

List of Figures.....vii

Nomenclature.....x

Acknowledgements.....xi

Dedication.....xii

Chapter 1: Introduction

1.1 Membrane Processes.....1
1.1.1 Membrane Fouling.....2
1.1.2 Membrane Fouling Reduction Techniques.....5
1.1.2.1 Cleaning.....5
1.1.2.2 Feed Pre-Treatment.....7
1.1.2.3 Membrane/Process Design.....7
1.1.3 Evolution of Centrifugal Membrane Processes.....10
1.2 CMDS Process Description.....13
1.2.1 Membrane Orientation.....16
1.3 Previous and Ongoing Academic Work on CMDS Process.....19
1.3.1 FRACT.....19
1.3.2 Computational Fluid Dynamic Models.....20
1.3.3 Angular Influences in CMDS Process.....22
1.4 Preliminary Calibration Experiments.....22
1.5 Principles of Experimental Work.....28

Chapter 2: Concentration Polarization

2.1 Introduction.....30
2.2 Experimental Procedure.....33
2.3 Results.....35
2.3.1 Orientation – 0,r,y.....35
2.3.2 Orientation – 90,r,y.....38

Chapter 3: Fouling

3.1 Introduction.....47
3.2 Humic Acid Fouling.....48
3.2.1 Introduction.....48
3.2.2 Experimental Work.....49
3.2.2.1 Preliminary Experiments.....49

3.2.2.2 Procedure For Fouling Experiments.....51
3.2.3 Results.....53
3.2.3.1 Roll 90/270 Results.....53
3.2.3.2 Roll 180 Results.....60
3.2.4 Microscopic Analysis of Fouling Layers.....64
3.2.4.1 Experimental Procedure.....64
3.2.4.2 SEM and EDX Results.....65
3.3 Colloidal Silica Fouling.....72
3.3.1 Introduction.....72
3.3.2 Experimental Work.....73
3.3.2.1 Preliminary Experiments.....73
3.3.2.2 Procedure For Fouling Experiments.....74
3.3.3 Results.....75
3.3.3.1 0,r,0 Results.....76
3.3.3.2 90,r,0 Results.....78
3.3.3.3 90,180,y Results.....79
3.3.4 Microscopic Analysis of Fouling Layers.....81
3.3.4.1 SEM Results.....81
3.3.4.2 EDX Results.....84
3.4 Nanofiltration.....86
3.4.1 Introduction.....87
3.4.2 Experimental Work.....90
3.4.2.1 Preliminary Experiments.....90
3.4.2.2 Procedure For Fouling Experiments.....91
3.4.3 Results.....92
3.4.3.1 Variable Pressure Results.....92
3.4.3.2 Fixed Pressure Results.....95
3.4.4 Microscopic Analysis of Fouling Layers.....96

Chapter 4: Conclusions

4.1 CMDS Process Conclusions.....100
4.1.1 Membrane Orientation.....102
4.1.2 Fouling in CMDS and Conventional Membrane Processes.....104
4.1.2.1 Fouling Feed Stream Differences.....104
4.1.2.2 Fouling Layer Permeability.....106
4.1.2.3 Adherence of Fouling Layer.....106
4.2 Toward Industrial Applications.....107

References.....109

LIST OF TABLES

Table 1.1	Industrial applications of membranes	2
Table 1.2	Foulant differences	3
Table 1.3	Physical Cleaning methods	6
Table 1.4	Pre-treatment methods	7
Table 1.5	FRACT operating ranges	20
Table 1.6	Summary of calibration experiments	25
Table 2.1	DS-3™ membrane material specifications	33
Table 2.2	90.r.y head experiments operating pressure ranges	35
Table 2.3	Relative flux values	46
Table 3.1	Filtration effectiveness and particle size	51
Table 3.2	Humic acid fouling experimental conditions	53
Table 3.3	α and κ values for roll 90/270 orientations	59
Table 3.4	α and κ values for roll 180 orientations	63
Table 3.5	DuPont Ludox properties	73
Table 3.6	Colloidal silica fouling experimental conditions	75
Table 3.7	α and κ values for 0.r.0 orientations	78
Table 3.8	α and κ values for 90.r.0 orientations	78
Table 3.9	α and κ values for 90.180.y orientations	80
Table 3.10	Typical solids content of whey	89
Table 3.11	DS-5™ membrane material specifications	90
Table 3.12	Whey solution fouling experimental conditions	92
Table 3.13	κ' values and "rollover" pressures for variable pressure experiments	94
Table 3.14	α and κ values for fixed pressure experiment (experiment #4)	96
Table 4.1	Summary of membrane orientation performance for flux enhancement	101-102

LIST OF FIGURES

Figure 1.1 Fouling mechanisms....3

Figure 1.2 Forces acting on a particle at the membrane surface (Spintek apparatus)....9

Figure 1.3 Taylor vortices in a rotating annular module....10

Figure 1.4(a) CRO apparatus....12

Figure 1.4(b) Typical spiral wound cartridge....12

Figure 1.5 CMDS Apparatus – door closed....13

Figure 1.6 CMDS Apparatus – door open....14

Figure 1.7 Membrane module stack....15

Figure 1.8 Membrane head configuration....15

Figure 1.9 Examples of membrane orientation....18

Figure 1.10 Static membrane apparatus....23

Figure 1.11 Temperature dependence on permeate flux....27

Figure 1.12 Membrane process comparison....28

Figure 2.1 Concentration profile during concentration polarization....30

Figure 2.2 0,r,0 orientation concentration polarization experiment (35000 ppm NaCl)....37

Figure 2.3 0,r,0 orientation concentration polarization experiment (70000 ppm $MgSO_4$)....38

Figure 2.4 90,90,0 orientation concentration polarization experiment (22500 ppm NaCl)....39

Figure 2.5 90,180,0 orientation concentration polarization experiment (22500 ppm NaCl)....40

Figure 2.6 Membrane module orientation and flow direction....41

Figure 2.7 Averaged surface mass fraction along the flow channel for various orientations....42

Figure 2.8 Relative flux results for concentration polarization experiments....44

Figure 2.9 90,180,y orientation effect of Coriolis forces experiment....45

Figure 3.1 Example of humic acid molecular structure....49

Figure 3.2 Membrane module orientation and feed flow direction (90,90/270,y)....54

Figure 3.3 Humic acid experiment #1.....55
Figure 3.4 Humic acid experiment #2.....56
Figure 3.5 Humic acid experiment #3.....57
Figure 3.6 Hypothetical fouling curve with quantification nomenclature.....59
Figure 3.7 Membrane module orientation and feed flow direction (90,180,y).....60
Figure 3.8 Humic acid experiment #4.....61
Figure 3.9 Humic acid experiment #5.....62
Figure 3.10 Location of deposit on membrane module after 90,180,90 experiment....63
Figure 3.11(a) Sample mounted on aluminum stub for surface image.....65
Figure 3.11(b) Sample mounted on modified aluminum stub for edge image.....65
Figure 3.11(c) Side view of SEM aluminum mounting stub.....65
Figure 3.12 Surface electron micrographs (1000x magnification) of: (a) unused membrane; (b) static humic acid fouled membrane; and (c) 90,270,0 orientation dynamic humic acid fouled membrane 66
Figure 3.13 Surface electron micrographs (1000x magnification) of: (a) unused membrane; (b) static humic acid fouled membrane; and (c) 90,270,0 orientation dynamic humic acid fouled membrane.....67
Figure 3.14 Edge electron micrographs (100x magnification) of: (a) unused membrane; and (b) static humic acid fouled membrane.....68
Figure 3.15 Edge electron micrographs (100x magnification) of: (a) 90,180,0 orientation dynamic humic acid fouled membrane; and (b) 90,180,90 orientation dynamic humic acid fouled membrane.....68
Figure 3.16 H_2O rinsed membrane surface electron micrographs (100x magnification) of: (a) static humic acid fouled membrane; (b) 90,180,0 orientation dynamic humic acid fouled membrane; and (c) 90,180,90 orientation dynamic humic acid fouled membrane.....71
Figure 3.17 Membrane module orientation and feed flow direction (0,r,0).....76
Figure 3.18 Colloidal silica experiment #1.....77
Figure 3.19 Colloidal silica experiment #2.....79
Figure 3.20 Colloidal silica experiment #5.....80
Figure 3.21 Surface electron micrographs of: (a) unused membrane (1000x); (b) static silica fouled membrane (1000x); and (c) static silica fouled membrane (500x).....82

Figure 3.22 Surface electron micrographs (1000x magnification) of: (a) static silica fouled membrane; (b) 90,180,90 orientation dynamic silica fouled membrane; and (c) 90,180,0 orientation dynamic silica fouled membrane.....83

Figure 3.23 Edge electron micrographs (100x magnification) of: (a) unused membrane; and (b) static silica fouled membrane.....84

Figure 3.24 H_2O rinsed membrane surface electron micrographs (100x magnification) of: (a) static silica fouled membrane; (b) 90,180,0 orientation dynamic silica fouled membrane; and (c) 90,180,90 orientation dynamic silica fouled membrane.....86

Figure 3.25 Gel polarization concentration profile.....88

Figure 3.26 Generalized NF transport relationship.....89

Figure 3.27 Whey experiment #1.....93

Figure 3.28 Whey experiment #3.....94

Figure 3.29 Whey experiment #4.....95

Figure 3.30 Surface electron micrographs (250x magnification) of: (a) unused membrane; (b) static protein fouled membrane; and (c) 90,180,90 orientation dynamic protein fouled membrane.....97

Figure 3.31 Edge electron micrographs (100x magnification) of: (a) unused membrane and (b) static protein fouled membrane.....98

Figure 3.32 Edge electron micrographs (100x magnification) of: (a) unused membrane and (b) dynamic (90,180,90 orientation) protein fouled membrane.....98

Figure 4.1 90,180,0 orientation with reference axis.....103

Figure 4.2 90,270,0 orientation with reference axis.....104

NOMENCLATURE

c_f	feed concentration
c_p	permeate concentration
d	particle diameter
d_p	pore diameter
j_v	volume flux across membrane
k	mass transfer coefficient
p	pitch angle
p_r	roll over pressure
r	roll angle
y	yaw angle
C_b	bulk fluid concentration
C_g	gel layer fluid concentration
C_w	wall fluid concentration
D or D_s	force due to back diffusion
F_D	force associated with the membrane flux
F_C	centrifugal force
G	gravitational force
J_v	mass flux across membrane
L_p	membrane permeability
R	membrane rejection
S:Si	sulphur to silica ratio
α	relative slope factor (fouling)
β	relative flux (concentration polarization)
δ	boundary layer thickness
ΔP	hydrostatic pressure difference
$\Delta\Pi$	osmotic pressure difference
κ	relative offset factor
κ'	modified offset factor
τ_r	radial shear force
τ_θ	tangential shear force

ACKNOWLEDGEMENTS

I would like to thank Dr. Tom Fyles for his guidance and supervision throughout the course of this degree program. I especially appreciate his tolerance with respect to me periodically taking time off to pursue my Naval Reserve career. His good sense of humour and easy-going nature made this project a little easier. Thanks are also warranted to the other guiding faculty members of the CMDS project, namely Dr. Geoff Vickers and Dr. Ned Djilali; their input has been appreciated.

Several colleagues have also helped to make the time spent at UVic better both professionally and personally. These people include, in no particular order, Jon Pharoah, Alvin Bergen, Lynn Cameron, Darryl Brousmiche, Dave Robertson and Scott Murphy. Two other gentlemen, who helped out significantly in the progress of this research with their machining expertise, are Roy Bennett and Richard Robinson.

Finally, I would like to thank my family and Annette for their support and patience throughout the pursuit of this degree. They can rest assured that this is finally the end, and there will be no more degrees forthcoming.

DEDICATION

To Dr. William Bridgeo, Dean Emeritus of Science at Saint Mary's University. This is the man who took a chance on a young, solid C student and showed him the world of research and introduced him to things that a Chemical Engineer might do. Thank you.

1 Introduction

In the field of membrane separation, fouling has long been considered one of the major drawbacks with respect to increased use of the processes. Simply stated, fouling is the process resulting in loss of performance of a membrane due to the deposition of suspended or dissolved substances on its external surfaces, at its pore openings and within its pores [1]. Fouling typically leads to higher operating costs because of the reduction in throughput, and because of the increased need for cleaning. The goal in fouling reduction, and subsequent flux enhancement, is to create an environment where suspended and/or dissolved particles are discouraged from migrating onto the surface of the membrane. One way to do this is to create unstable flow near the surface of the membrane. This may be accomplished by using hydrodynamic methods that will improve mass transport of the particles from the membrane surface, back to the bulk solution. The work contained in this dissertation evaluates performance of a system where unstable flow is developed in a centrifuge. The process is called Centrifugal Membrane and Density Separation (CMDS). The goal of work is to determine the nature and extent of flux enhancement and fouling reduction due to the rotating environment.

1.1 Membrane Processes

Membrane technology is a relatively recent development in the area of separation science. It was the development of the synthetic asymmetric membrane by Sourirajan and Loeb in 1960 that spawned the future development of membrane processes [2]. Though initially used in the desalination of seawater, membrane processes have now found their way into other process industries (examples in Table 1.1). They have the advantage over other types of separation, in that there is no phase change necessary for the separation to occur and operating costs are generally lower.

It may be first useful to define some of the technology that will be examined in the following chapters. Reverse osmosis is described as a pressure driven process that rejects solute from its carrier solvent via a semi-permeable membrane. This diffusive process has the ability to separate particles down to 5 Å in size from a solvent. Nanofiltration refers to the type of membrane that relies on size selectivity to achieve a separation of

solutes. Size selectivity can also refer to the molecular weight of solute components. The essential difference between RO and NF is that RO involves solvent diffusion through the bulk membrane material, while NF is a true filtration with the smaller solutes passing through voids in the membranes (< 10 Å particle size). Nanofiltration separations do not have the same rejection capabilities of reverse osmosis, but also do not require their higher driving pressure. They can be used to concentrate suspended or colloidal material in aqueous streams, remove dissolved macromolecules from the stream, and de-salt streams. Respective examples of these types of NF separations include: (1) dewatering of syrups; (2) protein fractionation/separation; and (3) removing NaCl from whey.

Industry	Application
Agribusiness	Dairy – effluent treatment, milk dewatering
	Food – starch, sugars separation
	Fermentation – wine, dairy
Industrial	Recovery of valuable products – paints, dyes
Metallurgy	Precious metal recovery and removal
Environmental	Recovery of hazardous by-products
	Pulp and paper – spent sulfite liquor
Municipal	Sanitary wastewater – tertiary treatment
	Water supply – desalination of brackish or seawater
Biotechnology	Pharmaceuticals – serum, deionized water
	Genetic engineering – fractionation, separation
	Fermentation – cell harvesting, enzyme clarification

Table 1.1 Industrial applications of membranes

1.1.1 Membrane Fouling

The primary subject of this dissertation involves fouling and how the CMDS process can minimize its deleterious effects. Therefore, it is worthwhile to examine fouling mechanisms and current trends used to alleviate fouling. Foulants themselves can be characterized by their size in such a manner: (1) particles - 10^4 to 10^5 Å, and include such things as white blood cells, red blood cells, bacteria, yeast, and platelets; (2) colloids - 10 to 10^4 Å, which include viruses, DNA, lipoproteins, albumin and antibodies; and (3) solutes - 1 to 10 Å, including insulin, antibiotics, sugars and salts. Table 1.2 illustrates the relative differences between these three types of foulants. Each type of foulant

affects membrane surfaces in a different manner, depending upon the capabilities of the membranes. For example, reverse osmosis membranes could potentially be fouled by all three of the above categories of foulants, where nanofiltration membranes would probably only be fouled by particles and colloids. It is for this reason, that foulant characteristics are important considerations in the selection of a membrane material for a given application.

	Diffusivity (cm^2/s)	Osmotic Pressure	Relative Viscosity
Particles	$< 10^{-9}$	negligible	high
Colloids	10^{-6} - 10^{-9}	low	moderate
Solutes	10^{-5} - 10^{-6}	high	low

Table 1.2 Foulant differences [3]

It is these foulant sizes that often dictate the type of fouling that will occur on the membrane surface. Figure 1.1 illustrates the three primary fouling mechanisms that may occur in RO and NF membranes, and how they relate to particle size.

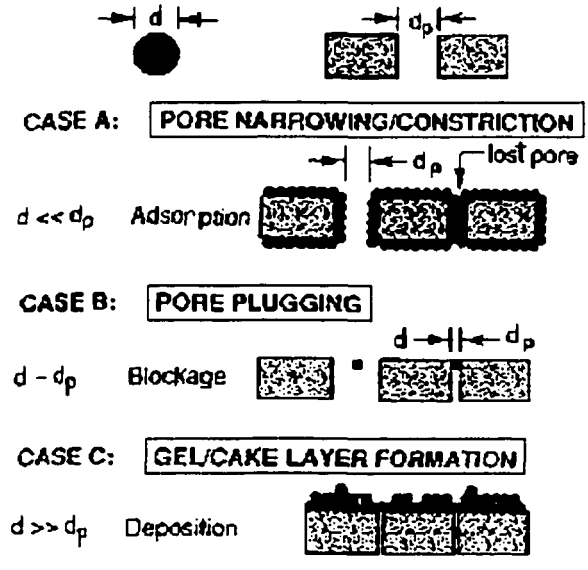

Figure 1.1 Fouling mechanisms (see Fig. 2 of [4])

Adsorption fouling, or pore narrowing occurs when particles in a feed stream are adsorbed onto the membrane's surface, thus reducing the available size of the pores. The chemistry of the membrane is such that dissolved molecules from the feed solution are quickly sorbed onto the membrane's surface. This may occur by a number of mechanisms that include the following: (1) electrostatic interaction; (2) hydrophobic effects; and/or (3) charge transfer (hydrogen bonding). In this fouling mechanism, the initial adsorption occurs quite rapidly, and when all of the adsorption sites are filled, a pseudo steady-state is reached. It is this initial adsorption of solute that creates a nucleation site for further build-up on the membrane surface (mostly within the membrane structure). After this occurs, a monolayer can form on the membrane's surface, and, in some cases, additional layers will eventually form, become compacted and impede both the crossflow and permeation velocities [3]. The phenomenon of adsorption is especially important in the area of nanofiltration where the pore size is large compared to reverse osmosis.

Pore blockage or plugging is the only one of the three discussed fouling mechanisms that is considered to be reversible. This type of fouling is caused by large diameter particles physically blocking the pores of the membrane, as illustrated in Figure 1.1. These contaminants are often aggregates of a particular solute in the feed solution. Upon being blocked, the pores can be cleared of its plugs by simply backflushing the membrane with permeate, which is one of the methods that will be discussed later in this section.

The final mechanism, gel layer formation, is associated with macromolecular fouling on the membrane surface. It is a type of concentration polarization associated with nanofiltration and ultrafiltration. The term concentration polarization refers to the concentration profile that has a higher level of solute nearest to the upstream membrane surface compared to the more-or-less well-mixed bulk fluid far from the membrane surface [1]. This is discussed further in the sections dealing with concentration polarization and nanofiltration (Section 2.1 and Subsection 3.4.1, respectively).

1.1.2 Membrane Fouling Reduction Techniques

There are three important ways in which fouling and concentration polarization can be minimized: (1) membrane cleaning; (2) feed pre-treatment; and (3) membrane/process design. Each of these techniques has been well researched, as flux decline is a serious problem in the acceptance of membrane separations as an economically viable process. The last two areas are considered preventive, but often it is the first area that is the more commonly practiced of the three, in conventional membrane processes.

1.1.2.1 Cleaning

When flux decline has reached the point where the membrane system is no longer performing at acceptable levels, cleaning of the membrane must be undertaken. Membrane manufacturers define this situation with the following guidelines: (1) 10% decline in flux while operating at constant pressure and temperature; (2) 10% increase in driving pressure required to maintain constant flux; or (3) 15 to 20% increase in differential pressure between feed and concentrate streams [5]. The method used to clean the system depends on the type of foulant and the material of the membrane. Cleaning can be divided into three categories: (1) chemical; (2) physical (sometimes subdivided into hydraulic and mechanical); and (3) physio-chemical. Chemical methods are typically used for irreversible fouling, and physical or physio-chemical methods are generally used for reversible fouling situations. Chemical cleaning methods are also more prevalent where reverse osmosis membrane restoration is concerned, and nanofiltration and ultrafiltration membranes rely more on the physical and physio-chemical methods.

Chemical cleaning acts to dissolve the fouling layer, or to create a reaction at the membrane's surface favourable for foulant removal. Chemicals are usually introduced with a low pressure, flushing stream into the membrane module. The type of chemicals which are used in membrane cleaning include the following: (1) acids (HNO_3, citric acid and H_3PO_4) - used in the removal of carbonate and sulphate scales; (2) bases (NaOH) - used after an acid wash to neutralize the membrane surface; (3) complexing agents (EDTA) - necessary for the removal of Ca precipitates; (4) enzymes - can clean protein

build-up on membranes; (5) detergents - remove oily deposits from membrane; (6) concentrated NaCl solutions - used to remove protein foulants; and (7) oxidants/disinfectants (NaOCl and H_2O_2) - remove biological slimes [6].

As mentioned above, physical cleaning methods are often characterized as being mechanical or hydrodynamic. Table 1.3 describes some of the more common mechanical and hydrodynamic cleaning methods that are currently being used for membrane restoration.

Method	Description
forward flushing	permeate is pumped into the feed section of the process to clean foulant from membrane surface
reverse flushing	direction of permeate flow is alternated between the forward and backward direction
permeate back pressure	reversing the flow of permeate by applying large back pressure, and at the same time, allowing a feed solution to go to the membrane and wash away loosened foulant particles
vibration	pneumatic hammers are used on the pressure vessel to loosen foulant particles, while maintaining a feed flush near the membrane's surface
air drain and water refill	the pressure vessel is evacuated with air, then immediately filled with water which creates turbulence at the gas/water interface (turbulence displaces the foulant particles
air sparge	periodic injections of air ahead of flush stream (useful for hollow fibre membranes)
sonication	ultrasonic cleaning with a wetting agent
sponge ball cleaning	polyurethane sponge balls are inserted into the pressure vessel for a few seconds to scrub the surface of the membrane (only works under turbulent flow conditions)

Table 1.3 Physical cleaning methods [6]

These physical methods are often used in conjunction with chemical cleaning methods to create the category of physio-chemical cleaning. Examples of these methods used for RO membrane treatment include: (1) using reverse flushing with a surfactant in the cleaning stream; (2) acid wash stream used in conjunction with foam ball scrubbing; and (3) peracetic acid and hydrogen peroxide working with a reverse flush technique [6].

1.1.2.2 Feed Pre-Treatment

In many situations, pre-treatment of the bulk feed solution can alter the conditions that may bring about fouling or concentration polarization at the membrane's surface. Effective pre-treatment requires knowledge of the nature of the fouling mechanism, and the membrane material (excessive pre-treatment may be harmful to the membrane). Examples of pre-treatment include: (1) pH adjustment; (2) heat treatment; (3) change in ionic strength; (4) use of sequestering agents; (5) chlorination; and (7) coagulation for pre-filtration. Table 1.4 gives examples of some of the different types of foulants, and what method of pre-treatment could be used for each.

Foulant	Treatment	Description
Ca salts	pH adjustment	acid addition replaces sulphates and bicarbonates with more soluble chlorides
silica	heat treatment	raised temperature increases solubility
colloids	coagulate and filter	colloids form larger particles which can be filtered out
bacteria	chlorination	removes (kills) bacteria
Fe precipitate	pH adjustment	acid dose stabilizes and keeps Fe in solution

Table 1.4 Pre-treatment methods [7]

1.1.2.3 Membrane/Process Design

The area of design can be broken down into one of two areas: (1) membrane material properties; and (2) membrane process modifications. The former deals with the surface bonding effects of fouling, and the latter with hydrodynamics. This form of fouling reduction typically costs less than post-process cleaning techniques, and also helps to better understand the nature of the feed stream, as well as the separation process itself.

In terms of membrane material, the pore size and the distribution often governs how a membrane will foul, therefore if the membrane is dense in its pore distribution (*i.e.* large number of pores), it is less likely to foul as quickly. Surface charge on the membrane can also be used to minimize the effects of fouling when used in conjunction with the charge associated with the foulant. Often colloids in the feed solution are negatively charged,

and thus a negatively charged membrane would act to repel the colloid from its surface. Another surface effect is the hydrophilic or hydrophobic nature of the membrane. If the membrane is very hydrophilic it will attract water to its surface, thus causing the membrane to remain "wet", and not allow particles to adhere to its surface as easily.

There are several techniques that have recently been developed in both the manufacturing and surface modification areas. Some of the manufacturing advances have come in the introduction of nitrogen-containing polymers, and the use of new manufacturing techniques such as dip coating, plasma polymerization, interfacial polymerization and water casting. The surface modification methods include plasma treatment, fluorination of hydrocarbon polymers, and grafting of phospholipids onto the membrane. Plasma treatment is an area that includes, depending on the degree of plasma discharge, reactions such as surface plasma etching, plasma modification of the chemical structure of the surface layer, and plasma polymerization [8]. The fluorination of the membrane's polymer film by using hydrofluoric acid or fluorosilic acid increases the hydrophilicity of the membrane, and thus reduces the ability of solutes to foul [9]. A phospholipid coating mimics the manner in which red blood cell plasma membranes resist protein fouling. In this sort of process, a microfiltration membrane's surface is plasma etched and then coated with a phosphorylcholine solution. This process reduces the amount of protein fouling at the membrane's surface, and creates a lower flux decline compared to untreated membranes [10].

For process modifications, hydrodynamics refers to the manner in which the bulk feed solution reaches the surface of the membrane. Some of these modifications include: (1) increasing crossflow velocity; (2) improving feed spacers and inserts; (3) use of pulse flow; (4) Taylor and Dean vortices; (5) short path lengths in flat membrane modules; (6) backpulsing of permeate; and (7) use of high surface area, low flux hollow fibers [11].

A method of interest that is capable of creating high shear rates due to the presence of Taylor vortices (flow instabilities) is the use of rotating membrane modules. In these types of system, the high shear rate is caused by the high membrane speed, as opposed to

a high crossflow fluid velocity. An example of this type of system is the Spintek rotary membrane disk used for ultrafiltration. It uses the action of a centrifuge to create shear forces at the surface of the membrane that act to reduce fouling on the surface. This is illustrated in Figure 1.2; where F_D is the force associated with the membrane flux, F_C is the centrifugal force[1] which is a function of particle mass and rotational speed, D is the force due to back diffusion, τ_r is the radial shear force, and τ_θ is the tangential shear force. A system such as this also reduces the solute build-up due the density difference between the polarized layer and the bulk solution (concentration polarization). Another membrane module that will give the high shear rate is the rotating annular module (Figure 1.3). This type of system relies on a rotating inner membrane module and a stationary outer cylinder (pressure vessel) to create the Taylor vortices on the membrane surface. This type of process is capable of continuous microfiltration in the turbulent Taylor-vortex regime [12]. The basic theory behind these enhanced shear force membrane separation processes is similar to that of the research to be discussed in this dissertation.

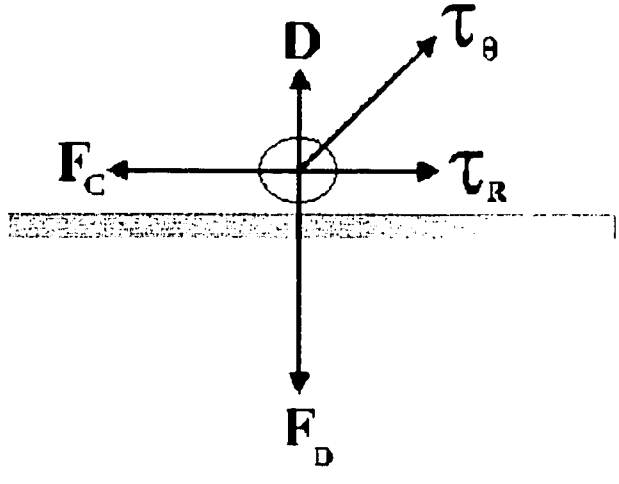

Figure 1.2 Forces acting on a particle at the membrane surface (Spintek apparatus) [11]

[1] The term "centrifugal force" is a postulated one. However, because the term has come into popular use, it will be used through out this dissertation to refer to the force directed outward from the axis of rotation.

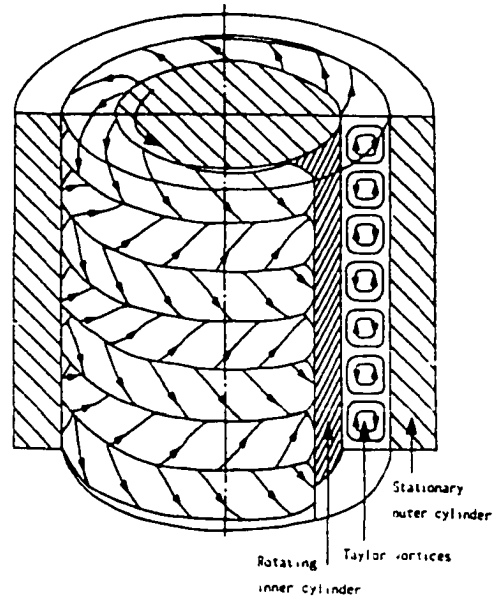

Figure 1.3 Taylor vortices in a rotating annular module (see Fig.1 of [12])

1.1.3 Evolution of Centrifugal Membrane Processes

As discussed above, advantages can be obtained by using rotating membrane processes to create turbulent, or at least unstable, flow at the membrane surface. Before describing in detail the process used for the experiments contained in this dissertation, it is worth looking at some at some of the earlier process design work done in this area. Work done in this area by Grenci [13] introduced a system where a rotating cylindrical membrane uses the centrifugal force generated to create the pressure necessary to drive the reverse osmosis process. In this system, the membrane is placed on the inside of a rotating cylinder wall, and the salt water feed is introduced in the center of the cylinder. The action of the centrifuge causes the migration of the salt water to the wall, and thus to the membrane. An invention by Keefer [14] addresses the problem associated with kinetic energy losses due to rotor windage in a rotary reverse osmosis process. An impeller feed pump, which is integral to the rotating membrane pressure vessel, creates the required feed pressure for the reverse osmosis process. The advantages of the centrifugal environment on the membrane's surface can still be achieved in this configuration. As the working pressure is due to the pump and not the centrifuge, lower rotating speeds are possible, and thus a reduction in windage losses.

The theory behind the process investigated in this dissertation was initially developed from work done by Wild and Vickers involving a centrifugal reverse osmosis (CRO) desalination system. In CRO, low pressure feed water enters the device along a rotational axis and moves to the periphery of a spinning rotor where the pressure developed is sufficient to drive the reverse osmosis process. Permeate is released at the periphery, and the retentate is returned to the rotational axis before leaving the device at low pressure. This critical aspect of CRO results in energy savings of 40-60% that of conventional high pressure reverse osmosis [15]. The patented design uses an evacuated enclosure to further reduce energy losses due to the rotor windage [16]. The developed CRO prototype uses sixteen conventional spiral wound membrane cartridges on the rotor. In using the circular pattern (Figure 1.4a) of spiral wound cartridges (Figure 1.4b) in the CRO process, an infinite number of membrane orientations were possible, with respect to the center of rotation. In this type of apparatus, there is no way of knowing if one particular membrane orientation is more advantageous than any other, with regards to exploiting centrifugal forces in the reduction of fouling.

The process referred to in this dissertation is the Centrifugal Membrane Density Separation (CMDS) process. CMDS applies the same process as CRO (feed along axis of rotation and permeate release at the periphery) to develop the process pressure, but unlike CRO, uses fixed orientations of the membranes with respect to the rotational axis. In a process such as the CMDS system, the membrane can be oriented in one of several ways relative to the axis of rotation, each of which is expected to create a specific type of reduction in fouling. This system utilizes centripetal acceleration and Coriolis forces, generated by a rotating centrifuge, to create the unstable flow necessary to reduce the fouling (including concentration polarization) at the membrane surface. The following sections will describe how the process works, membrane orientation, previous and ongoing academic work involving CMDS, and preliminary calibration experiments.

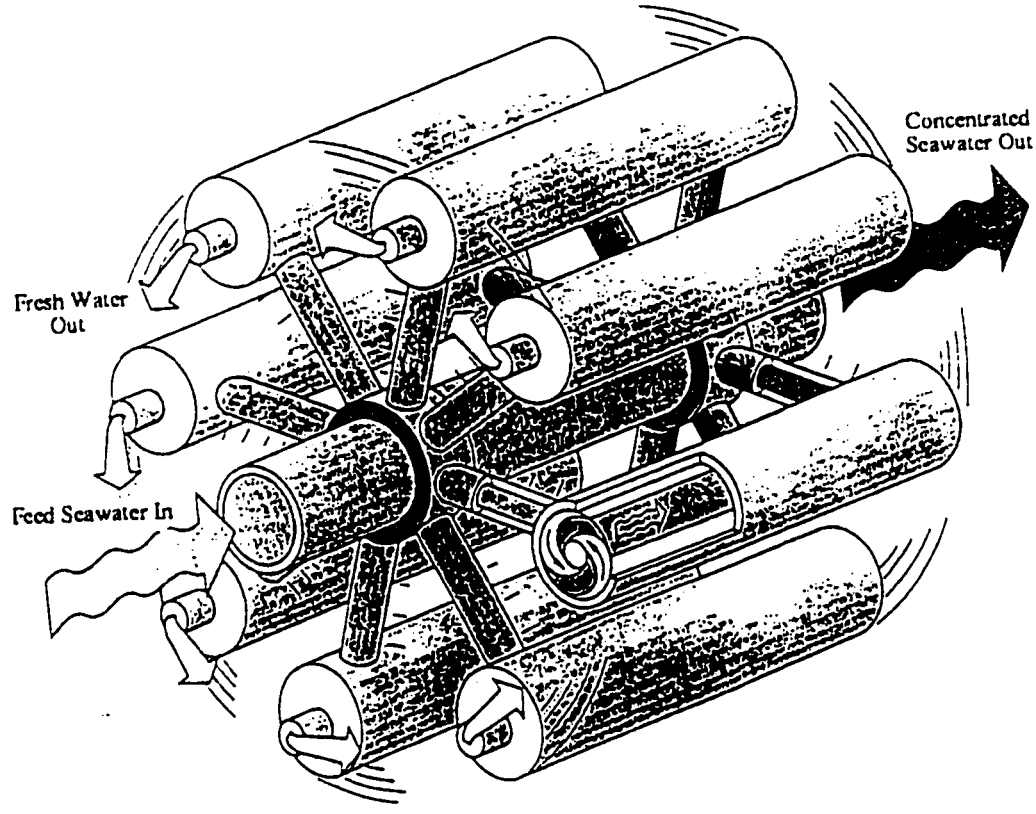

Figure 1.4(a) CRO apparatus (see Fig.1 of [15]); and

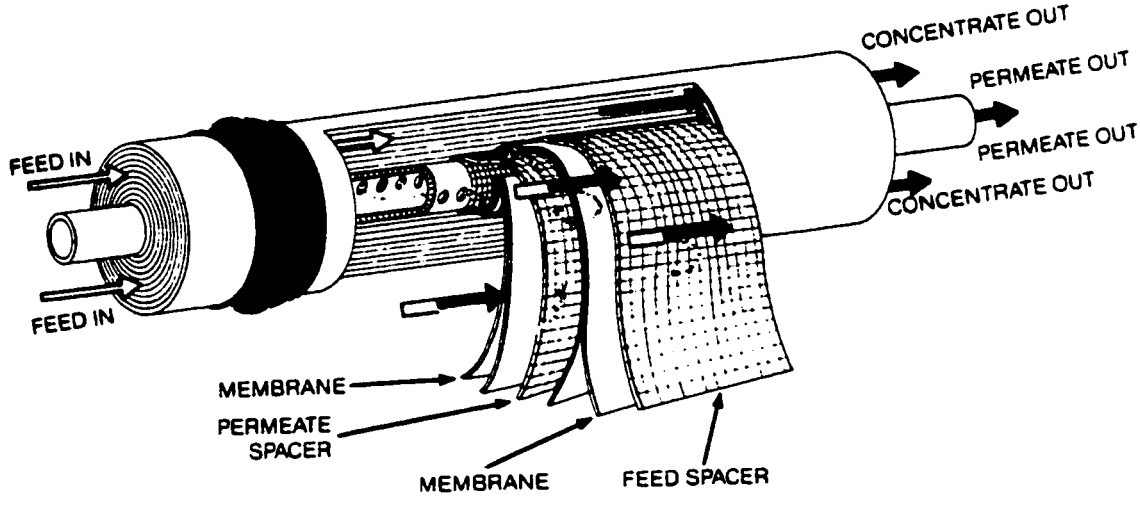

Figure 1.4(b) Typical spiral wound cartridge (see Fig 5.37 of [17])

1.2 CMDS Process Description

The experiments for this dissertation involve the use of an apparatus designed and constructed at the University of Victoria (Figure 1.5). A brief apparatus description follows, but a more complete description is available in [18]. The apparatus has been designed to accommodate rotors of varying geometries and operating speeds. The principal component of the design is a 5-foot diameter rotor housing which can be evacuated to minimize frictional power loss and heating due to windage. A 15 hp drive motor, disc brake, and oil lubricated bearings are mounted on the rear of the rotor housing, and the entire housing is mounted on vibration isolation feet to minimize the effects of minor imbalances in the test rotors. A circulation pump, tanks, heat exchanger, and plumbing take fluid to a rotary coupling which connects the spinning rotor to the stationary plumbing. The rotor system consists of an arm with a membrane head at one end and a counter balance at the other. The shaft and membrane head have been constructed out of titanium in order to reduce the weight and the stress problems associated with high g forces. Plumbing fixed to the arm carries the feed fluid to the membrane head and returns the retentate to the rotor axis (Figure 1.6). The rotor is capable of achieving pressures up to 8300 kPa, at rotational speeds up to 2200 rpm.

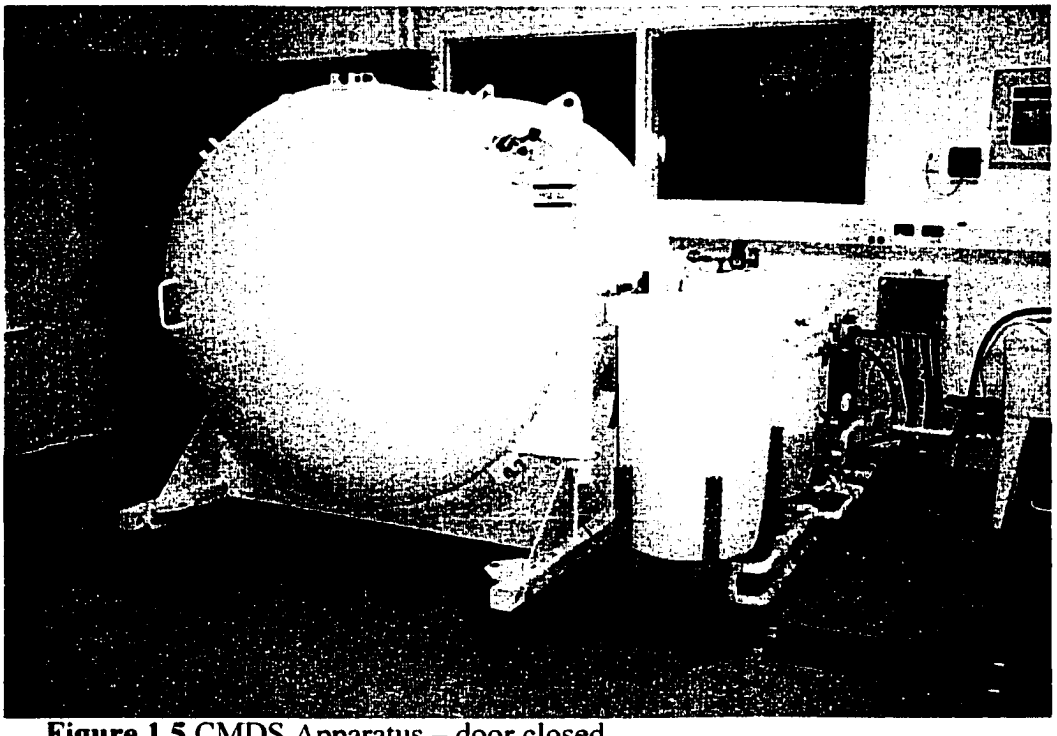

Figure 1.5 CMDS Apparatus – door closed

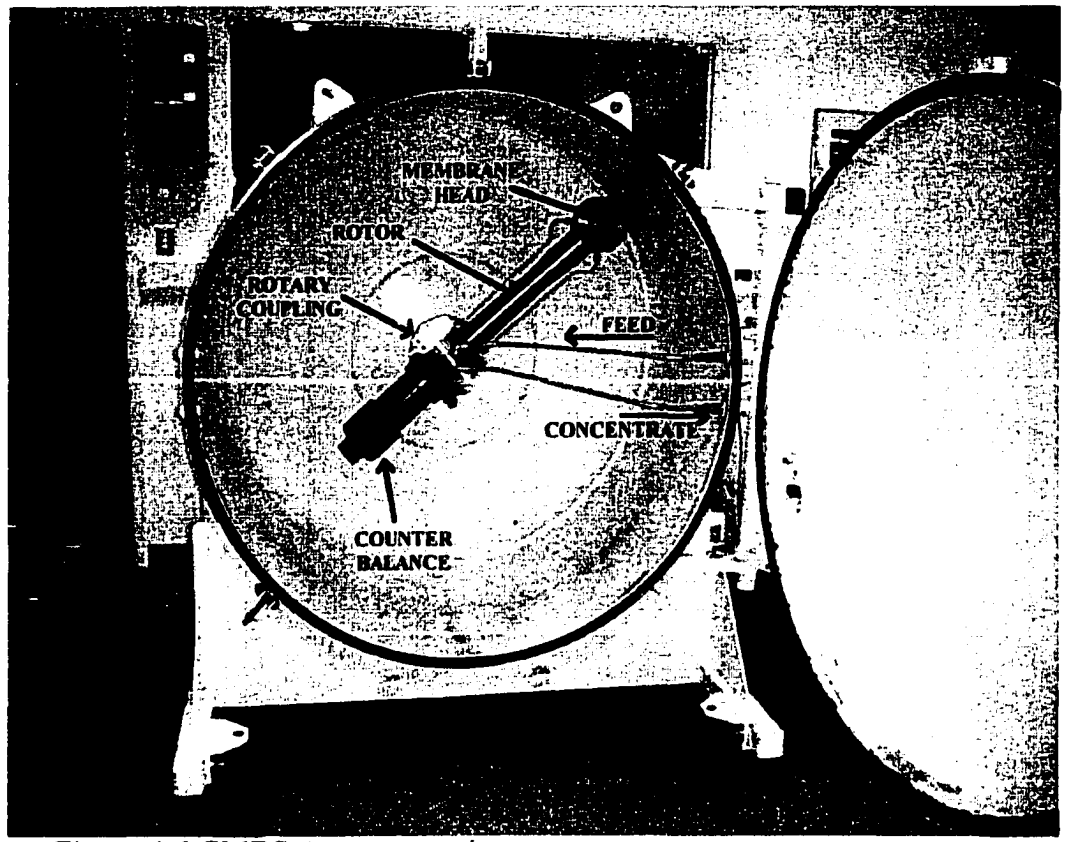

Figure 1.6 CMDS Apparatus – door open

Membrane modules used in this apparatus are stacked in a membrane holder, which is in turn placed in the membrane head that is attached to the rotor. Figure 1.7 shows how the individual membrane modules would be stacked in the membrane holder, and Figure 1.8 represents the membrane head configuration and its associated nomenclature. The membrane modules each consist of a permeate spacer fixed between an impermeable layer and a layer of membrane. The membrane modules, up to 9 in the membrane cell, all face in the same direction and are subject to the same relative direction of centripetal acceleration. Each module has an average membrane area of 50 cm^2. The permeate that flows through the membrane head is eventually released into the vacuum housing. Prior to this release, the permeate flow rate, conductivity and temperature are measured in a custom measurement cell (discussed further in Section 1.3.1). This instrumentation, along with other apparatus systems, report to a LabView™ interface which monitors and tracks performance, and in the event of failure, shuts down the apparatus.

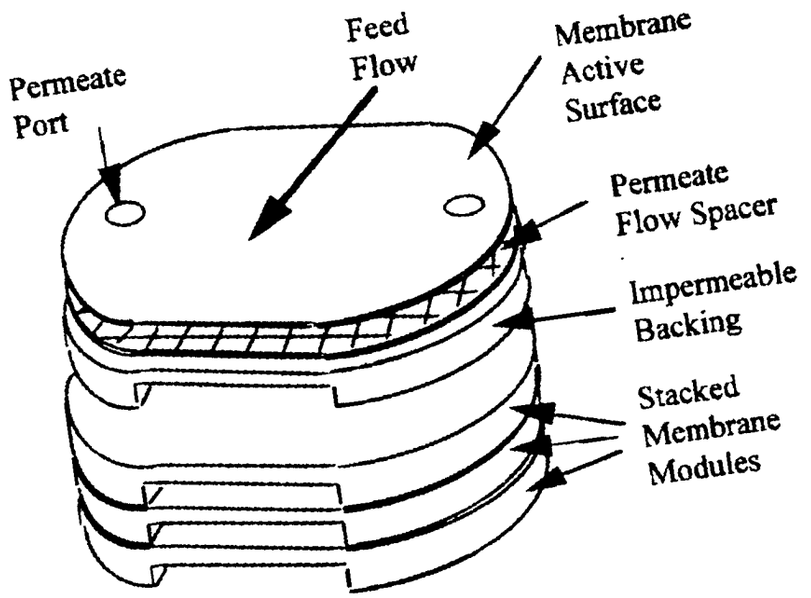

Figure 1.7 Membrane module stack [19]

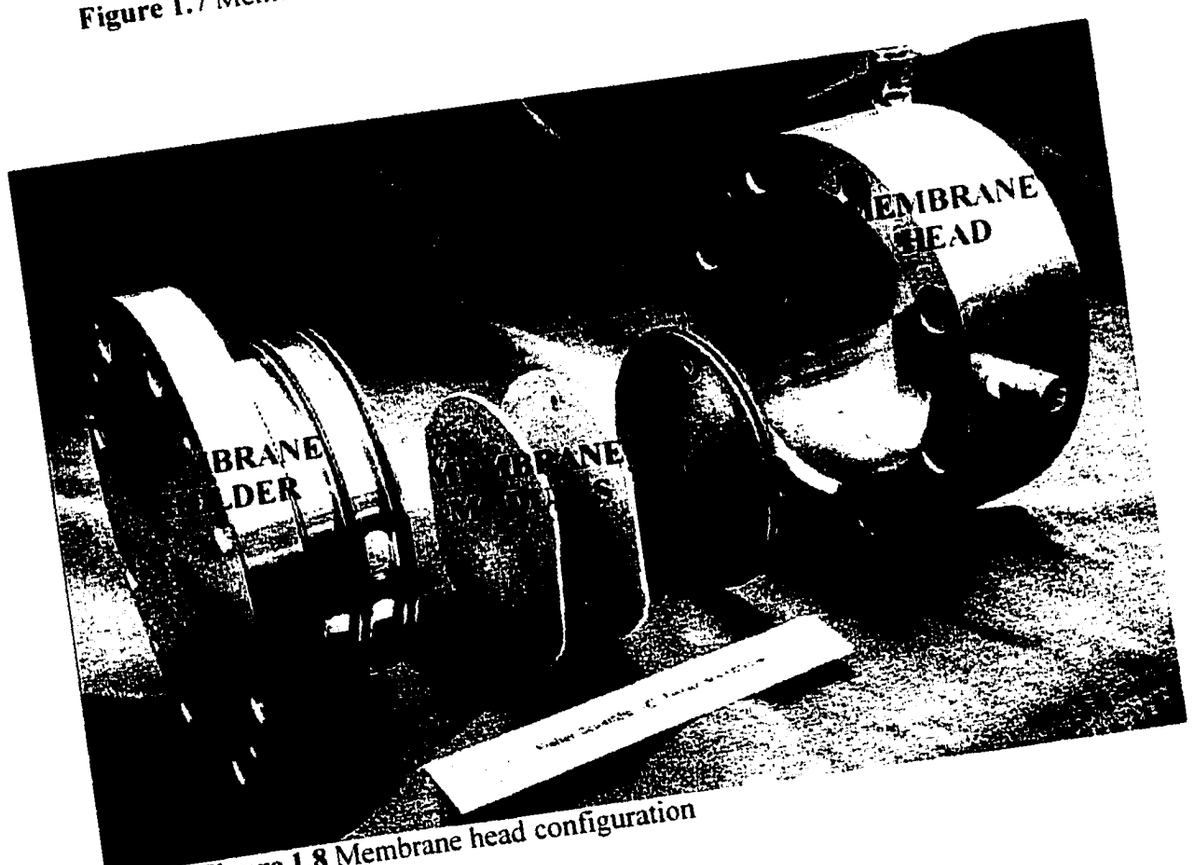

Figure 1.8 Membrane head configuration

Before the process is initiated, the membrane holder (containing the membrane modules) is secured into the membrane head with eight bolts. The vacuum housing door is sealed and the vacuum pump is turned on to bring the interior vacuum to approximately 28 in Hg. When the process begins, feed enters along the rotor axis and is pumped at low pressure to the membrane head at the rotor periphery. As the rotor spins the pressure increases with the rotational speed. It is this pressure that provides the driving force for the permeation across the membrane, and the permeate released at the periphery produces the transmembrane pressure. The concentrated feed returns to the rotary coupling and then exits the vacuum housing at low pressure to be returned to the process feed tank.

1.2.1 Membrane Orientation

As mentioned in Section 1.1.3, the membrane modules in the CMDS process can be fixed into one of several orientations. Membrane orientation plays an important role in the design of the experiments. Given orientations are available which will best exploit the benefits obtained from the Coriolis and centrifugal forces. In later chapters, this will come to light when describing the role each of these two forces play in the reduction of fouling and concentration polarization at the membrane surface.

In an effort to keep the nomenclature for these orientations straightforward, analogies have been developed which utilize the terms "pitch, roll and yaw". These three terms refer to the rotations about the z, x and y axes, respectively (refer to Figure 1.9). The pitch angle is achieved by using one of the two membrane heads available for the CMDS apparatus. Head #1 represents the 0° pitch angle, while head #2 represents the 90° pitch angle. Given the constraints of the hardware, these two pitch angles are the only ones currently available in the CMDS apparatus. The roll angles available depend on which of the two membrane heads is being used. For head #1, only two roll angles are possible, 0° and 180°, and these depend on how the membrane modules are placed into the membrane holder. If the modules are placed in the holder with the active membrane surface facing down, the roll angle is considered to be 0°. When the modules are placed in the holder with the active membrane surface facing up, the roll angle is considered to be 180°. When using membrane head #2, any roll angle, from 0° to 360°, is possible to obtain. As

is the case with head #1, membranes can be placed into the membrane holder with either the active membrane surface facing up or down. In these cases, the roll angles differing by 180° can be achieved without having to physically turn the rotor 180°. Yaw angles always refer to the way in which the membrane holder can be made to rotate within the membrane head. Given that there are eight bolts connecting the holder to the head, there are eight different yaw angles possible: 0°, 45°, 90°, 135°, 180°, 225°, 270° and 315°. Figure 1.9 illustrates examples of how the membrane is oriented with respect to the axis of rotation.

With these three descriptors, subsequent orientations will be given by 3 numbers, in the order of pitch, roll and yaw. For example, the orientation 0,180,90 refers to a pitch of 0°, a roll of 180° and a yaw of 90°. Occasionally, the letters p,r,y will be used if a generic description of the orientation is desired for experiment description. An example of this would occur when describing membrane head #2 experiments as 90,r,y experiments.

One other related component of membrane orientation is the direction of spin of the centrifuge rotor. The CMDS apparatus is capable of rotating in either a clockwise or counter-clockwise direction. However, for all of the experiments described in this, and the next two chapters, the direction of spin is always counter-clockwise as illustrated in Figure 1.9.

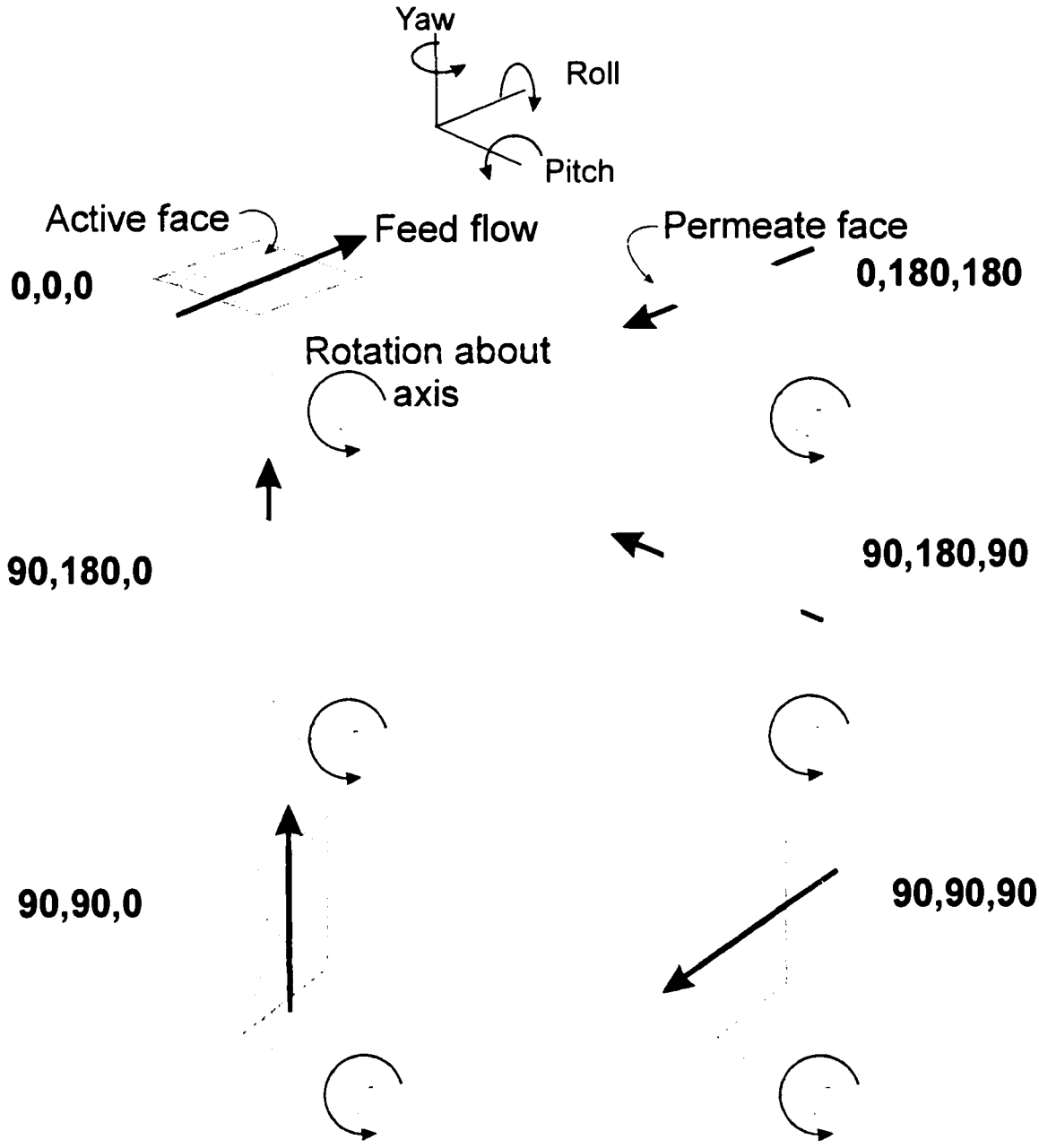

Figure 1.9 Examples of membrane orientation

1.3 Previous and Ongoing Academic Work on CMDS Process

Over the past few years, work involving the CMDS process has given rise to several academic works by other graduate students, aside from the work being described in this dissertation. These have included development of a custom measurement device, computational fluid dynamic models, and a determination of angular influences on the CMDS process. This section will provide brief descriptions of these works, and how they relate to the experiments to be described in this and later chapters.

1.3.1 FRACT

The flow rates produced by the experiments using the CMDS prototype were envisioned to be fairly low (< 20 mL/min), and thus it became necessary to measure the flow while the process was running. Due to this factor, and also the harsh environment present in the CMDS process (2000 rpm and 3200 G's), it was determined that there was a need for a custom made measurement device. This device, referred to as the CMDS Flow Rate and Conductivity Transducer (FRACT), was developed by Peter Byrnes in fulfillment of the thesis portion of his M.A.Sc. degree [20]. This was conceived, designed and built for use onboard the membrane head at the end of the rotor of the CMDS apparatus. In the concept phase of this work, it was determined that flow rate and conductivity were the target quantities to be measured by this device. These two quantities would help to determine how much permeate was passing through the membrane, and at what quality (% rejection = f(conductivity)). As the permeate was to be released into the vacuum housing, this device had to be made to capture, measure, and release the permeate. The challenge associated with this design was to build a device that could withstand high gravitational forces and vibrations, while being able to deliver signals from within the device to a user interface located outside.

From initial experiments, it was determined that the ranges for flow rate and conductivity should be 0.5-20 mL/min and 0-5 mS/cm, respectively. For the flow meter part of the device, a "fill and empty" chamber was envisioned for use. This chamber would have an electromagnetic actuated valve that would allow for the control of the filling and draining of the device. Inside of the fill chamber, fluid level-sensing electrical contacts would

create the signals necessary for the flow measurement determination. The conductivity measurement was to be determined by using two parallel platinum plates placed inside of the fill chamber. This measurement was temperature compensated based on a temperature-sensing channel within the FRACT. The conductivity voltage signal was converted to mS/cm (X), which in turn could be converted to ppm NaCl (Y) using the following 3rd order polynomial:

$$Y = -3.1509 + 486.54X + 10.176X^2 - 9.7453 \times 10^{-2}X^3 \qquad (1.1)$$

Once initial testing was complete, the FRACT was attached to the permeate port of the membrane head for dynamic testing. The performance of the FRACT during this testing is summarized in Table 1.5.

Measurement		Range	Precision
Flow Rate		0.5-20 mL/min	±2.5% (@10mL/min)
Conductivity	High Range	0.44-5 mS/cm	±0.3%
	Low Range	0-0.34 mS/cm	±0.1%
Temperature		15-45 °C	±0.5%

Table 1.5 FRACT operating ranges

1.3.2 Computational Fluid Dynamic Models

Numerical modeling of the CMDS process complements the experimental work conducted using the process. The CFD models were developed by Jon Pharoah in fulfillment of the thesis portion of his M.A.Sc. degree [21], as well as in his ongoing PhD dissertation research. The models consist of a three-dimensional flow channel with a permeable membrane surface, where the membrane itself is modeled using a boundary condition representing the preferential removal of one component of the solution [22]. Simulations involving both a conventional static membrane process and the rotating CMDS process were examined, and compared.

The fluid flow in the CMDS process is determined by the conservation of mass, the Navier-Stokes equations and a scalar transport equation. These governing equations are

outlined in both of the above noted references. The boundary conditions specified for these equations include inlet, outlet and no-slip conditions, as well as a selective membrane boundary condition. This membrane boundary condition is based on both the mass (J_s) and volume (j_v) flux across the membrane, represented by the following respective equations:

$$j_v = L_p(\Delta P - \Delta\Pi) \tag{1.2}$$

$$J_s = j_v \frac{(1-R)}{R}(c_f - c_p) \tag{1.3}$$

where R is the membrane rejection, c_f is the feed concentration, c_p is the permeate concentration, L_p is the membrane permeability, ΔP is the hydrostatic pressure difference and $\Delta\Pi$ is the osmotic pressure difference.

The model and boundary conditions are solved with a finite element analysis using the CFD code TASCflow3d. Some of the results for this analysis are related to the concentration polarization experiments conducted on the CMDS apparatus, and are discussed in Section 2.3 of this dissertation. In general, the CFD experiments help to highlight phenomena that may be occurring at the surface of the membrane, which in turn may be reducing the effects of concentration polarization and/or fouling. This type of work helps to show how the theoretical work can greatly enhance the overall quality of the experimental work. It can provide direction for the experiments, thus negating the need for a lot of "trial and error" work. This factor is important because of the significant amount of time necessary to conduct a single set of experiments. An example of this enhancement was highlighted by the CFD determination that showed that Coriolis forces were playing a significant role in the creation of the aforementioned flow instabilities on the membrane surface. It was this work which directed the experimental focus towards examining specific orientations (to be described in the next two chapters).

1.3.3 Angular Influences in CMDS Process

As the current CMDS apparatus is a prototype, a view towards eventual scale-up has been examined. This research was completed by Alvin Bergen in fulfillment of the thesis portion of his M.A.Sc. degree [18]. This work examines angles that need to be considered for an eventual module design that contains more membrane material. This thesis goes into great detail on the work that went into the mechanical design of the CMDS prototype apparatus. Bergen also examines such areas as temperature dependence and temperature control. This became an important issue, as it was determined that flux increased by 3.6% for every °C increase in temperature. He also expands upon the concentration polarization work (to be discussed in the next chapter) by taking a closer look at the relevance of the yaw angles to flux enhancement.

Based on his experimental work, Bergen determined that the membrane orientation in future CMDS membrane modules should employ radial feed flow with maximum Coriolis acceleration. This limits the module design to a configuration with annular rings or axial vanes. He determined that developing a cartridge design where the entire circumference of the rotor is filled with membrane material would maximize packing density but would be difficult to implement. A rotor design with discrete cylindrical pressure vessels and modular membrane cartridges was found to be a practical alternative. A cartridge design employing a series of double sided membrane disks aligned in the planar orientation would contain proper geometry to maximize performance and would simplify manufacturing. Bergen proposes that by incorporating the feed distribution channels into a split membrane disk support shell, a robust and easy to assemble cartridge design would result. The module would be functionally similar to the spiral wound modules used in the CRO rotor design [16], but optimized for the dynamic environment.

1.4 Preliminary Calibration Experiments

Initial experiments were conducted on a conventional pressure-driven membrane (static) apparatus (Figure 1.10). This apparatus has an identical membrane head to that used for the CMDS apparatus. This allowed for the same membrane holder, containing a given

set of membrane modules, to be used in comparison experiments. The static apparatus also consists of a high-pressure reciprocating pump, capable of producing applied pressures of up to 6900 kPa. Additional equipment includes a bladder accumulator to dampen the pump's pulses, two feed tanks, a backpressure regulator, pressure regulator, and associated plastic and stainless steel plumbing. Flow and conductivity are measured in the static process using a timed fill volume and a bench top conductivity meter, respectively.

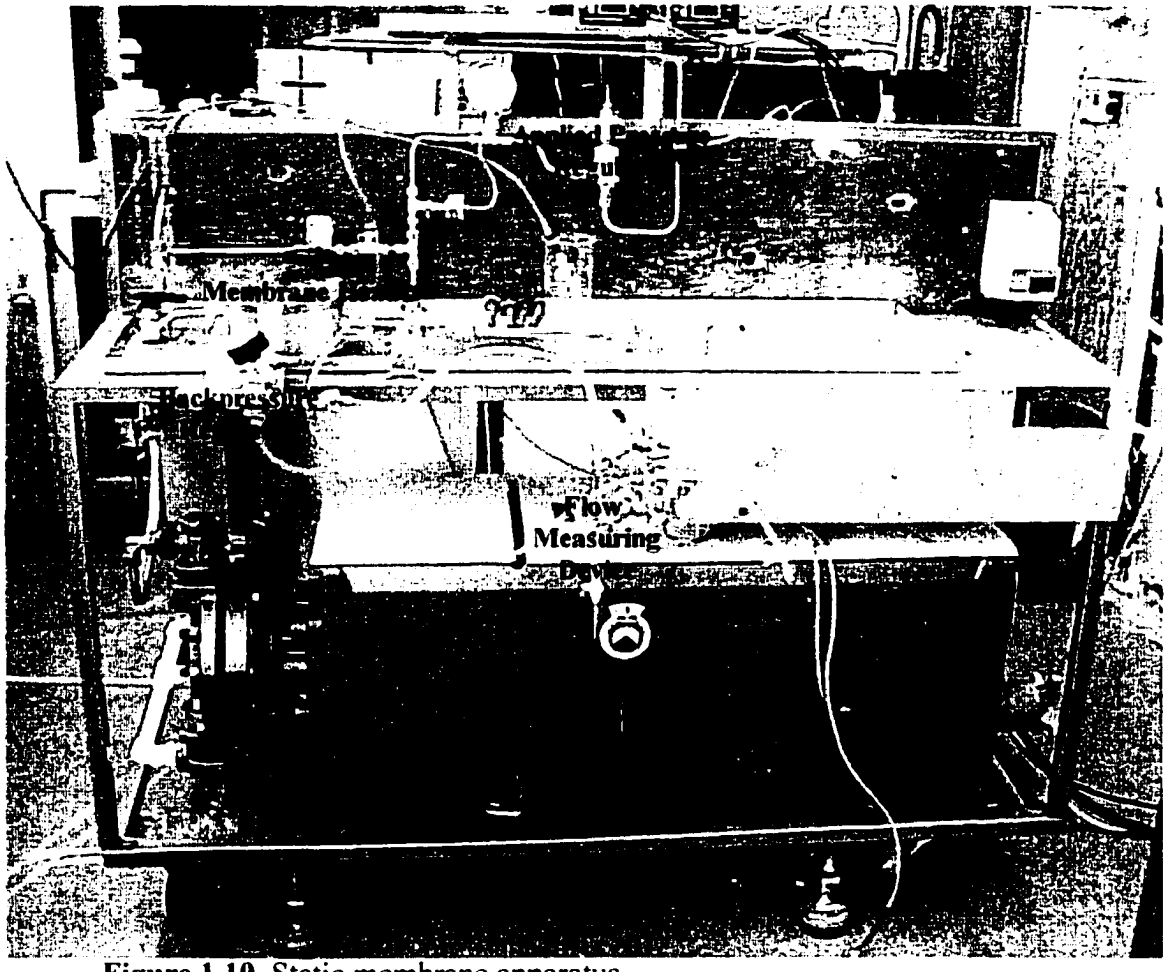

Figure 1.10 Static membrane apparatus

The initial calibration experiments were performed to see if there were any factors that contributed to improved flux performance, regardless of whether the process was dynamic or static. The experiments were conducted to examine membrane orientation within the membrane holder, flow inlet and outlet angles (*i.e.* yaw angles), feed flow rate,

backpressure, and temperature dependence. These experiments were conducted at a fixed pressure (3100 kPa) and NaCl solution concentration (500 ppm). Exceptions occur in the backpressure experiment, which was conducted at a transmembrane pressure of 4200 kPa, and in the temperature experiment, where the NaCl concentration was 18,000 ppm. The low NaCl concentration was chosen for most of these experiments in order to minimize concentration polarization effects. These preliminary experiments also helped in the development of process and membrane knowledge. This information became valuable later, as it provides "rule of thumb" experience on both the CMDS process and membranes.

Table 1.6 illustrates examples of the preliminary experiments conducted to test the effects of yaw, membrane orientation within the holder and feed flow rate using the static system. The position of the membrane is given in this table in the standard membrane orientation discussed in Section 1.2.1. Though no pitch exists in the static apparatus, it is designated as 0^{o} for the purposes of this presentation of data. In the experiments, the feed flow rate was varied from 2 to 7.5 L/min, 4 different yaw angles were examined and both the "up and down" of the membrane within the holder (roll = 0 and 180) was looked at. From these results, it was determined that little, to no, effect was observed. The only small observed trend occurred in the varying of the feed flow rate. When the feed flow rate was increased the permeate volume flux also increased. This is attributed to the corresponding increase in fluid velocity across the membrane. With the fixed area of the cell, the Reynolds Number increases slightly, but still remains in the laminar flow regime (Re ~ 200). Though the feed solution was low in NaCl concentration, the increased fluid velocity may have been reducing any small amount of concentration polarization that may have been occurring at the membrane surface.

Experiment #	Membrane Orientation	Feed Flow Rate (L/min)	Volume Flux (L/m^2 hr)
1	0,0,0	4.0	27.7 ± 1.1
2	0,180,0	4.0	29.3 ± 0.4
3	0,0,135	6.0	31.0 ± 2.0
4	0,180,135	6.0	30.4 ± 1.3
5	0,0,45	4.0	26.9 ± 0.8
6	0,0,135	4.0	29.2 ± 0.9
7	0,0,180	4.0	29.0 ± 0.5
8	0,0,0	2.0	26.3 ± 0.2
9	0,0,0	7.5	30.2 ± 1.4
10 (#8 repeated)	0,0,0	2.0	26.5 ± 0.3

Table 1.6 Summary of calibration experiments

The effect of backpressure was also examined on the static apparatus. This was deemed necessary because of the fact that the CMDS apparatus exerts a backpressure on the permeate due to the plumbing within the membrane holder. The permeate travels a short distance towards the rotor axis before release into the vacuum chamber, thus the radial difference between the membrane radius and the "critical release radius" [16,23] creates a backpressure on the membrane. Using the backpressure regulator on the static apparatus, the backpressure was varied from 0 to 1400 kPa in 350 kPa increments. The corresponding applied pressure was varied to ensure that the transmembrane pressure remained at a constant 4200 kPa throughout the experiment. These experiments showed that there was no difference in permeate flux or salt rejection when the backpressure was applied. Because of this, direct flux comparisons could be conducted between the static and dynamic processes without having to account for the inherent backpressure of the dynamic process.

The final preliminary experiment involved the dependence of flux on the temperature of the feed solution. During the earlier experiments, it was determined that the increase in temperature over time was causing an increase in permeate flux. This increase in temperature alters a number of properties of the feed stream: viscosity is decreased, density is decreased, diffusivity of ionic species is increased. All these factors combine to increase the flux across the membrane. An experiment was conducted to examine the

significance of this relationship (Figure 1.11). The linear regressions provided means for establishing how significant the effects were. The results for the static and dynamic processes were 0.50 L/m^2 hr per ° C and 0.79 L/m^2 hr per ° C, respectively. From these results, it was determined that subsequent experiments should be temperature controlled to ± 1 °C. This was achieved by using an existing single-pass, concurrent flow heat exchanger on the static apparatus, and a retrofitted heating/cooling system on the CMDS apparatus [18].

The next step in the preliminary experiments was a direct comparison between the static and dynamic systems. This experiment was also conducted at low NaCl solution concentration to minimize the effects of concentration polarization. In this case, the same membrane holder (titanium) and membrane modules were used for both the static and dynamic processes to obtain a direct comparison. The comparison involved determining the permeate volume flux as a function of pressure (Figure 1.12). This experiment was the first one to test if the CMDS apparatus worked at least as well as a conventional, pressure-driven membrane process. It was concluded from this experiment that the CMDS apparatus did work in a similar manner to that of a pressure-driven process.

As previously mentioned, the preliminary experiments helped in the development of "rule of thumb" process knowledge. For example, it became apparent that there was some variability of membrane modules. The variation between the membrane modules was found to be ± 10-15%, which occurred because of the different membrane material samples used and the manner in which the membrane modules were assembled. There also seemed to be minor day-to-day variations in the flux performance of the membrane modules (± 2%). These errors were unavoidable and had to be factored into the experiments as a potential source of unquantifiable error, especially with the ± 2% day-to-day variation. Because of this factor, the use of static experiments as reference experiments became even more important for each concentration polarization and fouling determination.

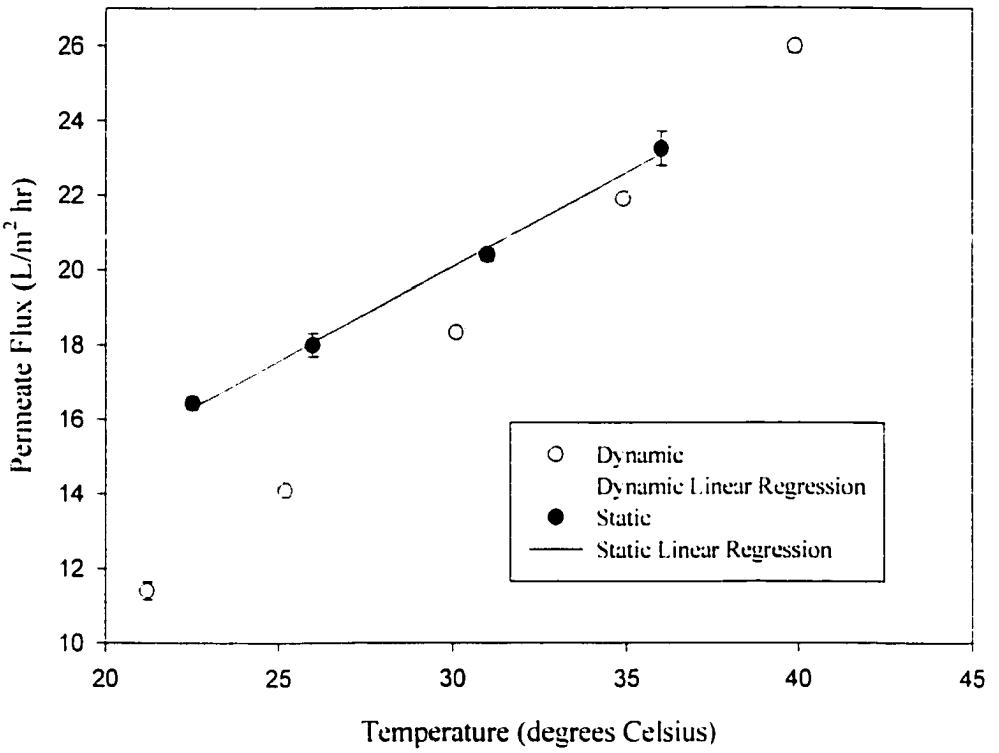

Figure 1.11 Temperature dependence on permeate flux

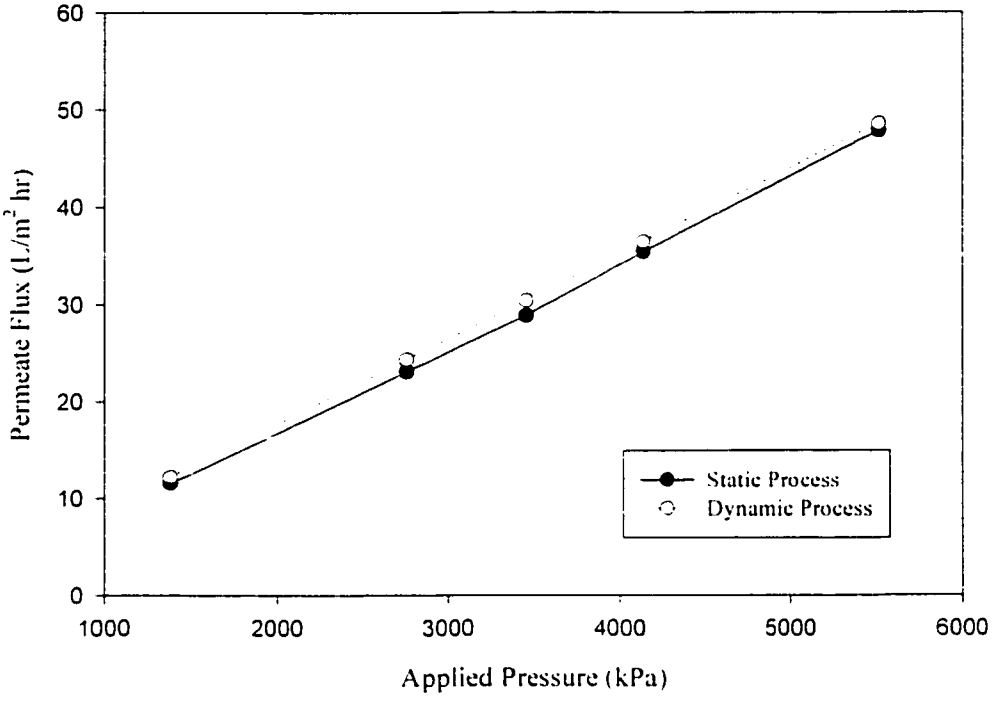

Figure 1.12 Membrane process comparison

1.5 Principles of Experimental Work

The previous information has laid the foundation for the experimental work that follows in the next two chapters. Previous work described in the literature, initial CMDS experiments and the preliminary CFD work has highlighted the possibility that secondary flow patterns can be developed on the surface of a membrane operating in a centrifuge. Exploiting the centrifugal and Coriolis forces can develop these flow patterns (instabilities), which in turn can lead to the reduction of fouling and concentration polarization on the membrane surface. Examining absolute flux and flux decline for various membrane orientations with respect to rotation, will provide information on how best to utilize the above-mentioned forces in the enhancement of membrane flux and reduction in fouling.

Concentration polarization is a useful area to start in the development of membrane orientation knowledge. The experiments associated with this phenomenon involve less complex feed solution preparation compared to those involved with the fouling experiments. The intent of the concentration polarization experiments is to compare the performance of the membranes in various orientations relative to results under the same conditions from the conventional static process. The performance will be quantified by examining the magnitude of the flux enhancement through various defined factors. These factors will help to illustrate the magnitude of the Coriolis and centrifugal forces being applied to the bulk solution near the membrane surface. These results will help to identify the "best" orientation, which may later be utilized in an ultimate scale-up of the process. They will also probe the relative importance of centrifugal and Coriolis forces in flux enhancement. Once again, these experiments lead to valuable "rule of thumb" knowledge with respect to the CMDS process, which can be utilized in future experiments.

The fouling experiments have several purposes in this dissertation. They will help in the understanding of the fouling mechanisms for colloidal solutions, and in the determination of the relative magnitude of flux enhancement associated with both Coriolis and centrifugal forces. The relative magnitude of flux enhancement, as well as the absolute flux, will also be quantified with defined factors. As some of the fouling feed streams are denser than the brine solutions, it is anticipated that the centrifugal forces will play an essential role in flux enhancement. As an additional part of the fouling experiments, fouling of nanofiltration (NF) membranes is also examined. NF processes employ a different type of transport across the membrane, and will thus help to illustrate two points. These include: (1) when required, the CMDS process works effectively for different types of membrane transport mechanism; and (2) Coriolis and centrifugal forces can help in the enhancement of flux for macromolecular feed solutions (proteins), with respect to membrane orientation.

2 Concentration Polarization

2.1 Introduction

Concentration polarization is one of the most pervasive problems encountered in membrane processes. Though considered to be a type of fouling, it often is discussed separately because of its different mechanism. It results from the buildup of a laminar boundary layer that increases solute concentration at the surface relative to the bulk solution. This occurs because water permeation at the membrane surface leaves the more concentrated solute layer that must diffuse back into the bulk liquid [24]. This in turn creates a reduction in the flux across the surface of the membrane, and thus a reduction in the process efficiency. This is particularly true for reverse osmosis membranes where osmotic pressure is also a consideration. In this case the flux is a function of applied pressure and osmotic pressure [flux = $L_p(\Delta P-\Delta\Pi)$], and as the latter increases, the flux will decrease. The increase in solution concentration in the boundary layer will create this higher osmotic pressure. Figure 2.1 illustrates this phenomenon by showing the solute concentration profile of the boundary layer, adjacent to the membrane surface (solid yellow area).

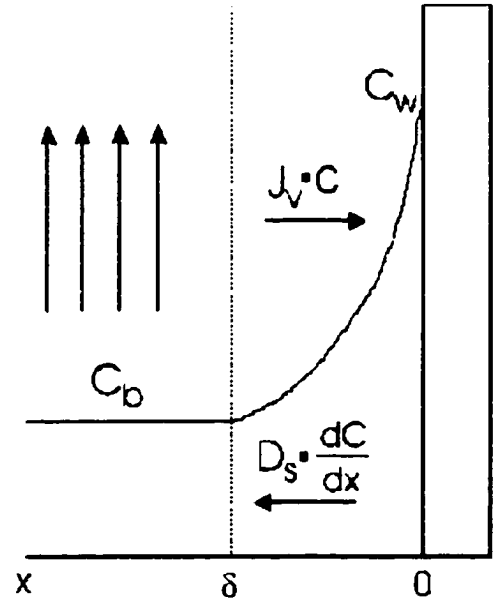

Figure 2.1 Concentration profile during concentration polarization

As the bulk solution flows across the surface of the membrane, it selectively permeates solvent through the membrane, leaving solute behind. This build up of concentration at the membrane surface can be expressed mathematically with a simple mass balance across the thickness of the boundary layer, δ, and is referred to as film theory [25]. This theory assumes that the bulk flow outside of the laminar film is better mixed and has a uniform concentration [26]. Therefore, the concentration gradient only exists in the laminar film, and accounts for all the resistance to mass transfer in the solution phase.

The solute convection to the membrane is given by a term $J_v \bullet C$, while for the back diffusion of solute to the bulk solution, it is $D_s \bullet dC/dx$. At steady state, the two fluxes will balance each other according to equation 2.1.

$$J_v \frac{dC}{dx} - D_s \frac{d^2C}{dx} = 0 \qquad (2.1)$$

If this relationship is integrated over the mass transfer boundary layer thickness, one arrives at the expression for flux across the membrane (equation 2.2).

$$\frac{C_w}{C_b} = exp \frac{J_v \delta}{D_s} \qquad (2.2)$$

Because the boundary layer thickness is unknown, the term D_s/δ is usually defined as k, or the mass transfer coefficient [26], and thus equation 2.2 can be redefined as:

$$\frac{C_w}{C_b} = exp \frac{J_v}{k} \qquad (2.3)$$

From this relationship it can be seen that as the permeation across the membrane increases (increasing J_v), the concentration at the membrane surface will also increase. As mentioned above, this increase in concentration will also create a higher osmotic pressure, which coupled with the back diffusion will increase the bulk concentration, thus

lowering flux. For reverse osmosis membranes and relatively dilute electrolytic feed solutions, there is no practical upper limit of the limiting wall concentration. This is not true for the nanofiltration of macromolecules where a phenomenon, known as gel polarization limits the wall concentration. Gel polarization will be discussed further in the section dealing with nanofiltration (Section 3.4.1).

Concentration polarization reduction is one of the primary goals of the centrifugal membrane process. Experiments were developed to see if the process could reduce concentration polarization, and with which membrane orientation was the reduction most effective. For future scale-up of the process, it is important to determine which orientations yield the best results. For example, it is assumed that membranes in the general 0.r.y orientation will show both an improvement and reduction in flux compared to the static process. For membranes in the 0.0.y orientation (*i.e.* active face facing outward with respect to the centre of rotation) it is assumed that the density effect of the centrifuge will act in such a manner to draw more concentrated solution away from the surface of the membrane. This will then enhance the flux relative to the static case. This density effect occurs because of the high rotational speeds of the centrifuge that creates significant centrifugal forces. It is these forces that cause the migration of dense objects away from the centre of rotation. Membranes in the 0.180.y orientation (*i.e.* active face facing inward with respect to the centre of rotation) should give the opposite results, with concentrated solution being held near the surface of the membrane by the gravitational forces, thus creating less flux relative to the static case.

As was discussed in Section 1.3.2, earlier computational fluid dynamic work had determined that Coriolis forces create instabilities in the flow patterns which may be partially responsible for the reduction of the laminar boundary layer at the membrane surface, and subsequent reduction of concentration polarization. Membrane orientations using the general 90.r.y orientation could be used to examine this effect. Some of the orientations are capable of producing minimum Coriolis forces, while others can produce maximum Coriolis forces. These orientations will also be compared to the 0.r.y orientations, discussed in the previous paragraph. In all cases, performance relative to the

static case will be examined to determine how well each orientation performs. This will be the main means of comparison between the orientations, and the actual method of comparison will be discussed in Section 2.3.

2.2 Experimental Procedure

The experiments involved the use of the two fixed heads (0,r,y and 90,r,y) that are representative of the two principal pitch angles possible in the dynamic apparatus. Initial work in the preliminary calibration experiments had developed a sufficient level of expertise where the process operating parameters were well established. All concentration polarization experiments were conducted with a feed recirculation rate set at 2 L/min, a feed temperature of 25 °C, and in all cases, four membrane modules were used. These four membrane modules have a combined area of approximately 200 cm^2. The membrane material used in the individual membrane modules was DS-3™, a thin-film composite reverse osmosis membrane from Osmonics (previously Desalination Systems). Table 2.1 summarizes some of the specifications for the membrane material. In the case of the dynamic experiments, the direction of rotation was always counter-clockwise.

Specification	Value
application	organic separations, landfill leachate, wastewater treatment
membrane rating	99.0% average NaCl rejection (based on 32000 ppm NaCl feed at 5,516 kPa operating pressure and 25°C).
pH range	optimum rejection at pH 5.5-7.0, operating range 2.0-11.0
typical operating pressure	5,500 kPa
maximum pressure	6,900 kPa
maximum temperature	50°C

Table 2.1 DS-3™ membrane material specifications [27]

Experiments were run using the fixed head with the pitch of 0° (designated as 0,r,y). These experiments involved the use of varying concentrations of NaCl in both the static and dynamic systems. The three NaCl concentrations that were used included 10000, 22500 and 35000 ppm, and were prepared using distilled water (reduced likelihood of

biological fouling commonly associated with tap water) and a coarse grade of NaCl. The concentrations were determined based on the conductivity calibration (equation 1.1) that was used when using the bench top conductivity meter in the sample preparation. The procedure for these experiments involved running the membrane modules on the dynamic system using both the inward and outward facing orientations (represented as 0,180,y and 0,0,y, respectively, as discussed in the previous chapter, Section 1.2.1). Upon completion of these dynamic experiments, the membrane head assembly was transferred to the static apparatus for duplicate experiments. This procedure was conducted separately for each of the three NaCl concentrations. The procedure involved varying the applied pressure from 2700 to 5500 kPa (in approximately 700 kPa increments) for each concentration of feed solution. Varying numbers of permeate samples were sequentially collected at each pressure to determine the flow rates. These sample flow rates were determined using the FRACT on the dynamic apparatus, and using a set volume vessel and stopwatch on the static apparatus. In both processes, the concentrate was recycled back to the feed tank, and a volume of fresh water was added periodically to make up that lost in the permeate stream.

In trying to determine how well the dynamic process would perform at even higher electrolyte concentrations, a problem with the FRACT was identified. The conductivity measuring capability of the FRACT had an upper limit for the permeate stream (as described in Section 1.3.1). This in turn limited how concentrated the feed solution could be based on a minimum membrane rejection value of 95%. In an effort to overcome the upper limit of the FRACT conductivity measurement, an electrolyte solution had to be used which allowed for higher concentrations, while keeping within the bounds of the dynamic system conductivity measurement. It was decided that $MgSO_4$ would be used for this purpose given its significant solubility coupled with its lower specific conductivity relative to NaCl. In effect, twice the weight fraction of that used for NaCl were used as $MgSO_4$ feed solutions for this part of the experiment using the 0,r,y head. The $MgSO_4$ experiments used the same procedure as the one described above for NaCl.

Another set of concentration polarization experiments were run using the fixed head with the pitch of 90° (designated as 90,r,y). In the case of this head, two roll angles of interest were examined experimentally; roll 0° and roll 90° (designated as 90,0,y and 90,90,y, respectively). The procedure for these experiments were altered somewhat in that all three NaCl concentrations were run consecutively on the dynamic system, and then, consecutively, on the static system. For these experiments, only NaCl solutions were used as feed solutions.

From the previous 0,r,y head experiments, an approximate operating pressure range for each concentration was determined. Therefore, unlike in the 0,r,y experiments, the applied pressure ranges varied for each feed solution concentration. Similarly, the pressures were increased in 700 kPa increments. Table 2.2 summarizes the operating pressure ranges used for the 90,r,y head experiments. The permeate samples were collected in the same manner described above for the 0,r,y experiments.

NaCl Feed Solution (ppm)	Orientation	Applied Pressure Range (kPa)
10000	Dynamic 90,90,0	1400 – 5500
	Static Comparison	2700 - 5500
22500	Dynamic 90,90,0	2100 – 5500
	Static Comparison	2700 – 5500
35000	Dynamic 90,90,0	2700 – 6200
	Static Comparison	2700 - 5500
10000	90,180,0	1400 – 4100
22500	90,180,0	2100 - 4800
35000	90,180,0	2700 - 5500

Table 2.2 90,r,y head experiments operating pressure ranges

2.3 Results

2.3.1 Orientation – 0,r,y

This set of concentration polarization experiments was conducted with the active membrane surface facing outward (0,0,0) and inward (0,180,0). To illustrate a typical

result, the flux performance for the experiment using the NaCl concentration of 35000 ppm is illustrated in Figure 2.2. This graph, like all done for concentration polarization experiments, shows permeate flux (L/m^2 hr) as a function of the applied pressure (kPa). This figure shows significant flux enhancement, and also shows that as the applied pressure increases, so does the flux enhancement.

To quantify the overall flux enhancement for each concentration and orientation, a slope analysis of the results was done using linear regression for each line. This was done using the linear regression tool on SigmaPlot 5.0™ [28]. At each concentration, a slope for the static case was determined, which was to be the value used for the comparison. The slopes were then determined for the lines representing the 0,0,0 and 0,180,0 cases. These slopes were then divided by the slope of the static case, and thus the relative flux enhancement (or decrease, as the case may be) was produced. This factor is referred to as β, and any value of this factor that is greater than one is indicating an enhancement of flux. The value of these factors provides a means of comparison for other results from other orientations, concentrations and feed solutions, and thus the higher the value of β, the better. A summary of these results is given in Table 2.3.

The next experiment used the different electrolyte ($MgSO_4$) to see if the results obtained for NaCl could be duplicated with much higher concentration feed solutions. The results for these experiments follow the same trends as those exhibited for the NaCl solutions, but with greater flux enhancement and slightly better rejection values (Figure 2.3 and Table 2.3). It is assumed that for this particular solution, the density was higher than that of the NaCl solutions. Because of this, it was likely that the density effect inherent in the centrifuge (discussed in Section 2.1) would be more pronounced. Figure 2.3 illustrates this by showing a greater difference in the 0,0,0 and 0,180,0 orientations, with respect to the static case. In Figure 2.2, we see that this effect is not as pronounced, and actually shows the 0,180,0 orientation and the static case to be fairly similar in slope and permeate flux magnitude. This leads to the conclusions that the dynamic process in the 0,0,0 orientation gives the greater enhancement of flux compared to the 0,180,0 orientation, and at higher feed concentration and density, this orientation also performs increasingly

better. This latter statement is quantified by the flux relative to static case factor (β) given in Table 2.3.

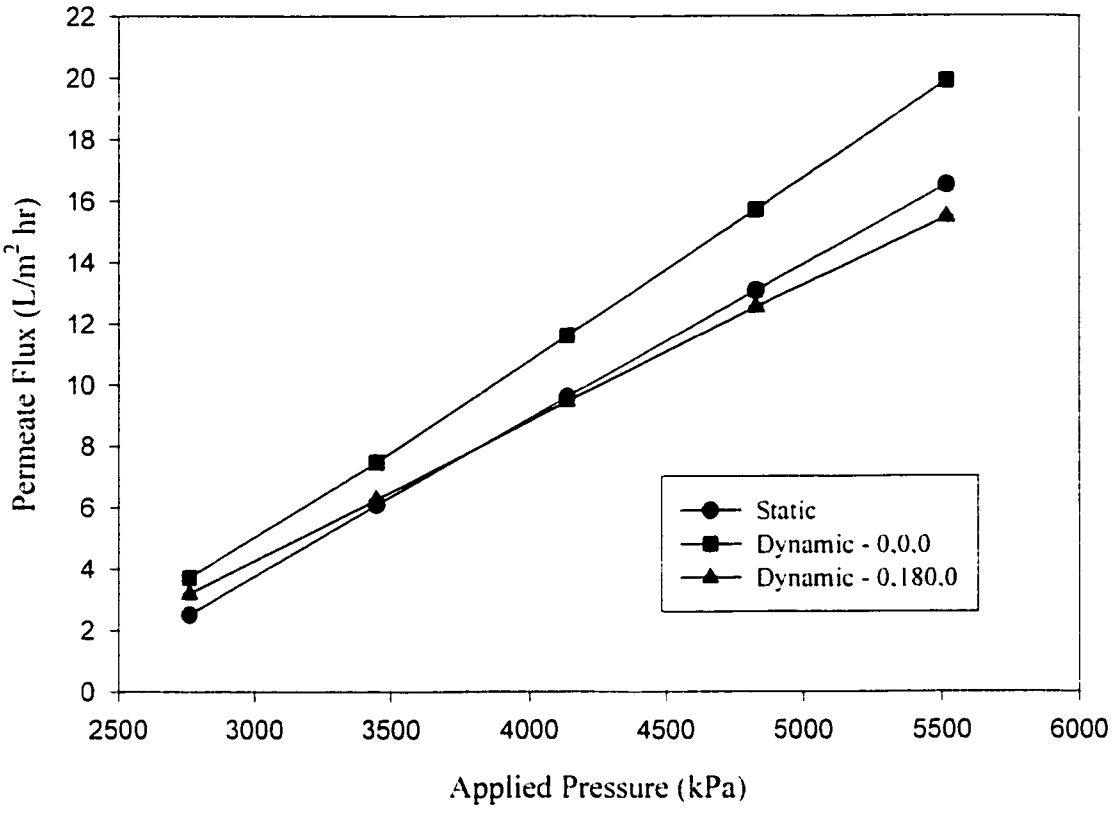

Figure 2.2 0.r.0 orientation concentration polarization experiment (35000 ppm NaCl)

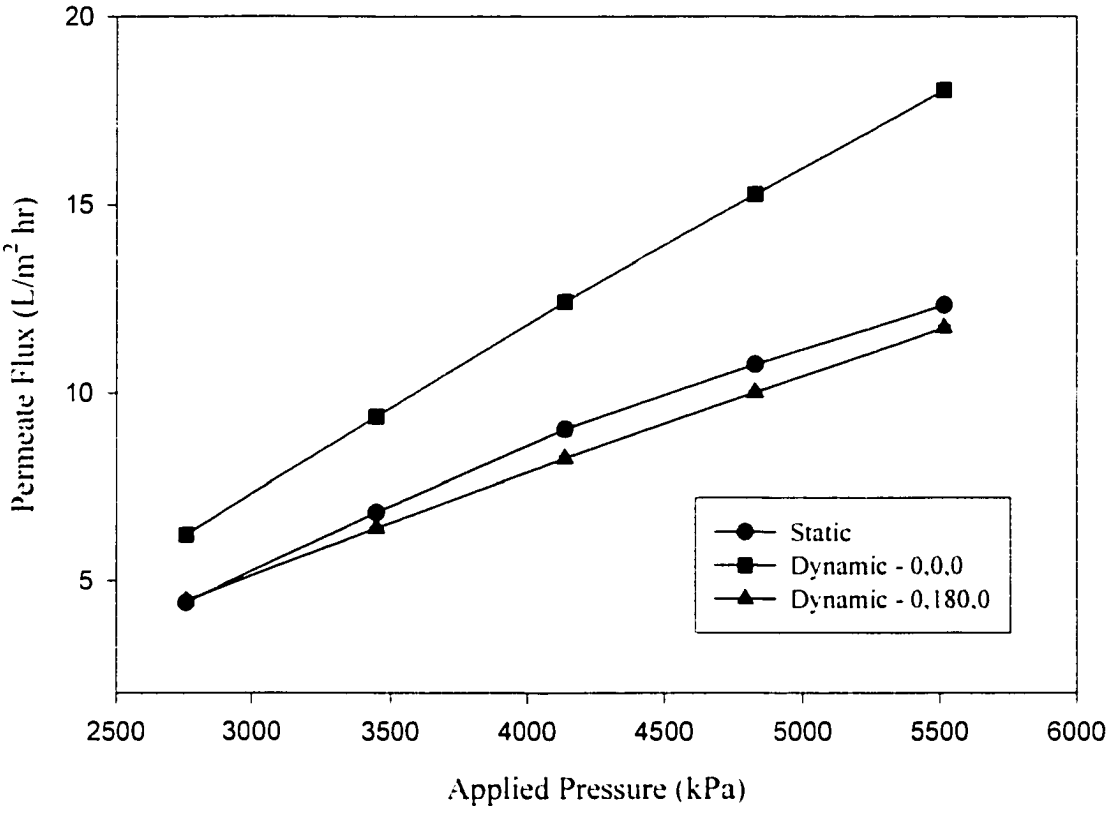

Figure 2.3 0,r,0 orientation concentration polarization experiment (70000 ppm $MgSO_4$)

2.3.2 Orientation – 90,r,y

The concentration polarization experiments conducted here involve the second fixed head (90,r,y orientation). They show that there was a greater increase in flux enhancement with higher pressures and higher feed concentrations. Typical results for the 90,90,0 and 90,180,0 orientations are shown in Figures 2.4 and 2.5, respectively. According to the relative flux analysis (β values) shown in Table 2.3, the 90,180,0 orientation appeared to perform the best when compared to the other results for NaCl of similar concentrations.

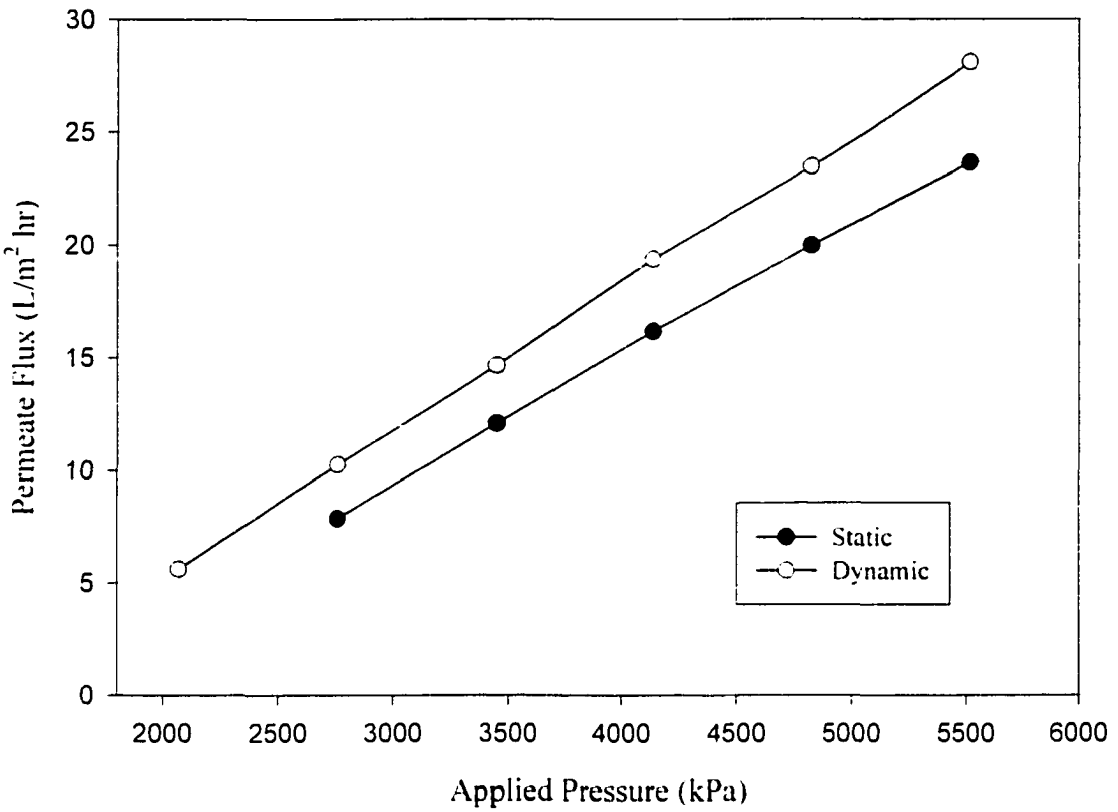

Figure 2.4 90,90,0 orientation concentration polarization experiment (22500 ppm NaCl)

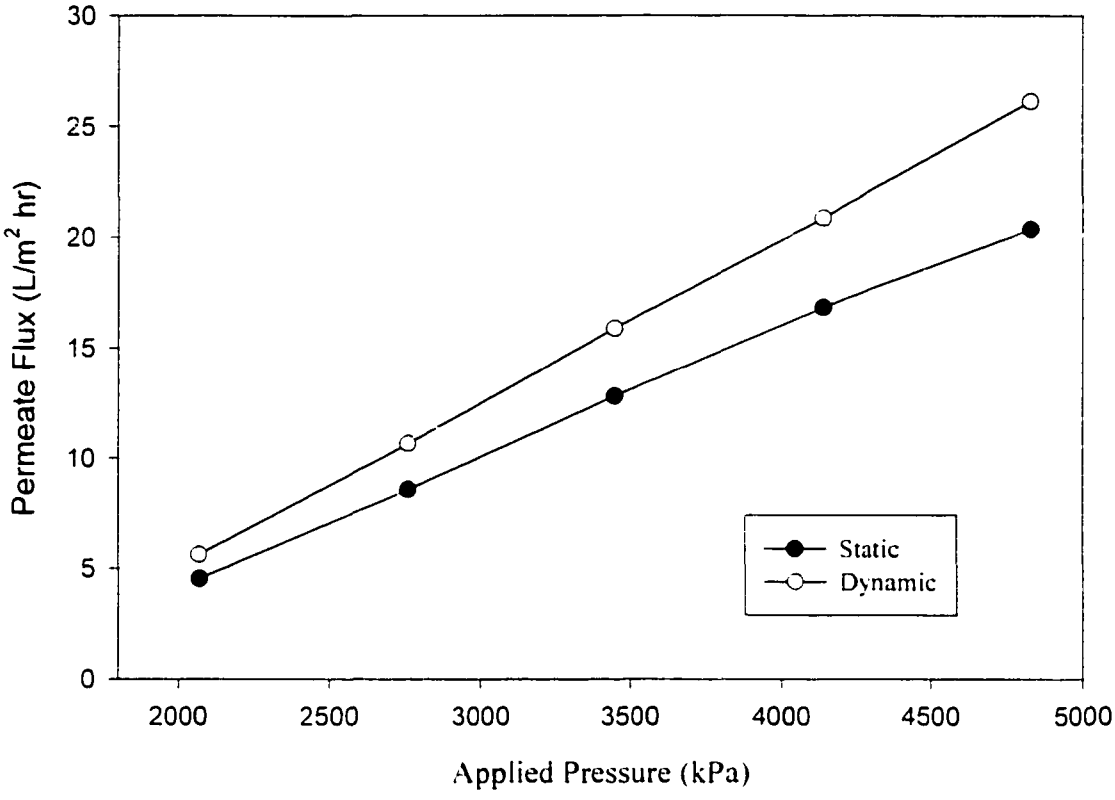

Figure 2.5 90,180,0 orientation concentration polarization experiment (22500 ppm NaCl)

Direction of flow relative to the orientation of the membrane and direction of rotation in the dynamic apparatus is depicted in Figure 2.6. This figure shows the three orientations that gave significant improvement in flux, relative to the static case. These figures visualize what is happening at the membrane's surface. The summary in Table 2.3 indicates that the increasing improvement in flux enhancement for these three orientations, were obtained with the 0,0,0, 90,90,0 and then 90,180,0 orientations, respectively. Computational fluid dynamic (CFD) models predict that orientations with Coriolis acceleration occurring along the length of the membrane's flow channel (*i.e.* 90,r,y orientations) offer enhanced permeate production [29]. The 0,r,y orientations have

the Coriolis acceleration directed away from the surface of the membrane. Additionally, in the case of the 0.r.y orientations, density effects are playing a more significant role in any flux enhancement relative to the static case.

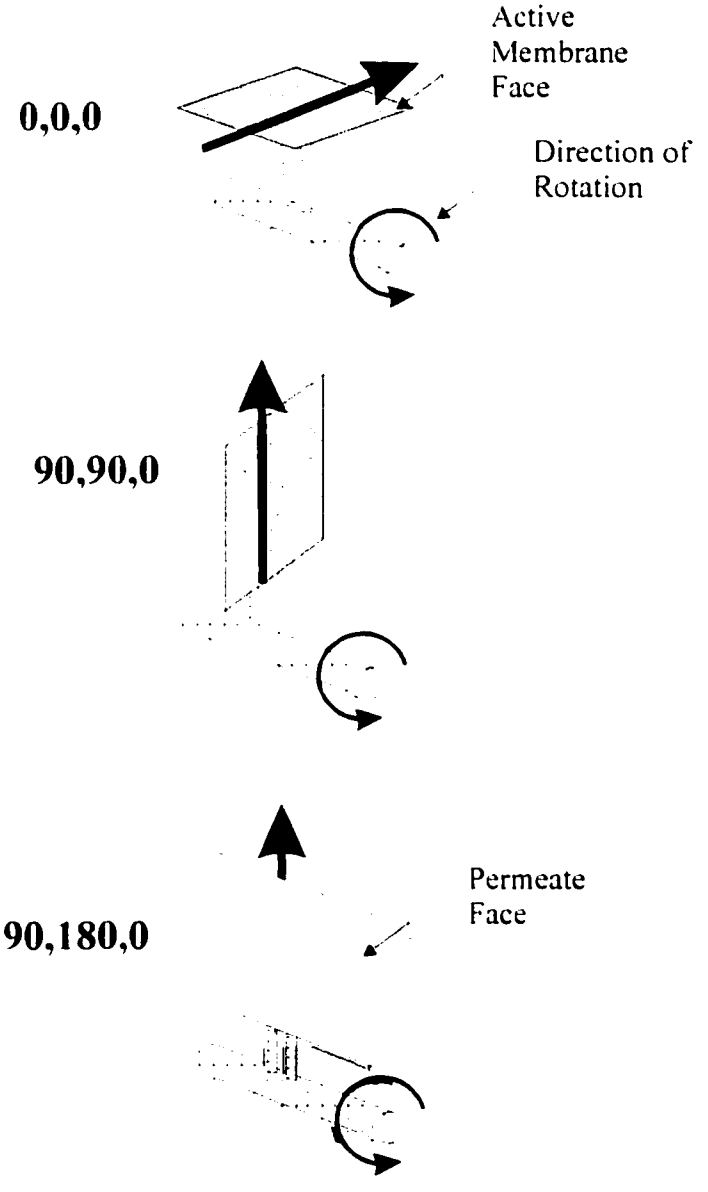

Figure 2.6 Membrane module orientation and flow direction

These CFD models also help to predict what is happening along the surface of the membrane, which gives a better understanding of why a given orientation works better than another does. Figure 2.7, which shows how the concentration of NaCl at the surface

is distributed along the length of the membrane, is a useful theoretical summary of some of the experiments described above [30]. Unfortunately, data for the 90,180,0 orientation was not available at the time of the writing of this dissertation.

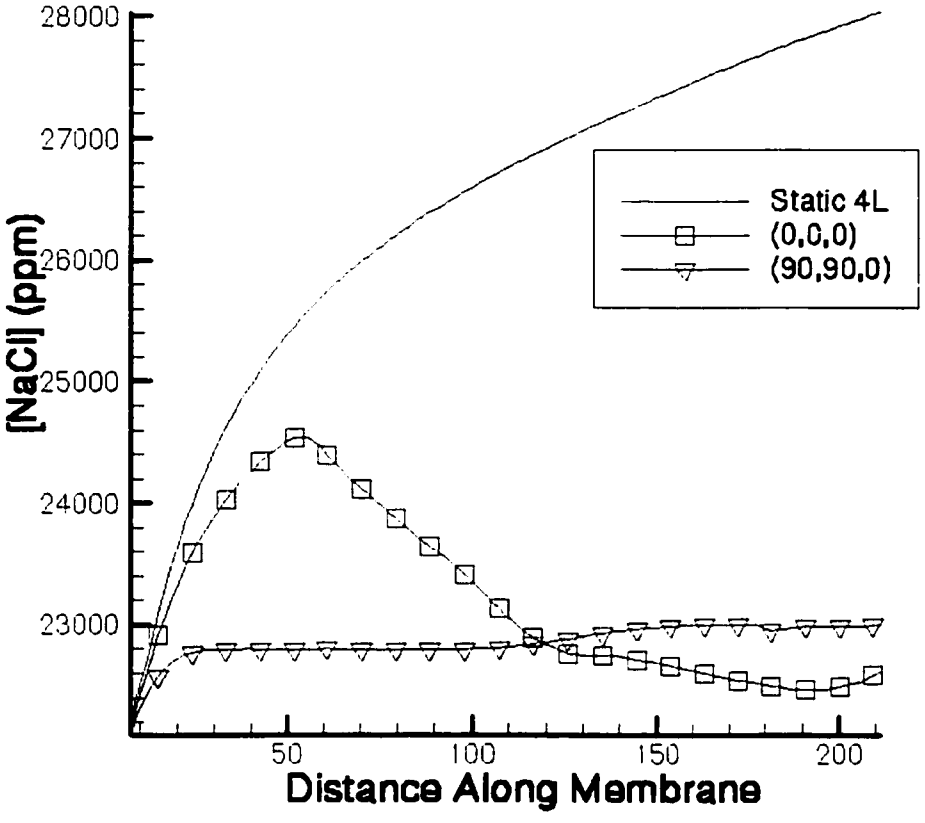

Figure 2.7 Averaged surface mass fraction along the flow channel for various orientations [30]

One can see from this figure how the 90,90,0 orientation shows virtually no variation of NaCl concentration from the beginning to the end of the flow channel. This cannot be said for the 0,0,0 orientation where there is an increase in NaCl concentration for the first 25% of the distance along the membrane. This would indicate that the flux in the 0,0,0 case should be less than that encountered in the 90,90,0 case for 22500 ppm NaCl due to concentration polarization effects shown in this first 25% of the distance along the membrane. However, this is not the case, according to the β results shown in Table 2.3, where the 0,0,0 and 90,90,0 cases have nearly identical values.

The results for the four orientations examined in the concentration polarization experiments (0.0.0, 0.180.0, 90.90.0 and 90.180.0) are illustrated graphically in Figure 2.8. From this, it was determined that all of the orientations, with the exception of the 0.180.0 one, showed an improvement in flux relative to the static case. It can be concluded that the 90.180.0 orientation shows the largest relative flux enhancement. It was also determined that there was a difference in flux relative to the static case when comparing NaCl and $MgSO_4$ solutions at a given orientation. This was due in part to the density differences between solutions. For example, at 0.35M, the density of NaCl is 1.01 kg/L and for $MgSO_4$ it is 1.04 kg/L [31]. The density difference is a significant consideration when related to the centrifugal forces developed at the high rotational speeds of the centrifuge. The difference is also a function of osmotic pressure, as $MgSO_4$ has a lower osmotic pressure than NaCl. In this case, the flux is greater because of the lower osmotic pressure creates the higher applied pressure (ΔP-$\Delta \Pi$) necessary to drive the process. However, the osmotic pressure is only a factor when comparing the results using different electrolytes.

Aside from showing the greatest relative flux, the 90.180.y orientation is also interesting because it is this orientation that gives both maximum and minimum Coriolis acceleration, depending on the yaw angle used. An analysis using four different yaw angles and 22500 ppm NaCl yielded interesting results [19]. Graphically (Figure 2.9), it does not seem to be a very significant result, however, in performing the relative flux analysis (as given in Table 2.3) there is a significant difference between the two minimum and the two maximum Coriolis cases (approximately 10%). This is important, as it will become useful later in describing how Coriolis forces may be utilized in the reduction of particulate fouling in the dynamic apparatus.

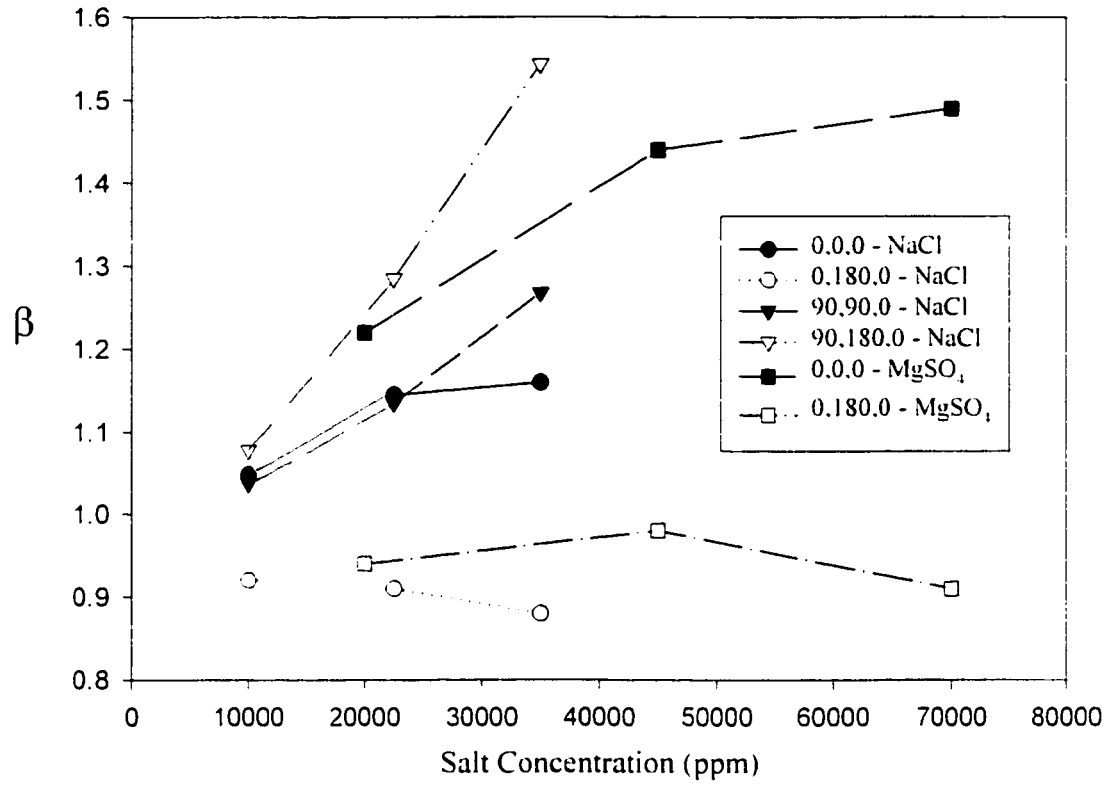

Figure 2.8 Relative flux results for concentration polarization experiments

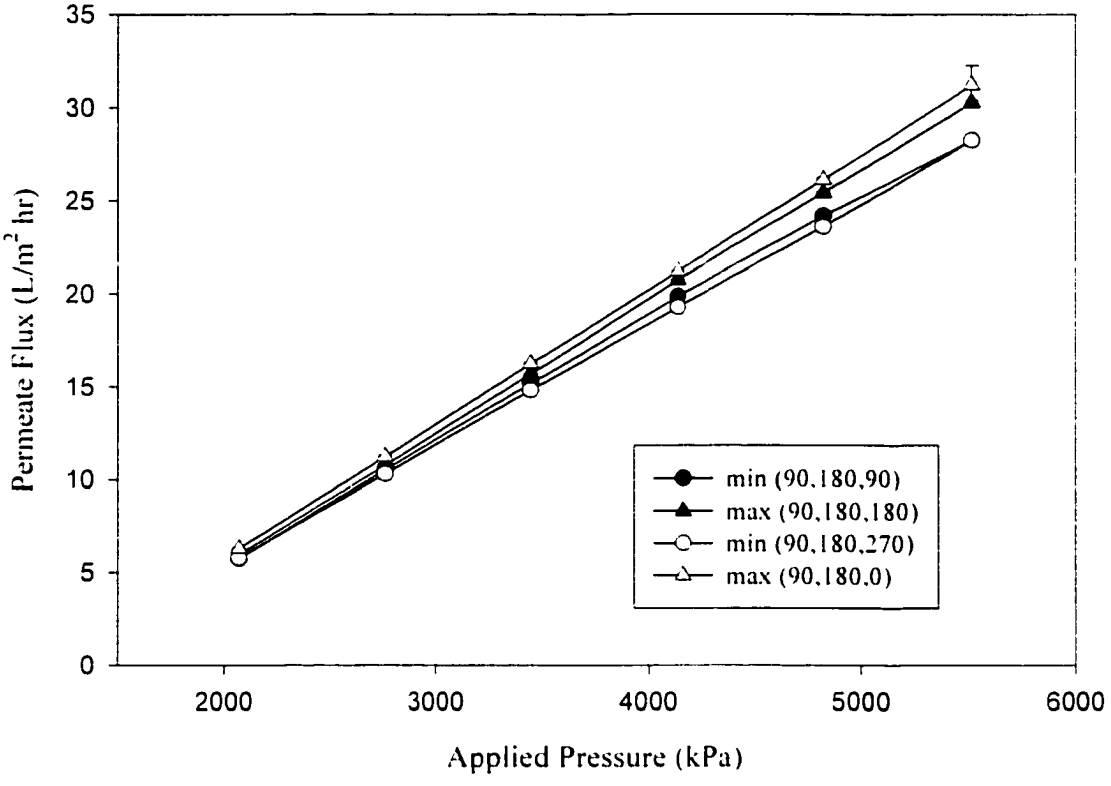

Figure 2.9 90,180,y orientation effect of Coriolis forces experiment

Electrolyte Solution	Feed Concentration (ppm)	Membrane Module Orientation (p,r,y)	Mean % Rejection	β
NaCl	10000	0,0,0	97.2	1.05
NaCl	22500	0,0,0	97.2	1.15
NaCl	35000	0,0,0	96.8	1.16
NaCl	10000	0,180,0	95.2	0.92
NaCl	22500	0,180,0	95.5	0.91
NaCl	35000	0,180,0	97.0	0.88
$MgSO_4$	20000	0,0,0	98.3	1.22
$MgSO_4$	45000	0,0,0	98.6	1.44
$MgSO_4$	70000	0,0,0	99.0	1.49
$MgSO_4$	20000	0,180,0	97.2	0.94
$MgSO_4$	45000	0,180,0	97.5	0.98
$MgSO_4$	70000	0,180,0	97.6	0.91
NaCl	10000	90,90,0	96.2	1.04
NaCl	22500	90,90,0	95.8	1.14
NaCl	35000	90,90,0	96.3	1.27
NaCl	10000	90,180,0	98.2	1.08
NaCl	22500	90,180,0	98.5	1.29
NaCl	35000	90,180,0	98.6	1.54
NaCl	22500	90,180,0	99.1	1.25
NaCl	22500	90,180,90	99.2	1.12
NaCl	22500	90,180,180	99.0	1.22
NaCl	22500	90,180,270	98.7	1.12

Table 2.3 Relative flux values

All of the trends discussed above will again be scrutinized in the following chapter on fouling. Though concentration polarization is a subset of fouling, its mechanisms are different from those of the type of fouling to be discussed next. Thus, the information gained in this chapter will have to be utilized cautiously. Direct comparison between the fouling involving electrolyte solutions (dissolved solids), and that involving colloidal and macromolecular foulants (suspended solids) is not completely valid. However, information gained about the effect Coriolis force has upon flux enhancement will prove to be useful in the fouling analysis.

3 Fouling

3.1 Introduction

Colloids, one of the foulants identified in Chapter 1, are a stabilized dispersion of particles in a continuous medium [32]. There are several types of these systems, and can include aerosols (fog or smoke), foams (fire extinguisher foam), emulsions (milk), and sols (silica particles in water), to name but a few. Colloids are considered to be one of the principal causes of membrane fouling [33]. They have the ability to foul both reverse osmosis (RO) and nanofiltration (NF) membranes, though the mechanisms for the fouling of these membranes are poorly understood [34]. The research presented in this chapter will show how fouling is minimized and flux enhanced by the CMDS process, and will qualitatively examine colloidal fouling mechanisms. The particular feed solutions utilized in the experiments include humic acid and silica. In addition, fouling of NF membranes with whey feed solutions will also be examined in this chapter. The use of NF membranes in fouling experiments will help to illustrate how flux enhancement in the CMDS process is not limited to the diffusive transport of reverse osmosis membranes.

As discussed in the previous chapter (Subsection 1.1.2), fouling reduction is often accomplished through feed solution or membrane modification. This is often done in an effort to create the favourable particle-membrane interactions. Though the research in this dissertation is concerned with a process, rather than with solution or membrane modifications, it is still useful to take a brief look at these particle-membrane interactions. Surface properties for colloids dictate the manner in which they foul. These may create an environment were the particles are attracted to each other, to the surface of a membrane, or to retained particles on the membrane surface. These interactions are controlled by solution chemistry, and by the chemical characteristics of colloids and membrane [34]. In the research associated with this dissertation, each particular feed solution has different chemical properties, and the specific effects of these will be discussed further in the subsequent sections for each feed solution. These surface interaction factors can be considered when examining potential flux enhancement using the CMDS process. If the interactions are significant, the Coriolis and centrifugal forces

working to reduce the fouling in the process will have to be large enough to overcome them.

Colloidal fouling on the membrane surface can either occur by the adsorption or pore blockage mechanisms. Once on the surface, the particles undergo one of several fates: (1) they can become part of a well structured cake-like layer; (2) given sufficient shear force, they can flow tangentially across the surface of the membrane; or (3) they can continue through the membrane provided they are small enough or relatively immune to the adsorption process [35]. It is the combination of the nature of the cake formation, and the shear forces that will dictate how the CMDS process reduces fouling and enhances flux in colloidal environments.

3.2 Humic Acid Fouling

3.2.1 Introduction

Humic substances are the result of chemical and biological degradation of plants and animal residues, and the synthesis activities of microorganisms [36]. Along with fulvic acids, they represent the major fraction of dissolved organic matter in aquatic environments [39]. These substances are also important constituents of the organic colloidal phase and are one of the major fouling agents during filtration of surface waters in reverse osmosis [40]. They also affect water quality by creating an undesirable brownish colour.

Humic acid consists of a mixture of complex macromolecules with carboxylic and phenolic structures attached. It is the presence of these functional groups that creates an overall negative charge for the molecules. For humic acid molecules, the molecular weight ranges from 300 to 10000 g/mol [3]. An example of a molecular structure for humic acid is illustrated in Figure 3.1.

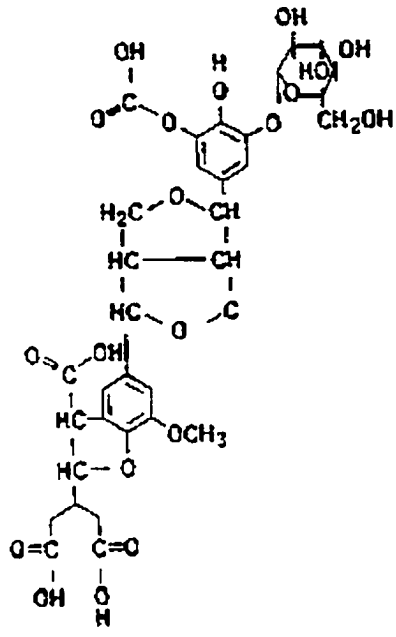

Figure 3.1 Example of humic acid molecular structure

Humic acid fouling on the surface of a membrane is dictated by two primary considerations. First, adsorption on the surface is greater when there is significant surface roughness, and second, at lower pH and/or higher ionic strength the humic acid is more strongly adsorbed on the surface [41]. For the latter consideration, there is a trade-off with respect to its ability to remain a colloidal solution; at low pH humic acid solutions tend to precipitate. As the fouling study for this dissertation involves colloids, higher pH is a requirement. For the purposes of this research, membrane porosity is not examined, as it is the process, and not the membrane material, which is the focus.

3.2.2 Experimental Work

3.2.2.1 Preliminary Experiments

Prior to the fouling study of the humic acid and the CMDS process, feed solutions were characterized to determine chemical and physical properties. The humic acid used for the feed solutions was a technical grade of humic acid, sodium salt from the Aldrich

Chemical Company. It is made up of small, dark brown flakes and has a measured molecular weight of 2300 g/mol [42].

The effect of pH was first examined to determine which range would be suitable for the humic acid feed solutions. In other experiments conducted using humic acid, a pH of 11 was deemed to be suitable [43]. For this determination, 15 mL of three concentrations of humic acid (85, 500 and 3000 mg/L, in distilled water) were placed in four 25 mL test tubes each, and their respective pHs were altered in three of the test tubes using either 0.5M NaOH or HCl. The pH of the unaltered humic acid solutions was found to be 9.5, while the altered solutions pH values ranged from 1.0 to 13.5. After a 24-hour period, no noticeable changes were visible: the solutions were a uniform, cloudy, dark brown. To the samples with a pH of 1.0, an additional few mLs of 0.5 M HCl was added to the test tubes. After a 2-hour period, it was noted that the acidified solutions were clear and a brown precipitate had formed on the bottom of the test tubes. From this analysis, it was determined that the humic acid solutions were stable to a wide pH range, but to ensure stability, subsequent feed solutions for fouling experiments were altered to a pH of 10 or 11.

The effect of ionic strength on humic acid colloid stability was also examined in these preliminary experiments. In this experiment, humic acid solutions were made up in NaCl solutions, rather than in distilled water. Solutions of 300 mg/L humic acid were made using 10000, 22000 and 35000 ppm NaCl solutions. After a 24-hour period, no changes in the solutions were noted. From this it was assumed that feed solutions could be made in 10000 ppm NaCl for future fouling experiments, with no risk to colloid stability.

Another important characterization was that of particle size distribution, which was established using dynamic light scattering (Nicomp Submicron Particle Sizer – Model 370). This was critical in determining whether or not the feed solution has particles that are in the colloidal range (1nm to 1000 nm). This technique was also useful in determining what level of pre-filtration was necessary to obtain a solution in the right particle size range. It was decided that a concentrated solution of humic acid could be

prepared that had a mean particle diameter of less than 400 nm. Once prepared, the concentrated solution could be diluted in a 10000 ppm NaCl solution, and used as a feed for the membrane fouling experiments. Several types of pre-filtration were examined, but from a cost and time point of view, a two-stage gravity filtration was chosen to prepare the humic acid concentrate. The effectiveness of the filtration on 3000 mg/L humic acid solutions is summarized in Table 3.1.

Filtration Method	Mean Particle Diameter (nm)	99% of Distribution Less Than
none	775	2841 nm
#1 Whatman	242	826 nm
#1 followed by #42 Whatman[2]	189	645 nm
Millipore 5 μm Teflon	262	839 nm
Millipore 0.45 μm	186	678 nm

Table 3.1 Filtration effectiveness and particle size

Finally, total organic carbon (TOC) analysis were done to both determine the concentration, and to act as a form of quality control to ensure each concentrated humic acid solution was being made in a similar manner. These analyses were done outside of the University of Victoria by Norwest Labs of Surrey, British Columbia. In each case, a 100 mL sample of the humic acid concentrate was sent for analysis.

3.2.2.2 Procedure For Fouling Experiments

Once the characterization of the humic acid had been completed, the preparation of the feed solution could be undertaken. A concentrated solution of humic acid was prepared by mixing the Aldrich humic acid with distilled water. This solution was then filtered consecutively through #1 and #42 Whatman filter paper. The filtered solution was then diluted 10 fold with a 10000 ppm NaCl solution (made with distilled water). The salt solution was added to the humic acid in order to provide a means of identifying the quality of the permeate in both the static and the CMDS apparatus, which was done by measuring the conductivity of the permeate. If the NaCl is rejected at values greater than

[2] chosen method of filtration

95%, then the larger humic acid particles are likewise being rejected at or above 95%. This type of relationship is especially important in the CMDS apparatus where the permeate is not captured for visual inspection. Therefore the use of the FRACT as a means of not only measuring permeate flow rate, but also conductivity, becomes important. As mentioned in the previous section, this small addition of NaCl to the humic acid shows no effect and its concentration is thought to remain homogenous throughout the humic acid feed solution. For this reason, it is a good indicator of permeate quality. The pH of the resulting solution was checked, and if it was found to be below 10, it was raised by the addition of 0.5 M NaOH. Once prepared, the humic acid feed solution had a dark amber colour.

In the fouling experiments, the feed solution was first used on a set of membrane modules in the static apparatus, and then later in the CMDS apparatus. The experimental conditions used in all of these experiments include an applied pressure of 4100 kPa, a feed recirculation rate of 2L/min and a temperature of 25 °C. In all of the experiments, a 10000 ppm NaCl solution was circulated through the membrane modules for the first 70-80 minutes to provide data for the normalization of the humic acid flux results. This was followed by an approximately 5-hour period of humic acid feed solution circulation through the membrane modules to observe the flux decline due to fouling. In the static apparatus, the flow rate was measured (by the same method described in the previous chapter) more frequently in the first 90 minutes of the humic acid feed solution addition. This was done because of the rapid decay of the flux over time (for example, refer to Figure 3.3), where it was important to better define this initial rapid flux decline. Upon completion of some runs, all of the membrane modules were removed and rinsed with jets of distilled water in order to remove any humic acid particles from the surface. In other cases, a membrane module was removed for later analysis, and the rest were rinsed with the distilled water. Once rinsed, the membrane modules were re-stacked in the membrane holder and were ready for the next fouling experiment. The membrane modules used in the humic acid fouling experiments were made of the same reverse osmosis membrane material (Osmonics DS-3™) described in Table 2.1.

3.2.3 Results

Fouling analysis using the CMDS apparatus for humic acid solutions was conducted using the head with the fixed pitch angle of 90°. A summary of the humic acid fouling experiments is given in Table 3.2, which includes feed concentration and membrane module orientation.

Experiment #	Membrane Module Orientation	Humic Acid Concentration (mg/L)	TOC (mg/L)	Mean Particle Diameter (nm)
1	90,r,0 (r = 90 & 270)	300	78	189
2	90,r,0 (r = 90 & 270)	300	81	80
3	90,r,y (r = 90 & 270, y = 0 & 90)	800	140	390
4	90,180,y (y = 0 & 90)	300	79	242
5	90,180,y (y = 0 & 90)	300	73	162

Table 3.2 Humic acid fouling experimental conditions

3.2.3.1 Roll 90/270 Results

Each of the three experiments consists of three parts: (1) static; (2) 90,90,0 – dynamic; and (3) 90,270,0 – dynamic (Experiment #3 also contains 90,270,90 – dynamic orientation). Figure 3.2 illustrates the orientation of the membrane modules for these experiments (dark colour represents active surface of membrane module). Each of these experiments was conducted on consecutive days, using the same feed solution. In the static experiment, the permeate was returned to the feed tank after measurement, and in the dynamic experiments, the feed solution was replenished with an appropriate amount of 10000 ppm NaCl solution every hour.

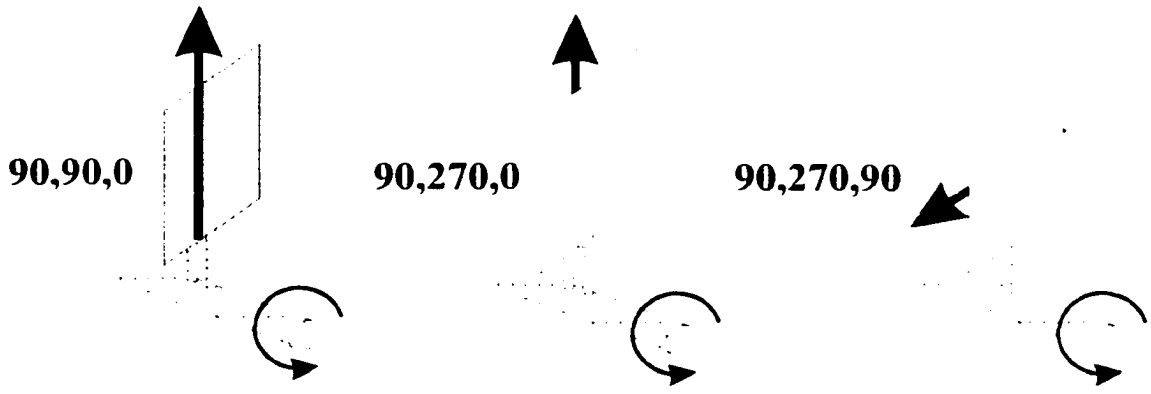

Figure 3.2 Membrane module orientation and feed flow direction (90,90/270,y)

The results from each experiment were collected and graphs of the relative flux over time were produced (Figures 3.3 to 3.5). Elapsed time is given relative to the point where the humic acid feed was started. The relative flux was determined by dividing the observed flux by the mean flux for the initial part of each experiment; *i.e.* the part where only the 10000 ppm NaCl solution was initially passed through the membranes (elapsed times prior to 0 minutes). It is also worth making a comment about the "noise" displayed in the dynamic process data in these three curves. The nature of the plotting software tends to magnify the flow meter data from the FRACT. Rather than smooth the data out by filtering, it was decided that all data points should be used (800 – 1000 points).

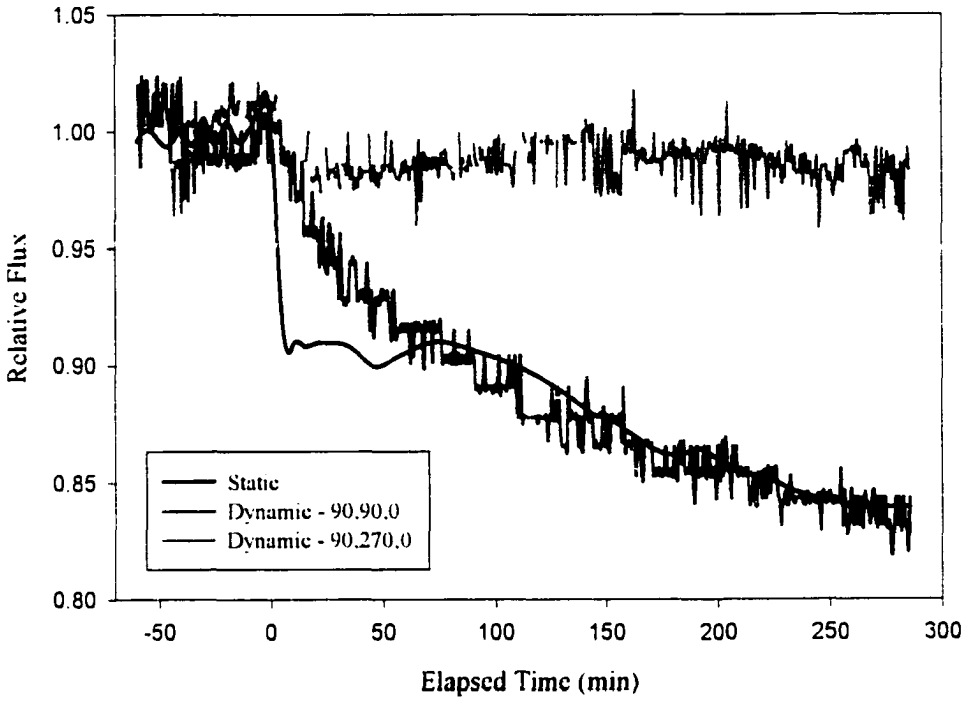

Figure 3.3 Humic acid experiment #1

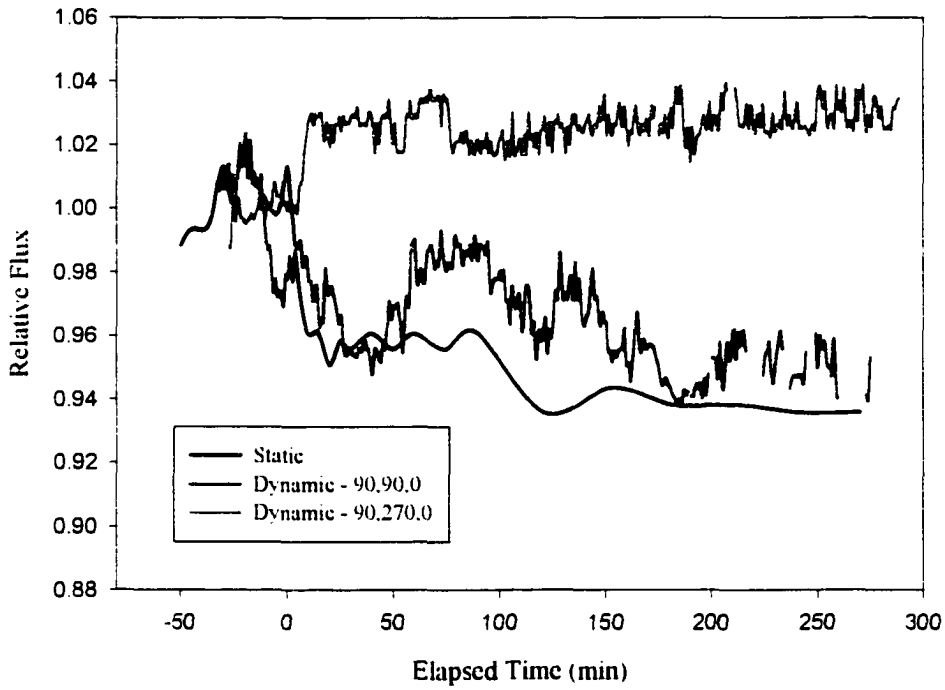

Figure 3.4 Humic acid experiment #2

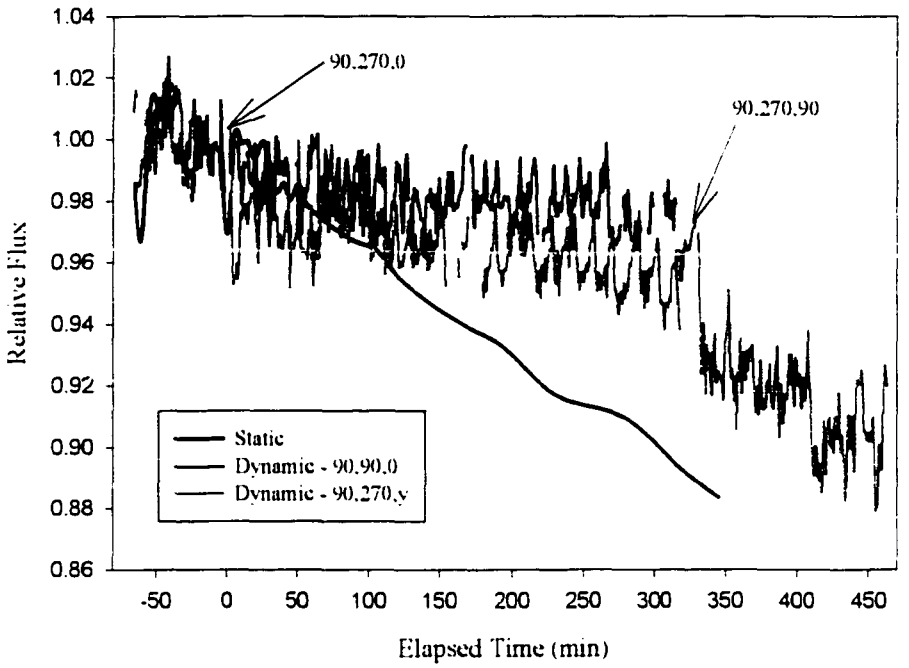

Figure 3.5 Humic acid experiment #3

From these graphs it is apparent that the CMDS process is capable of influencing the flux decline associated with the humic acid fouling of the membrane surface. However, it is necessary to quantify the benefit obtained by using this process. This was achieved by conducting a linear regression analysis of specific portions of the graph. The initial flux decline portion of the graphs (if present) was ignored in this analysis. Instead, the longer-term effect of fouling with respect to the static and dynamic processes was examined. Two trends are noted in the graphs: (1) the static case often has a steeper slope relative to the CMDS process; and (2) in cases where the CMDS process slope is similar or steeper than the static case, the flux offset is still greater. Both of these trends can be quantified by use of the linear regression data obtained from the selected portions of the graphs. These results are determined using the linear regression tool in SigmaPlot 5.0™ [28].

Consider the hypothetical relative flux over time curve illustrated in Figure 3.6. The relative slope factor, α, and the relative offset factor, κ, are defined by the following relationships (using the static and dynamic – orientation 1 cases from Figure 3.6):

$$\alpha = \frac{Slope\_1}{Slope\_s} \tag{3.1}$$

$$\kappa = \text{Offset Value 1} - \text{Offset Value s} \tag{3.2}$$

With this type of analysis a good result would be described as one where α is less than one and κ is positive. With respect to α, a value less than one indicates that the flux for the dynamic case is not decaying as fast as that for the static case, and thus the smaller the value, the better. As for κ, a positive value indicates that the relative flux for the dynamic case is greater than that for the static case, indicating that more permeate is passing through the membrane. The results for these analyses are summarized in Table 3.3.

For this particular analysis, the term "middle" refers to a 120-minute period selected from the middle of the graphs, and "final" refers to the final 90 minutes of the elapsed time on the graph. An exception to the latter occurs in experiment #3 where the "final" section applies for both the 90,270,0 and the 90,270,90 cases (see Figure 3.5). In this particular experiment, the yaw angle was changed to see if any effect could be observed.

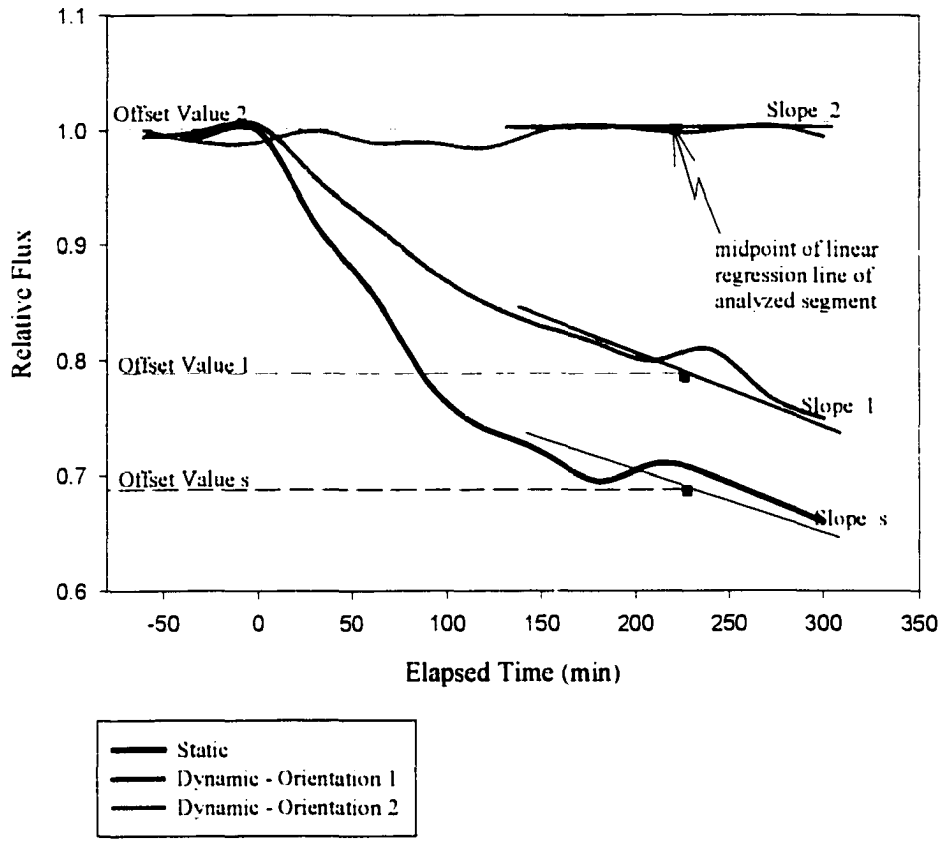

Figure 3.6 Hypothetical fouling curve with quantification nomenclature

Orientation & Experiment #		α_{middle}	α_{final}	κ_{middle}	κ_{final}
Static	1	1.0	0.00	0.00	1.0
	2	1.0	0.00	0.00	1.0
	3	1.0	0.00	0.00	1.0
90,90,0	1	1.1	-0.01	-0.01	1.1
	2	1.5	0.02	0.02	2.4
	3	0.07	0.04	0.07	0.26
90,270,0	1	0.03	0.10	0.14	0.39
	2	0.02	0.08	0.09	0.81
	3	0.12	0.02	0.05	0.44
90,270,90	3	N/A	N/A	0.04	0.70

Table 3.3 α and κ values for roll 90/270 orientations

This analysis showed that the 90,270,0 orientation provided significant flux enhancement relative to the static case. In this case, the value of α was always less than one, thus indicating that the rate of flux decline was less than the corresponding static case. In some cases, a flux decline does not really exist at all for the orientation. In addition to this, the 90,270,0 orientation always had a positive κ value, indicating that a higher absolute flux was occurring in this orientation relative to the static case.

3.2.3.2 Roll 180 Results

For this set of experiments, the orientations (see Figure 3.7) were chosen to see the effect of Coriolis forces upon the reduction of flux decline due to humic acid fouling. As mentioned in Section 2.3.2 of the previous chapter, the 90,180,0 orientation yields maximum Coriolis forces, while the 90,180,90 orientation gives the minimum Coriolis forces in the CMDS apparatus. The experiments for this section were conducted in the same manner as for those mentioned in the previous section. The particulars for these experiments are given in Table 3.2 of the previous section, where they are denoted as Experiments #4 and #5. For Experiment #4 and #5, the resulting relative flux over time plots are illustrated in Figures 3.8 and 3.9, respectively.

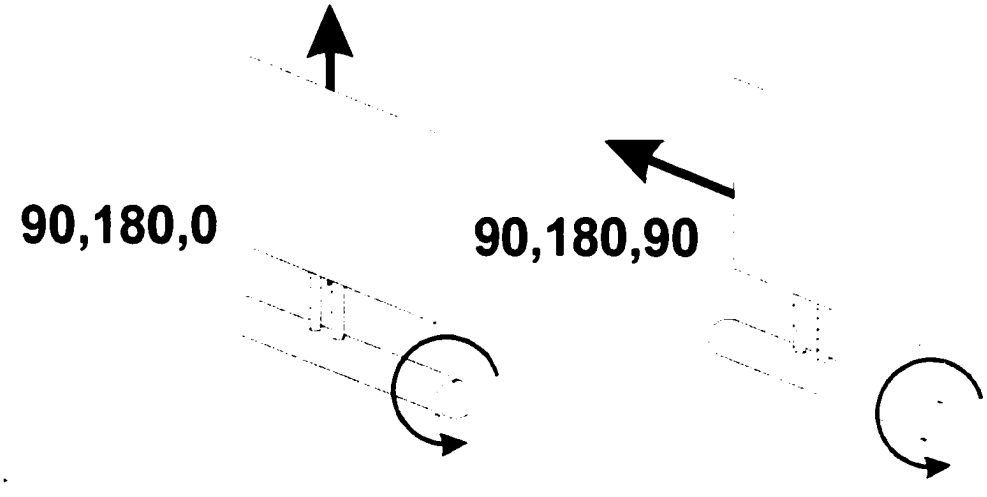

Figure 3.7 Membrane module orientation and feed flow direction (90,180,y)

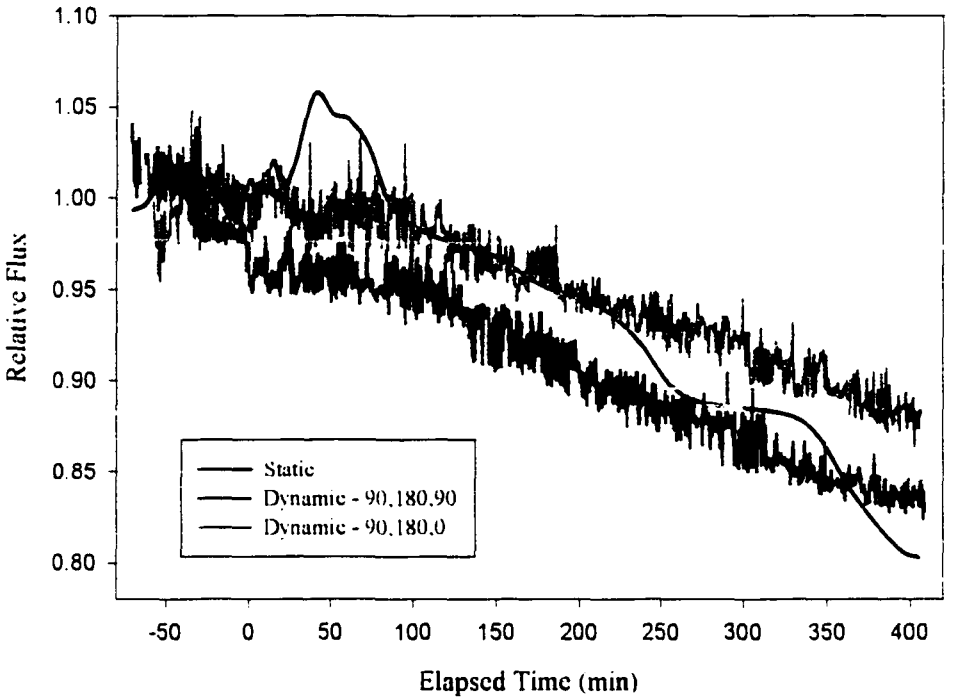

Figure 3.8 Humic acid experiment #4

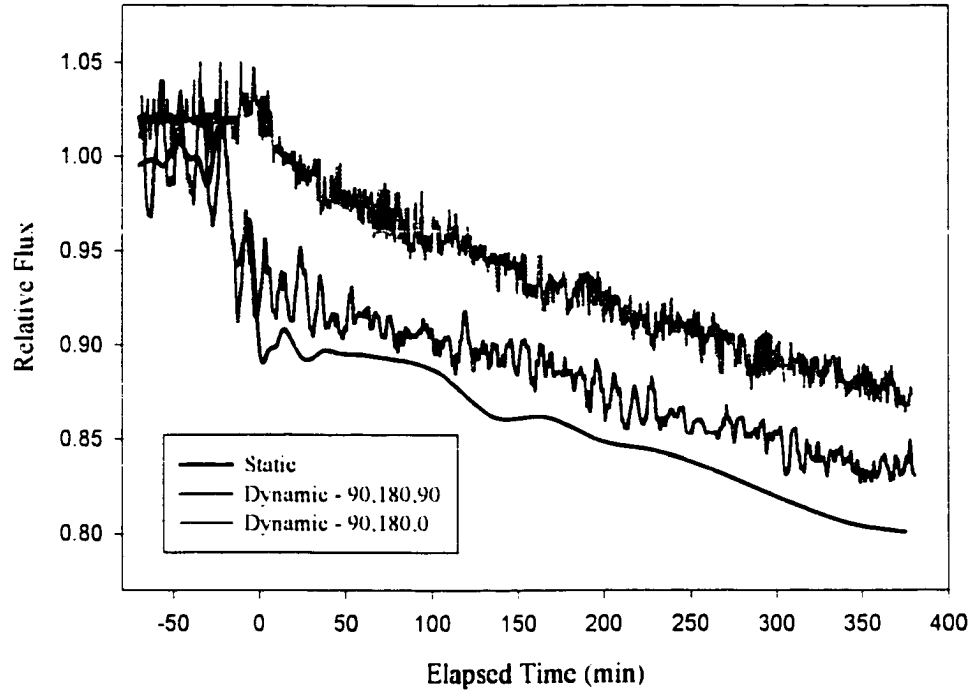

Figure 3.9 Humic acid experiment #5

It is interesting to note how these results differed from those given in the previous subsection (3.2.3.1). There is a noticeable flux decline over time for both the minimum (90,180,90) and maximum (90,180,0) Coriolis orientations. As the flux declines were fairly linear in all cases for both experiments, the α and κ values were determined for nearly the entire fouling experiment (from the 60-minute mark to the end of the run), and they are given in Table 3.4. This slightly different analysis does not allow this subsection's experimental results to be directly compared to the previous subsection's results. However, this is not necessary, as examination of the relative flux over time plots show that the 90,270,0 orientation is the only one that does not show flux decline over time, and is thus the "best" of the orientations examined.

Orientation & Experiment #		α	κ
Static	4	1.0	0.00
	5	1.0	0.00
90,180,0	4	0.61	0.01
	5	1.2	0.07
90,180,90	4	0.69	-0.03
	5	0.97	0.03

Table 3.4 α and κ values for roll 180 orientations

After the 90,180,90 experiments, an interesting phenomena was observed when the membrane stack was taken apart and the modules were removed. A brown deposit of material approximately 3mm thick was found on the flow channel portion of the membrane modules (Figure 3.10). The same material was also found in a build-up at the top of the interior of the membrane head. It appears from this, that the fouling layer is flowing towards the periphery, and this leads to the determination that a density effect is involved in the CMDS process. It indicates that particles are moving across the surface of the membrane and are being deposited at the periphery of the membrane head. This same phenomena was observed for the 90,180,90 orientation in the silica and whey experiments, which will be discussed in the next two sections of this chapter. Further conclusions regarding the effect of density and Coriolis forces will be presented in the final chapter of this dissertation.

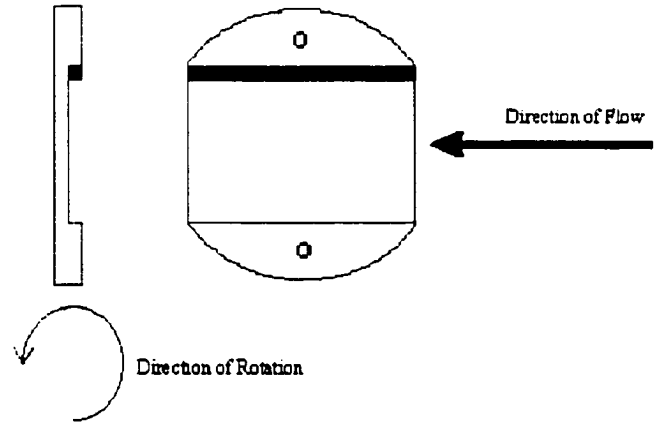

Figure 3.10 Location of deposit on membrane module after 90,180,90 Experiment

3.2.4 Microscopic Analysis of Fouling Layers

In an effort to better understand the mechanism(s) involved in the fouling of a reverse osmosis membrane by a humic acid feed solution, a microscopic analysis was undertaken. This analysis involved the use of scanning electron microscopy (SEM) and its associated energy dispersive x-ray (EDX) detector. The objects of these analyses were to qualitatively examine the surface of the membrane, and to attempt to measure the thickness of the fouling layer.

The SEM was chosen over a light microscope because it has a larger depth of field, which allows a large amount of the sample to be in focus at one time. The SEM also produces images of high resolution, which means that closely spaced features can be examined at a high magnification [44]. This fact will be important for examining surface fouling characteristics on the membrane samples. The energy dispersive x-ray (EDX) attachment on the SEM permits the detection and identification of the x-rays produced by the impact of the electron beam on the sample thereby allowing qualitative and quantitative elemental analysis. The SEM used for these analyses was a Hitachi S-3500N model with an Oxford Instruments ISIS 300 EDX interface, operated by Dr. C Singla of the Department of Biology at the University of Victoria.

3.2.4.1 Experimental Procedure

Sample preparation was done in one of two ways: (1) surface images; and (2) edge images. For the surface images, small squares (~25 mm^2) of membrane material were cut with a scalpel from the humic acid fouled membrane modules. These samples were fixed onto the surface of the aluminum stubs (Figure 3.11) used for mounting SEM samples with double-sided tape. For the edge images, strips (1x10 mm) were cut from the humic acid fouled membrane modules. Aluminum stubs were modified by machining off a portion of the diameter (Figure 3.11). This was necessary because of the way in which the samples have to be mounted in the SEM. The strips were mounted to the sides of the stubs in such a manner so the edge of the strip would be facing the electron beam.

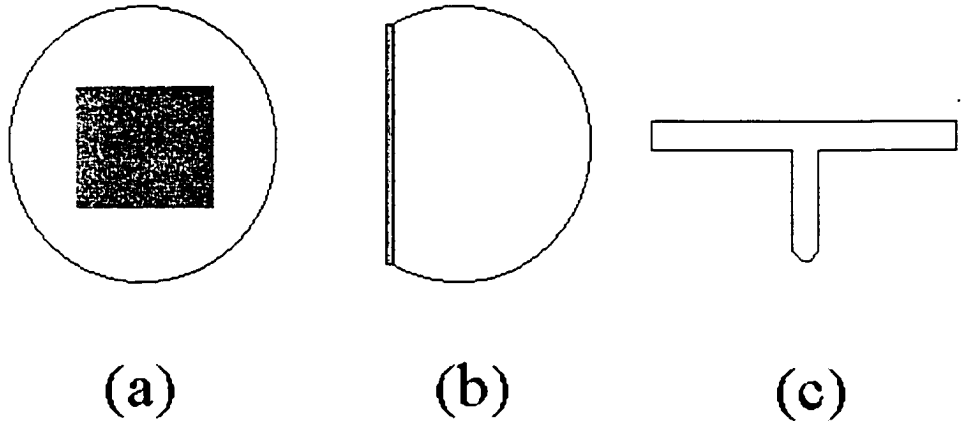

Figure 3.11 **(a)** Sample mounted on aluminum stub for surface image: **(b)** Sample mounted on modified aluminum stub for edge image: and **(c)** Side view of SEM aluminum mounting stub

In both cases, the samples were allowed to dry for approximately 24 hours in a desicator. This was followed by sputter coating the samples with gold. Once the coating process was complete, the samples were ready for viewing with the SEM.

3.2.4.2 SEM and EDX Results

One of the initial aims of the SEM analysis was to look at the surface of the humic acid fouled membranes, and obtain an understanding of how this fouling layer is deposited. Figure 3.12 gives a comparison of membrane fouled in the static process and membrane fouled in the dynamic process, and as a reference, a piece of unused membrane is also shown in this figure. It appears that the static fouled membrane shows a significant build up of a substance that looks like "dried mud", where the dynamic fouled membrane does not show this same level of fouling. The cracks in Figure 3.12(b) are from the dehydration necessary for the gold sputtering process. This image is misleading in that the cracks appear to have depth. This is not the case, as SEM only examines the surface of the image, and this apparent depth is akin to an "electron produced shadow". However, the magnitude of the shadow can be related to the height of the feature, though this cannot really be quantified in these images.

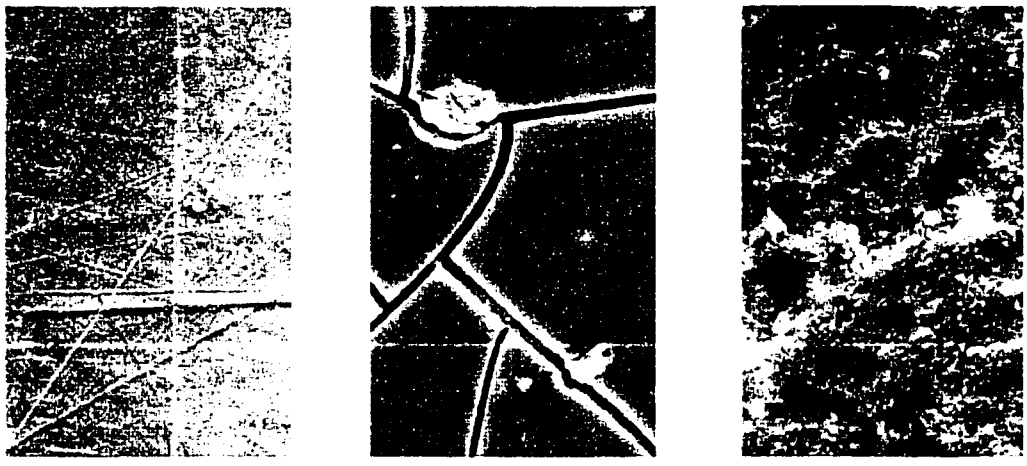

Figure 3.12 Surface electron micrographs (1000x magnification) of: (a) unused membrane; (b) static humic acid fouled membrane; and (c) 90.270.0 orientation dynamic humic acid fouled membrane

This same process was duplicated for humic acid fouled membranes in the roll 180 experiments. Figure 3.13 shows membranes fouled by humic acid in the static process and by the dynamic process in the roll 180 orientations. These images show fouling at approximately the same level for each process and orientation. This is consistent with the information presented in the relative flux over time plots (Figures 3.8 and 3.9). In these plots there appears to be a uniform decline in flux of relatively equal slope, thus indicating a similar level of fouling in each process and orientation. The fouling itself exhibits the same sort of "dried mud" appearance as that illustrated in Figure 3.12(b). It is difficult to ascertain the fouling mechanism at work here because of the fact that only the surface is being examined. It is therefore necessary to examine the cross section of the fouling layer. This is accomplished by using the edge image process described in the previous subsection.

Figure 3.13 Surface electron micrographs (1000x magnification) of: (a) static humic acid fouled membrane; (b) 90,180,90 orientation dynamic humic acid fouled membrane; and (c) 90,180,0 orientation dynamic humic acid fouled membrane

The edge image process was only performed on membrane material from the roll 180 experiments, as the samples used in the roll 90/270 experiments were no longer available at the time of this analysis. As this analysis is used for determining fouling layer thickness and possible deposition mechanisms, the use of membrane material from the roll 90/270 experiments is not considered necessary. Figures 3.14 and 3.15 show how the humic acid fouling layers are built up on the surface of the membrane. It is also interesting to see in Figures 3.14(b) and 3.15 how the membrane becomes compacted upon use, compared to that shown in Figure 3.14(a). The fouling layer appears to be fairly dense in all cases, and indicates an adsorption fouling mechanism is probably taking place. There seems to be an initial adsorption of material followed by a build up with concurrent compaction of the fouling layer. This compaction is supported by the micrographs, where there does not appear to be any stratification of built up layers. In terms of fouling layer thickness, there does not appear to one particular orientation that shows a thicker fouling layer than the others. In general, the layers are not always easy to differentiate, so the fouling layer thickness analysis is not completely definitive.

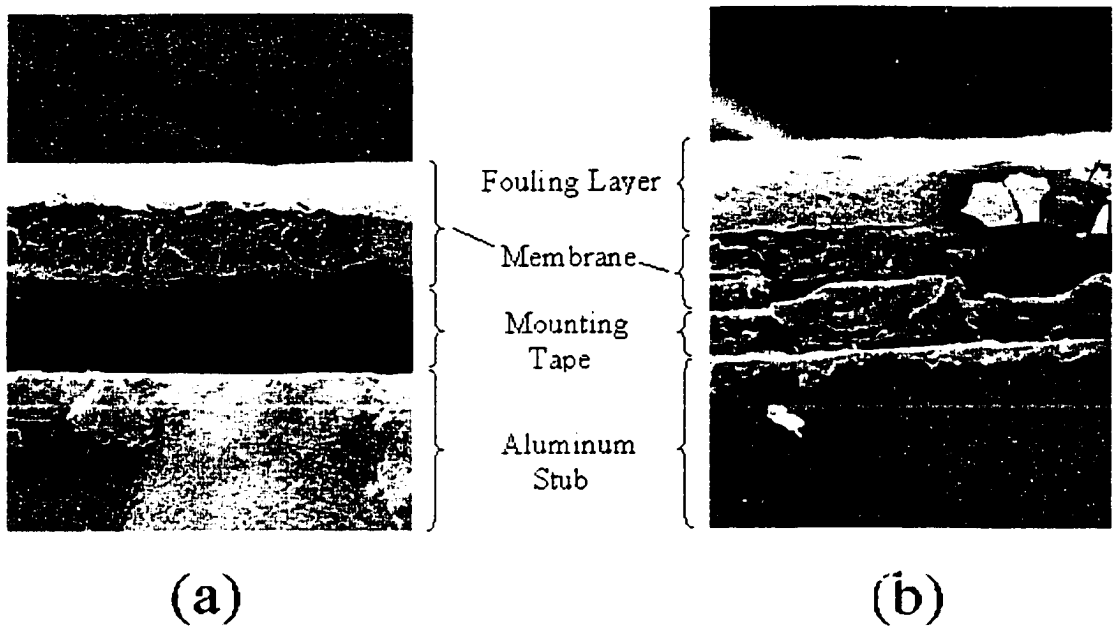

Figure 3.14 Edge electron micrographs (100x magnification) of: (a) unused membrane; and (b) static humic acid fouled membrane

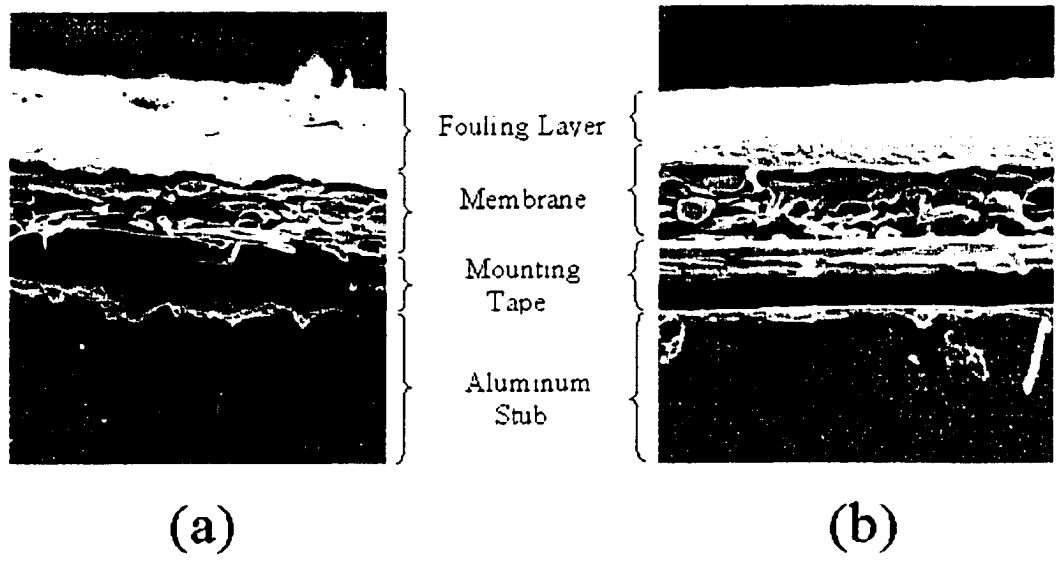

Figure 3.15 Edge electron micrographs (100x magnification) of: (a) 90,180,0 orientation dynamic humic acid fouled membrane; and (b) 90,180,90 orientation dynamic humic acid fouled membrane

Differentiation between the layers was attempted by using the energy dispersive x-ray (EDX) detector on the SEM. The combination of the imaging of the SEM and the elemental analysis capabilities of the EDX creates a means of conducting this differentiation. One of the advantages of this method was the fact that there was no need for sample preparation, as the SEM samples discussed above could be used for this study. The technique involves focusing on a particular part of the sample, capturing the image, and then scanning for emission from one or more elements. In the output file for the scan, the quantities of each element selected are relative to each other, and not absolute. For example, if only sodium and potassium are chosen, each of their quantities will add up to 100%, even though other elements may be present in greater amounts. The EDX can scan and determine which elements are prevalent, however, it was determined that specified elements would be scanned for all of the samples. The elements selected for the analysis were sulfur and silica, as it was thought that they would be present in different quantities for the foulant and for the membrane.

It was thought that a "pin point" analysis could be performed based on the type of images given by the SEMs (Figures 3.14 and 3.15, for example). However, once the image was captured onto the EDX interface, the image became very unfocussed. For this reason, the EDX analysis was only capable of giving trends in the various samples. The first scan involved the analysis of an unused piece of membrane, for reference. Looking at Figure 3.14(a), one can see that the membrane has two distinct layers; a polymer film and a porous support below. The EDX scan showed that in going from the polymer film to the porous support, the relative ratio of S:Si increased from 65:35 to >99:1. The next step was to examine the humic acid fouled membranes. The first scans were of the surfaces of the humic acid fouled membranes (static, 90,180,0 and 90,180,90 orientations), which showed that the humic acid foulant had a S:Si ratio of >1:99. Once this was done, scans of the edge images could be looked at to see if the fouling layer existed. In the case of the dynamic (90,180,0 orientation) fouled membrane (Figure 3.15(a)), in moving from the fouled surface to the aluminum support, the relative S:Si ratio went from >1:99, to 21:79, to 73:27 to >99:1. A similar trend with similar numbers was determined for the static fouled membrane (Figure 3.14(b)). These results, along with the ones for the

unused piece of membrane indicated the presence of a distinct fouling layer, which confirmed the allocation of the layers in Figures 3.14 and 3.15. The results also helped to show the similarity of the fouling layer for both the static and dynamic fouled membranes in the 90,180,y orientation experiments. The presence of silica in the humic acid fouling layer occurs because of inert inorganic matter present in the commercial humic acid flakes used for the feed solutions. Inert inorganic material found in soil often contains levels of silica.

The EDX analysis was also used to determine how well the humic acid foulant adhered to the surface of the membranes used in different processes and orientations. In this experiment, humic acid fouled membranes were rinsed with distilled water, dried, and then samples of each were prepared for SEM/EDX analysis. Figure 3.16 illustrates what the humic acid fouled membranes look like after they have been washed with distilled water. The EDX analysis showed that the relative S:Si ratio for the static, dynamic-90,180,0 and dynamic-90,180,90 were 86:14, 52:48 and 75:25, respectively. This leads to the conclusion that the fouling layer seems to adhere better to the membrane surface in the CMDS process. Though this experiment was not repeated for humic acid, a similar trend occurring in the silica fouling experiments (Subsection 3.3.4.1) confirming that this is a feature in the CMDS process.

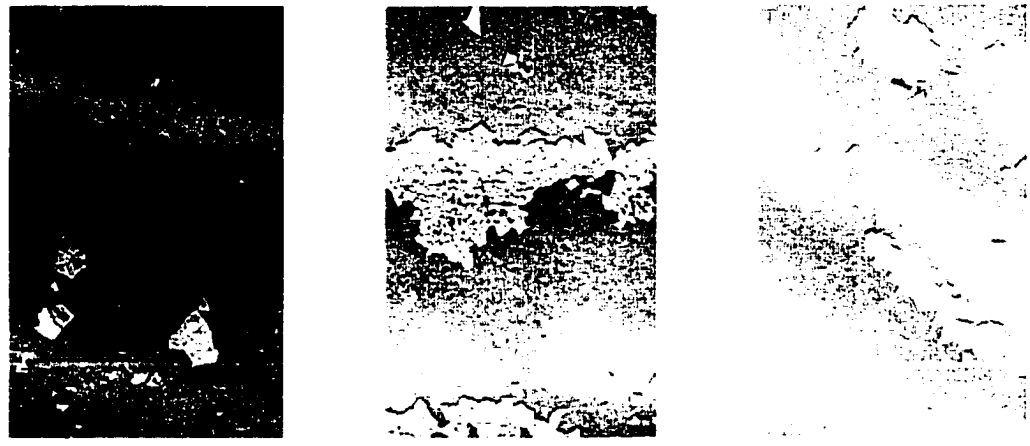

(a) (b) (c)

Figure 3.16 H_2O rinsed membrane surface electron micrographs (100x magnification) of: (a) static humic acid fouled membrane; (b) 90.180.0 orientation dynamic humic acid fouled membrane; and (c) 90.180.90 orientation dynamic humic acid fouled membrane

3.3 Colloidal Silica Fouling

3.3.1 Introduction

Silica represents one of the inorganic colloids that may be encountered in natural waters [43]. Colloidal silica reacts with other natural water contaminants to form scale deposits in water distribution systems. Conventional filtration equipment often fails to effectively remove colloidal silica, and most ion exchange resins are capable of removing only soluble silica [44]. Because of this, membrane filtration has provided a viable means of removing the silica from natural waters. However, with the use of membrane separations, comes surface fouling. Colloidal silica can foul the surface of a membrane by either the adsorption or the pore blockage mechanisms [35].

Fouling of reverse osmosis (RO) membranes by inorganic colloids has been previously investigated in a conventional membrane system [34,38]. In this work it was determined that electrokinetic and hydrodynamic forces influence the development of the fouling layer. For neutrally- or negatively-charged particles, the electrokinetic forces create an interaction between the surface of the membrane and the particles, thus creating the initial fouling layer. Once this layer is formed, the like-charged particles and the fouling layer tend to repel each other (more so for the negatively charged particles). However, this is minimized at higher ionic strengths (NaCl concentrations > 0.1M), which will be the case in the subsequent silica fouling experiments (NaCl concentration = 0.17M). The hydrodynamic forces are due in part to the permeation forces, which are often sufficient to overcome the particle repulsive forces. The permeation forces aid in the formation of a thick fouling layer, which once formed will reduce the flux through the membrane.

The colloidal silica of this research refers to an aqueous colloidal dispersion of silica particles that have high specific surface area. The particles in the dispersion are discrete uniform spheres that have no internal surface area or detectable crystallinity [45]. This type of colloidal silica has several industrial applications that include some of the following: (1) pulp and paper - paper coating; (2) computers and electronics – silicon wafer polish; (3) metal and metalworking - polishing agent; and (4) marine - antiskid

coating. The next section will discuss the chemical and physical properties of the particular colloidal silica solution used in the fouling experiments.

3.3.2 Experimental Work

3.3.2.1 Preliminary Experiments

Much of the physical and chemical characterization of the colloidal silica was conducted as part of an undergraduate research project by George Collins [46], the results of which will be summarized below. Two types of colloidal silica were used for the fouling studies; DuPont Ludox TM and HS-40. The manufacturer's supplied properties for these solutions are outlined in Table 3.5. From this table, it is noted that the silica particles have a negative charge, as the humic acid particles did in the previous fouling study (Section 3.2). However, the colloidal silica is stabilized with sodium ions, thus creating an overall, neutrally charged particle. The particle charges of the fouling solutions, and how they relate to fouling, will be discussed further in the concluding chapter of this dissertation (Chapter 4).

Property	Ludox Grade	
	HS-40	TM
stabilizing counter ion	Na	Na
particle charge	negative	negative
average particle diameter, nm	12	22
specific surface area, m^2/g	240	140
silica (as SiO_2), wt%	40	50
pH (25 °C)	9.7	9.1
viscosity (25 °C), cP	20	37
specific gravity (25 °C)	1.31	1.4

Table 3.5 DuPont Ludox properties

The effects of pH, ionic strength and temperature on the stability of the colloidal solutions were examined using solutions with a silica concentration of either 5g/L or 25 g/L. For all of these determinations, the particle size was monitored over time using the dynamic light scattering method described in Subsection 3.2.2.1. In the pH determination, the solutions were altered with the addition of either small quantities of HCl or NaOH. From this study, it was found that the solutions remained as stable

colloids at a pH between 5 and 6. This corresponds to the manufacturer's reported isoelectric point of 5.6.

The effect of ionic strength was examined by using varying concentrations of NaCl solution (500 to 20000 ppm) to make up the colloidal silica solutions. From this experiment, it was concluded that colloid stability degraded at higher ionic strength, and at higher silica concentration. For the fouling experiments to be discussed in the next subsection (3.3.2.2), silica concentrations below 25 g/L are chosen and the corresponding NaCl solution concentration are to be 10000 ppm. According to the ionic strength study, this combination will give a solution that will remain stable for at least 2 days.

Finally, the effect of temperature on colloid stability was examined. In this case, the 5 g/L and 25 g/L solutions were place placed in a thermostated water bath at 40 °C, and also left at room temperature (~21 °C). It was determined that the rate of coagulation increased with increasing temperature. For the solution specifications to be used in the fouling experiments, the solutions will remain stable for a minimum of 2 days.

3.3.2.2 Procedure For Fouling Experiments

With the information for the characterization of the colloidal silica known, the preparation of the feed solution could be carried out. The concentrated silica solutions from the manufacturer were diluted with a 10000 ppm NaCl solution (made with distilled water). As mentioned in Subsection 3.2.2.2 for humic acid, the salt solution was added to the silica in order to provide a means of identifying the quality of the permeate in both the static and the CMDS apparatus. The pH of the resulting solution was checked, and if it was found to be above 6, it was lowered to approximately 5.5 by the addition of 0.5 M HCl. Once prepared, the feed solution had a cloudy, grayish blue appearance. This feed solution was usually prepared fresh for each experiment, but in no case was a solution ever used more than 24 hours after its initial preparation. As mentioned above, two different types of colloidal silica concentrate solutions were used in the experiments, and this is indicated in Table 3.6.

The procedure for the colloidal silica fouling experiments was identical to that described for humic acid in Subsection 3.2.2.2. The experimental conditions used in all but one of these experiments include an applied pressure of 4100 kPa, a feed recirculation rate of 2L/min and a temperature of 25 °C. The only exception to this was Experiment #3 (see Table 3.6), which was run at the lower feed flow rate of 0.6 L/min. In all of the experiments, a 10000 ppm NaCl solution was circulated through the membrane modules for the first 70-80 minutes to provide data for the normalization of the silica flux results. This was followed by an approximately 5-hour period of silica feed solution circulation through the membrane modules to observe the flux decline. As was the case in some of the previous experiment, a membrane module was occasionally removed for later SEM/EDX analysis. The membrane modules used in the silica fouling experiments were made of the same reverse osmosis membrane material (Osmonics DS-3™) described in Table 2.1 of the previous chapter.

3.3.3 Results

Fouling analysis using the CMDS apparatus for the colloidal silica solutions was primarily conducted using the head with the fixed pitch angle of 90°. However, a result from a previous investigation [19] utilized the head with the fixed pitch angle of 0°. This particular result is included in this dissertation for comparison purposes. A summary of the experiments is given in Table 3.6.

Experiment #	Membrane Module Orientation	Colloidal Silica Concentration (g/L)	Mean Particle Diameter (nm)	Ludox Grade Used in Experiment
1	0,r,0 (r = 0 & 180)	15	30	TM
2	90,r,0 (r = 90 & 270)	21	25	TM
3	90,270,0	21	13	HS-40
4	90,270,0	5	12	HS-40
5	90,180,y (y = 0 & 90)	21	13	HS-40
6	90,180,y (y = 0 & 90)	21	14	HS-40

Table 3.6 Colloidal silica fouling experimental conditions

3.3.3.1 0,r,0 Results

The orientations for this experiment are shown in Figure 3.17. These are the same as the orientations described in Subsection 2.3.1 in the previous chapter on concentration polarization. This particular experiment helps to illustrate the nature of the density separation aspect of the CMDS apparatus. The two orientations represent the extremes of the action of the centrifugal forces acting on particles on the membrane surface. The graph of the relative flux over time (Figure 3.18) is produced in the same manner as that described for humic acid in Subsection 3.2.3.1. The same can be said for all of the silica fouling graphs produced in Subsection 3.3.3.

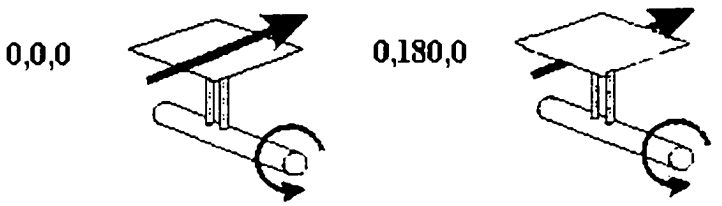

Figure 3.17 Membrane module orientation and feed flow direction (0,r,0)

In this experiment, the 0,0,0 orientation has the centrifugal forces acting in such a manner as to direct particles away from the surface of the membrane, while with the 0,180,0 orientation the opposite is true. As the colloidal silica solution has particles with a specific gravity of 2.6, the density separation effect inherent in the CMDS process is highlighted fairly well in this orientation. This is especially true when comparing these results with the ones obtained for the neutrally buoyant NaCl solutions discussed in Subsection 2.3.1 of the previous chapter. With the NaCl solutions, the negative impact of the centrifugal forces, *i.e.* in the 0,180,0 orientation, were not as dramatic as those associated with the silica (Figure 2.2 *vs.* Figure 3.18).

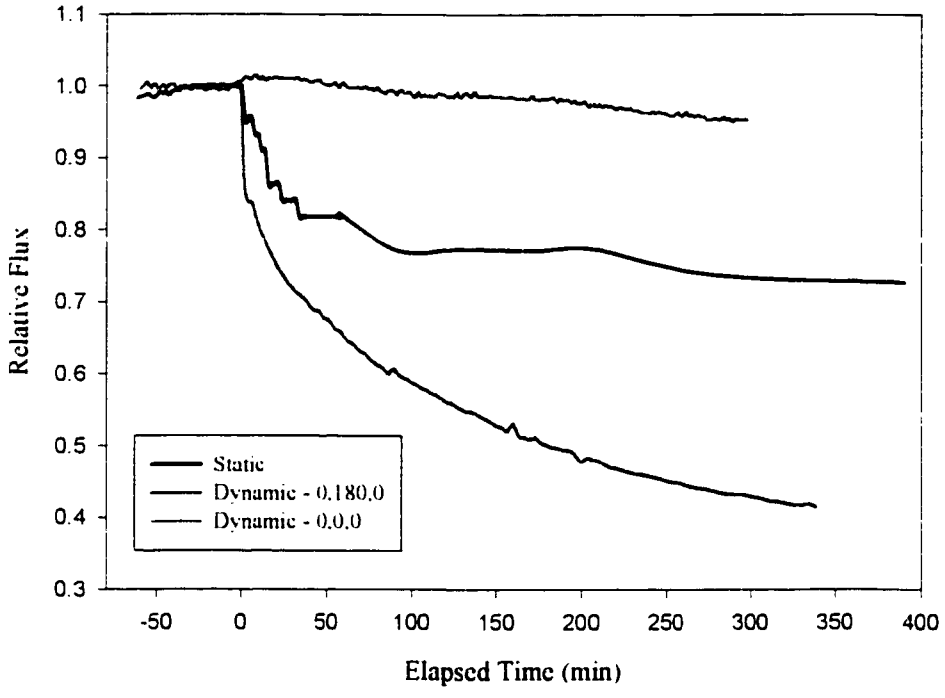

Figure 3.18 Colloidal silica experiment #1 [47]

The method of quantification for the plots is the same as that discussed in Subsection 3.2.3.1 of this chapter. The quantification for this orientation, and for all subsequent silica experiments, will include the area of the data from the 60-minute mark until the end of the run. In all of the plots to be given in this subsection the same characteristic exists; for the reference static case and the unfavourable dynamic orientations there is a fairly rapid flux decline over the first 60 minutes. As previously mentioned, this initial flux decline portion of the graphs is ignored in this analysis, and instead, the longer-term effects of fouling with respect to the static and dynamic processes are examined.

The quantification of the results illustrated in Figure 3.18 is given in Table 3.7. Using the knowledge obtained in the previous section, it can be determined numerically that the 0,0,0 orientation is superior to the 0,180,0 orientation based on a positive value of κ and a value of α that is lower than one. While this appears fairly obvious, the numbers will

allow for a comparison with the subsequent orientations used in the silica fouling experiments.

Orientation & Experiment #		α	κ
Static	1	1.0	0.00
0,0,0	1	0.87	0.21
0,180,0	1	3.7	-0.26

Table 3.7 α and κ values for 0,r,0 orientations

3.3.3.2 90,r,0 Results

Of the three experiments done in this subsection, only experiment #2 used two different roll angles, 90 and 270 (for reference, refer to Figure 3.2 for membrane module orientation relative to flow; in all cases the flow is in the same direction as that of the centrifugal force). Once this initial experiment was conducted, it became apparent that the 90,270,0 orientation was similar to the 90,90,0 orientation, so no further orientation experiments were conducted for the 90,r,0 orientation. Instead, the next two experiments (#3 and #4) investigated the effects of feed flow rate and colloidal silica feed concentration. The relative flux over time plots for this orientation are all very similar, therefore a typical result for this orientation is given in Figure 3.19. The α and κ values are also presented, in Table 3.8.

Orientation & Experiment #		α	κ
Static	2	1.0	0.00
	3	1.0	0.00
	4	1.0	0.00
90,90,0	2	5.9	0.53
90,270,0	2	1.7	0.53
	3	0.14	0.59
	4	-0.06	0.33

Table 3.8 α and κ values for 90,r,0 orientations

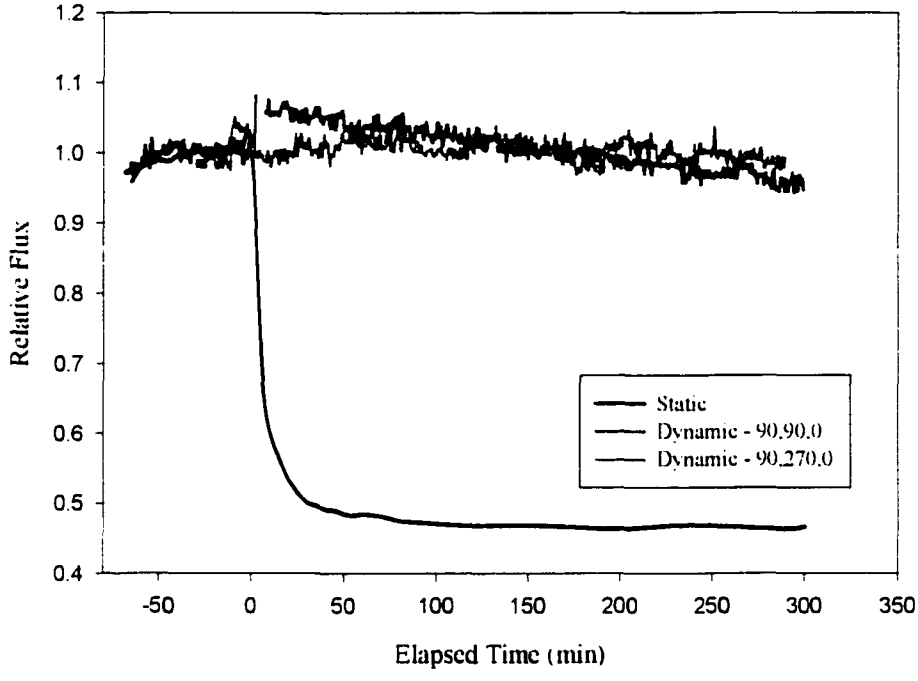

Figure 3.19 Colloidal silica experiment #2

The results showed that the 90,270,0 orientation performed the best of the 90,r,0 orientations examined. Though the value of α obtained for experiment #2 in the 90,270,0 orientation is greater than one, it is not that significant given that the other two results for the same orientation are well below one.

3.3.3.3 90,180,y Results

As mentioned in Subsection 3.2.3.2, the 90,180,y orientation (for reference, see Figure 3.7) is useful in helping to examine the effects of Coriolis forces in the CMDS process. The 90,180,0 orientation is capable of giving maximum Coriolis forces, while the 90,180,90 orientation gives the minimum forces. A typical result for this analysis is given in Figure 3.20, and upon examination of the curves, a similar trend to that shown for humic acid fouling at the same orientation (Figures 3.8 and 3.9) is noted. That is, this

analysis does not show a significant difference between the minimum and maximum Coriolis force orientations. The differences between the two different fouling solutions' flux declines will be examined further in the concluding chapter (Chapter 4).

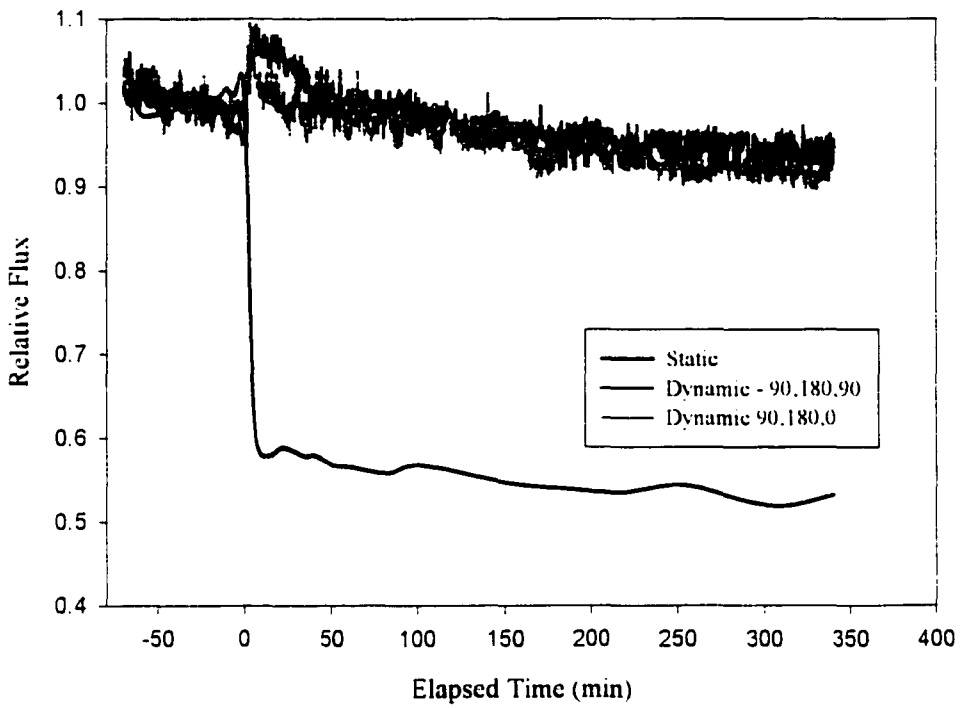

Figure 3.20 Colloidal silica experiment #5

Orientation & Experiment #		α	κ
Static	5	1.0	0.00
	6	1.0	0.00
90,180,0	5	1.8	0.40
	6	0.09	0.42
90,180,90	5	1.4	0.42
	6	0.14	0.33

Table 3.9 α and κ values for 90,180,y orientations

The values of α and κ (Table 3.9), for the most part, fall into what is apparently typical of the CMDS process, based on the full set of experiments already completed in these orientations. The slope analysis is a little misleading in that the α values for experiment #5 are slightly above one, indicating poorer performance relative to the static case. However, this result can also be tempered against the high κ values obtained in the experiments. It is also very clear in the relative flux over time figures that the performance of the dynamic process is superior to that of the static process, under the same conditions.

3.3.4 Microscopic Analysis of Fouling Layer

3.3.4.1 SEM Results

The procedures used in the preparation of samples were described in Subsection 3.2.4, and were used to examine silica fouled membrane samples. However, some difficulties were encountered in using these samples. Once dry, the silica layers tended to crumble, thus removing the deposits from the surface. This made it very difficult to prepare the edge samples for fouling layer thickness analysis. From the wet samples, a visual inspection noted fouling layers that appeared to be thin, glassy sheets.

Figure 3.21 gives a surface view of the silica fouled membrane samples and compares them to an unfouled piece of membrane material. In looking at the surface of the statically fouled membrane under 1000x magnification (Figure 3.21(b)), it was difficult to get a good understanding of what was happening at the surface. For this reason, an additional view at 500x magnification was done (Figure 3.21(c)). This image shows the "plate-like" structures that were identified in the visual inspection of the membrane, and also how the fouling layer flaked off of the membrane surface upon drying. The shadows in the image help to give a sense of the size of the structures, which appear to be larger than the ones illustrated for humic acid (Figure 3.12). It seems that the silica fouling layer is an agglomeration of material that forms "plates" on the surface.

Figure 3.21 Surface electron micrographs of: (a) unused membrane (1000x); (b) static silica fouled membrane (1000x); and (c) static silica fouled membrane (500x)

Micrographs of the 90.180.y experiments are presented in Figure 3.22. In this series of images it is interesting to see the distinct differences in the nature of the fouling layers on the static and dynamic samples. The static sample (Figure 3.22(a)) is very similar to the one given in Figure 3.21, while the dynamic fouling layers seems to have fouling "plates" which are smaller and somewhat better adhered to the membrane surface. Unfortunately, only the static case could be examined in the edge profile (Figure 3.23), and thus the fouling thickness of the dynamic orientations could not be studied. As mentioned before, this was due to the fact that the silica fouling layer degraded considerably once dried. The difference between static and dynamic cases is not a surprise given the considerable difference in their respective relative fluxes (Figure 3.20). The surface study of the micrographs seems to indicate that the dynamic fouling layers are more porous or possibly thinner, and thus more permeable.

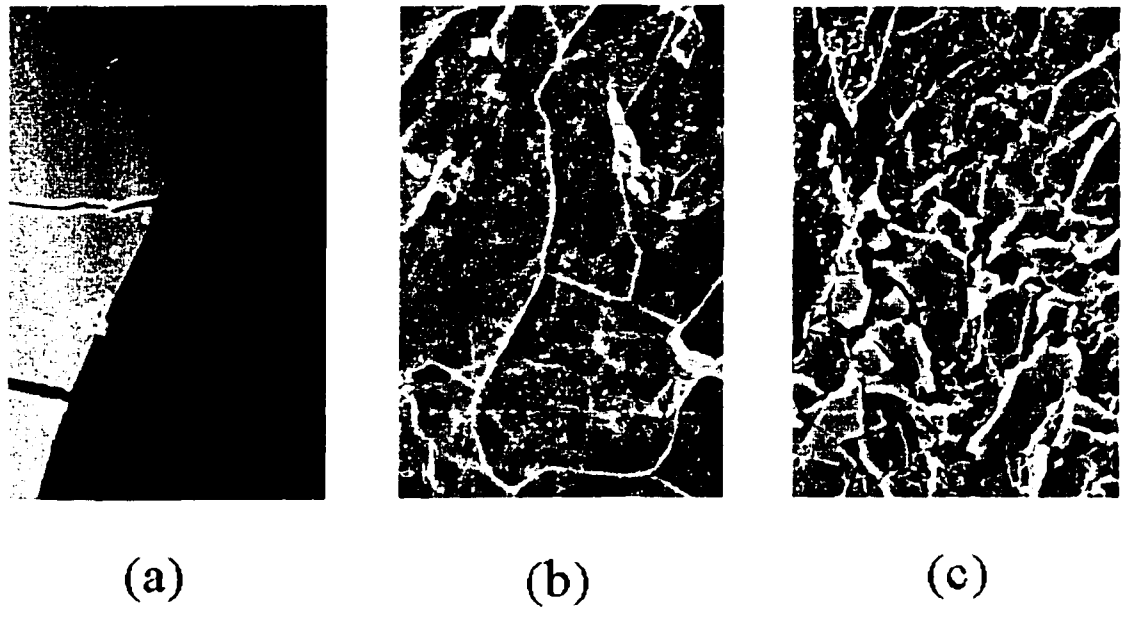

Figure 3.22 Surface electron micrographs (1000x magnification) of: (a) static silica fouled membrane; (b) 90.180.90 orientation dynamic silica fouled membrane; and (c) 90.180.0 orientation dynamic silica fouled membrane

The thickness of the static fouling layer (Figure 3.23(b)) gives some insight into the nature of the fouling layer. It seems to have the same characteristics as that shown for humic acid in the edge view of the static fouled membrane (Figure 3.14(b)). There appears to be a built up layer that is quite dense, indicating an absorptive fouling mechanism. One source of error, not discussed in the humic acid section, concerns the preparation of the samples. The edge samples were prepared by cutting the sections with a scalpel. In doing this, the image presented in the micrograph may represent a compaction caused by the cutting action of the scalpel. This could have been determined definitively if samples for the dynamic orientations could have been prepared from the fouled membrane modules.

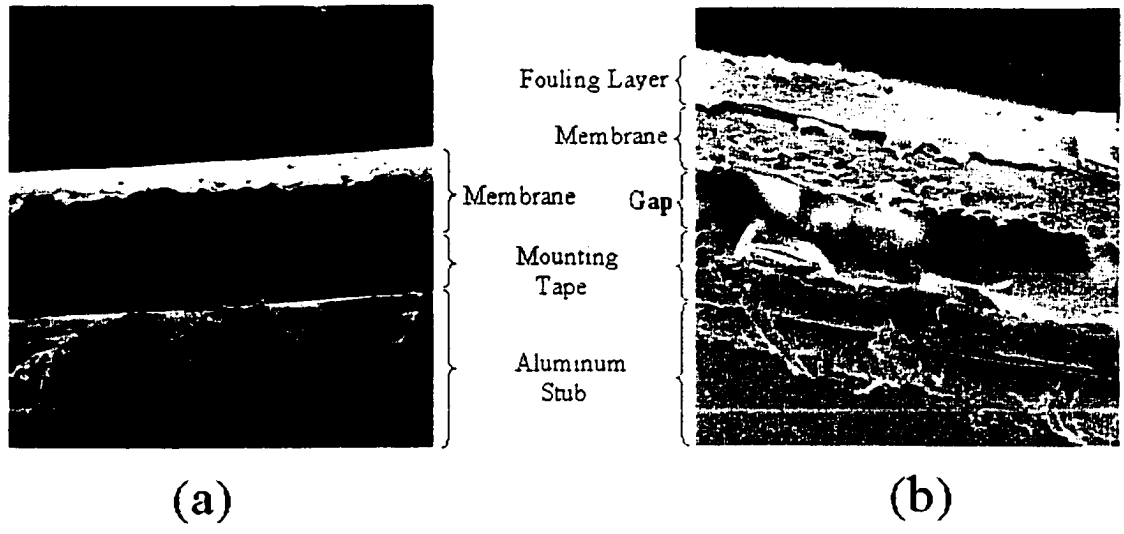

Figure 3.23 Edge electron micrographs (100x magnification) of: (a) unused membrane; and (b) static silica fouled membrane

3.3.4.2 EDX Results

The elements selected for the analysis were again sulfur and silica, as it was assumed that they would be present in different quantities for the foulant and for the membrane material. As was mentioned in Subsection 3.2.4.2, the EDX analysis was only able to identify trends with respect to the fouling layers, and not identify their exact interfaces on the edge micrographs (Figure 3.23). The first scan involved looking at the surface of the silica fouled membranes to see what the S:Si ratios were. For the static, 90.180.0 and 90.180.90 orientations, the ratios were found to be 71:29, 13:87 and 25:75, respectively. As a reference, these values can be compared to the ratio for the unused membrane material, 87:13. The high ratio for the static membrane sample may be misleading given that more of the dried foulant was probably gone from the membrane surface, compared to the dynamic fouled samples (Figure 3.22).

An analysis of the edge view of the static fouled membrane (Figure 3.23(b)) indicated that a silica fouling layer exists on the membrane surface. This analysis was not as critical as the one performed for the humic acid, as the silica fouling layer is quite apparent in the edge view image (Figure 3.23(b)), as compared to that for the humic acid (Figure 3.15, for example). In this experiment the S:Si ratios were, going from the

fouling surface towards the aluminum support, as follows: 26:74, >1:99, >1:99, 98:2 and >99:1. The 26:74 value is anomalous, however, as described above, this may have been due to some surface silica removed upon drying.

Finally, the EDX analysis was also used to determine how well the silica foulant adhered to the surface of the membranes used in different orientations. Once again for this procedure, the silica fouled membranes were rinsed with distilled water, dried, and then samples of each were prepared for SEM/EDX analysis. Figure 3.24 illustrates what the silica fouled membranes look like after they have been washed with distilled water. These images indicate that there is more material on the surface of the dynamic fouled membranes (surface has a rougher appearance), thus indicating better adhesion. The EDX analysis showed that the S:Si ratios for the static, 90.180.0 and 90.180.90 membranes were 87:13, 20:80 and 39:61, respectively. As determined in Subsection 3.2.4.2 on EDX analysis of unused membrane material, a "clean" membrane should have a high S:Si ratio. Thus, this is a further indication that more foulant has adhered to the dynamic fouled membranes. This result, along with the similar one obtained for humic acid, illustrates the apparent contradiction of how the foulant is better adhered to the membrane surface in the CMDS process, while still obtaining higher fluxes relative to the static case.

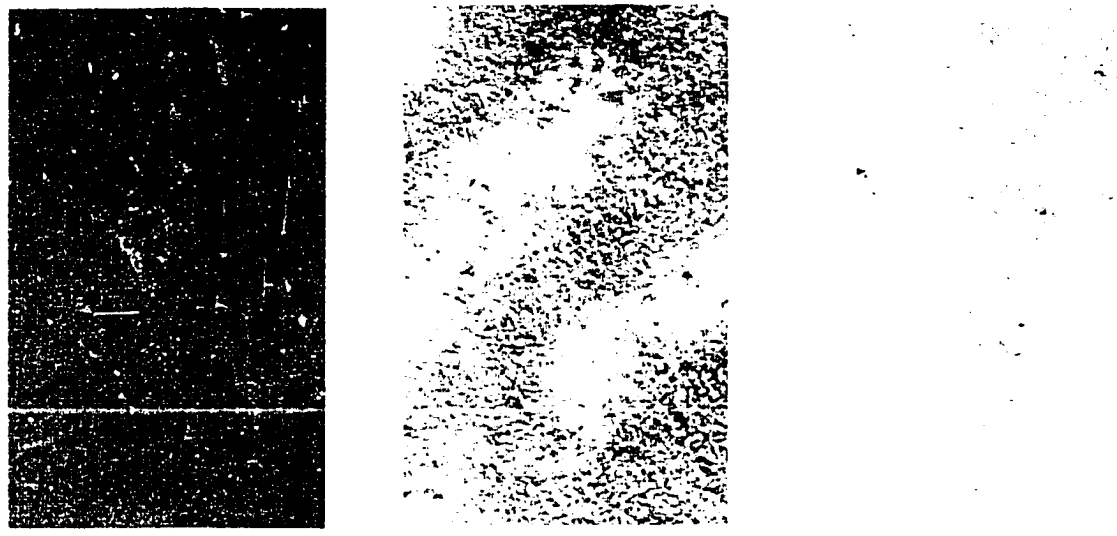

Figure 3.24 H_2O rinsed membrane surface electron micrographs (100x magnification) of: (a) static silica fouled membrane; (b) 90,180,0 orientation dynamic silica fouled membrane; and (c) 90,180,90 orientation dynamic silica fouled membrane

3.4 Nanofiltration

This section examines the nanofiltration of a feed solution containing protein, and thus changes the focus of the fouling from smaller particles to macromolecules. However, more importantly, the focus has shifted from reverse osmosis membranes to nanofiltration membranes, enabling the study of a different transport mechanism in the CMDS process. Nanofiltration (NF) membranes have pore sizes that are twice that found in reverse osmosis (RO) membranes (10-20 Å *vs.* 5-10 Å) [3]. The factors that effect separation for the two types of membrane also differ somewhat. Reverse osmosis transport is primarily dependent upon diffusivity and solubility of the solvent within the membrane matrix, where nanofiltration transport depends primarily on the relative size of particles *vs.* pore. NF membranes have a high permeability for monovalent salts (NaCl and KCl for example) and organic compounds with low molecular weight (<500 Daltons). However, they have very low permeability for higher molecular weight organic compounds (>500 Daltons) such as proteins [49]. This section will illustrate how the

CMDS process is universal in its application for both significantly different feed solutions and for different transport mechanisms.

3.4.1 Introduction

In the past few years, there has been considerable interest in the use of membrane separation processes for the fractionation of complex protein mixtures [48]. Membranes are also being used for de-watering dairy products, rather than using energy-intensive evaporation methods. With the use of membranes for these protein separations comes the inevitable problem of protein fouling on the surface of the membrane.

When using feed solutions that contain macromolecules, such as proteins, the fouling that occurs on the membrane surface is a form of concentration polarization. This is governed by the same equations as those described by equations 2.1 through 2.3 in Section 2.1. However, in this case, a macromolecular solute can build up on the surface of the membrane and a gel layer will begin to form. Once this layer forms and reaches a point limited by the solute's concentration, any further build up of solute must occur by a thickening of the existing gel layer at the membrane's surface. This creates a reduction in flux, which eventually reaches the point where the convective transport is equal to the diffusion backflow transport. In this situation the permeate flux becomes constant and C_w is replaced by C_g giving equation 3.3:

$$\frac{C_g}{C_b} = exp\ \frac{J_v}{k} \qquad (3.3)$$

; where C_g is the concentration of the solute at the gel layer surface. This is what is referred to as the "gel polarization model", and is represented by Figure 3.25. In this figure, the area directly adjacent to the membrane (yellow area) is the gel layer (blue area). This gel polarization representation of concentration polarization shows that water flux (J_v): (1) is independent of pressure upon formation of the gel; (2) decreases with increasing feed concentration; and (3) depends on fluid dynamics (*i.e.* laminar or turbulent flow conditions) [26]. The flux behaviour of this fouling model is generalized

in Figure 3.26, which shows at what point the gel layer forms on the membrane and what transport mechanisms are governing the flux.

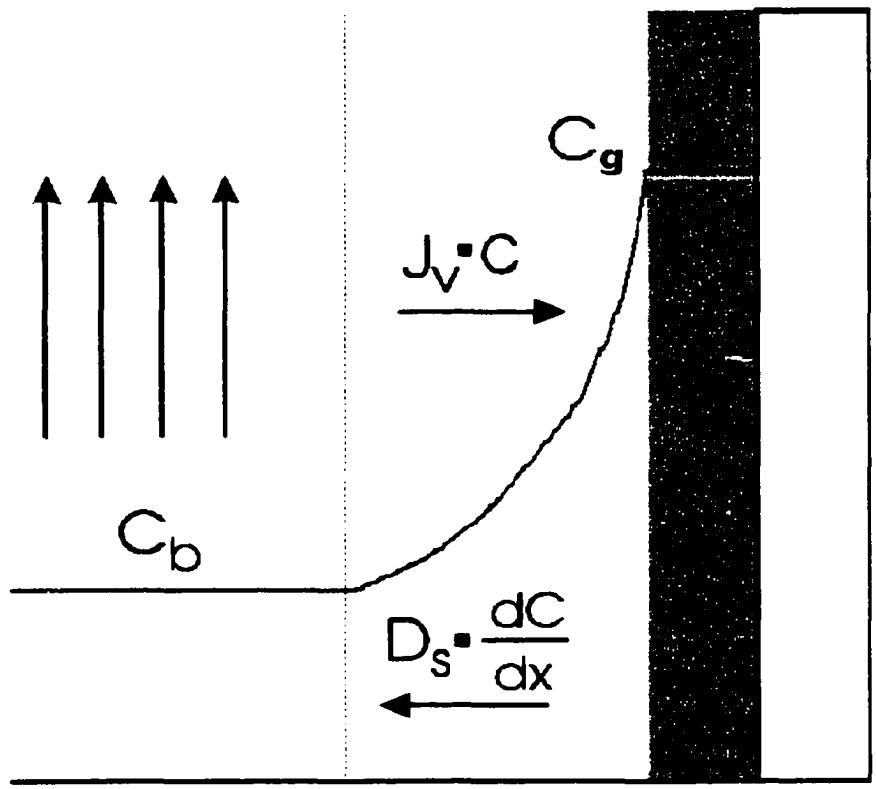

Figure 3.25 Gel polarization concentration profile

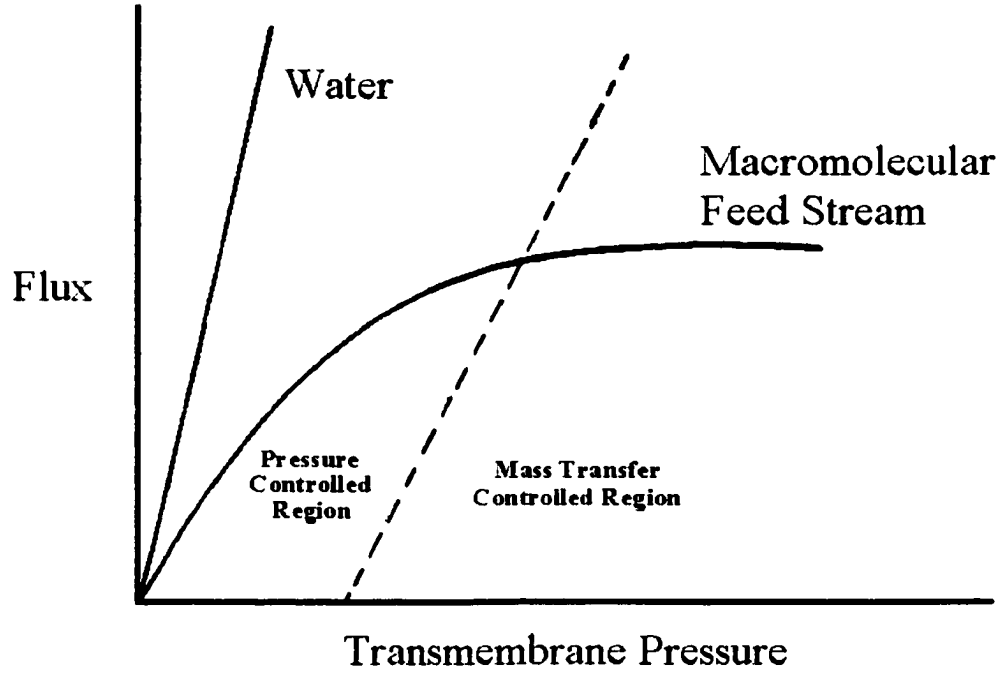

Figure 3.26 Generalized NF transport relationship (after [49])

The feed solution that was chosen to be used in the nanofiltration experiments was that of whey. Whey contains four major proteins: (1) β-lactoglobulin; (2) α-lactalbumin; (3) bovine serum albumin; and (4) immunoglobulin G [50]. However, for this study the term "protein" will used to represent all of the protein present in the whey feed solution. In addition to the protein there are other solids present in whey, which are represented in Table 3.10.

Constituent	Percentage of Total Solids
Fat	0.9
Protein	10.2
Non-protein Nitrogen	2.7
Lactose	74.0
Lactic Acid	2.2
Soluble Salts	9.6
Insoluble Salts	0.4

Table 3.10 Typical solids content of whey [51]

The molecular weights of the major constituents are below 500 Daltons (for example – lactose is 342 Daltons [52]), and thus it is mostly the protein that will retained by the

nanofiltration membranes. It is this retention that will manifest itself as a gel layer, as described above.

3.4.2 Experimental Work

3.4.2.1 Preliminary Experiments

The source of whey selected for the experiments was a commercial whey powder (Sigma Aldrich Co.), which had a minimum protein content of 11% (manufacturer's guarantee). The primary characterization of the whey powder involved determining its solubility. Information provided by Sigma-Aldrich indicated that the powder was soluble at 50 g/L [53], and tests confirmed that this was the case. A test solution with a concentration of 50 g/L was prepared with the addition of the whey powder to distilled water, followed by 5 minutes of gentle, mechanical stirring. The resulting mixture was a light yellow, turbid solution. This solution was allowed to sit 24 hours, and a subsequent observation found that there was no precipitation, or degradation of the solution. This remained the case for another 48 hour period, at which time the solution began to precipitate. A "spoiled milk" odour also began to become prevalent during this period, indicating the bacterial breakdown of the lactose to lactic acid. This experiment indicated that the feed solution would remain stable for a period of at least 24 hours. However, it was decided that fresh whey solution would be prepared for each day's experiments.

For these experiments, the membrane material used in the membrane modules was DS-5™, a thin-film nanofiltration membrane from Osmonics. Table 3.11 summarizes some of the specifications for the membrane material.

Specification	Value
application	Dye removal/concentration, heavy metals removal, and acid purification
pH range	2.0 - 11.0 operating range and 1.0 - 11.5 cleaning range
typical operating pressure	500 – 2800 kPa
maximum pressure	3500 kPa
maximum temperature	50°C

Table 3.11 DS-5™ membrane material specifications [54]

As all of the experiments done thus far involved reverse osmosis membranes, NaCl concentration (via conductivity measurements) of the permeate was used to determine how well the membrane was working. In the case of nanofiltration membranes, NaCl is not retained, and thus a new method of determining membrane integrity had to be developed. The main aspect of these experiments involves protein retention, therefore a method to quantify protein concentration in the permeate was necessary. A protein assay procedure based on the Bradford dye-binding procedure was chosen for this quantification (BioRad reagent) [55]. This colourmetric determination (595nm) is useful for protein concentrations of up to 1.4 g/L. This value represents a % rejection measurement of 25% based on a 50 g/L whey feed solution, thus it is effective in the 25-100 % rejection range. This analysis was to be done using the permeate from the static process experiments, as it was the only process capable of capturing the permeate. In all cases it was found that the membranes were not leaking protein into the permeate streams.

An experiment similar to that described in Section 1.4 was also conducted on the nanofiltration membrane modules to see if backpressure was a factor to be considered. This experiment was done after the integrity of the membranes had been confirmed with the protein assay of the permeate. In this procedure, distilled water was run through the NF membranes at a constant transmembrane pressure of 690 kPa (varying the applied and backpressures correspondingly). No effect was observed using a range of backpressures from 0 to 1400 kPa.

3.4.2.2 Procedure For Fouling Experiments

The procedure for these experiments differed somewhat from that used for the humic acid and colloidal silica fouling experiments. One type of experiment was done to try to reproduce the flux curves, illustrated in Figure 3.26, for both the dynamic and the static processes. The other type of experiment conducted was identical to the ones in the two previous sections on fouling, though at a lower applied pressure. For all of these experiments, a feed solution of whey was prepared to a concentration of 50 g/L by adding

the appropriate amount of whey powder to distilled water in the feed tanks (no NaCl was added, as with the humic acid and silica feed solutions).

The first type of experiment involved circulating whey feed solution first through the static process, and then through the dynamic process. This was done by varying the transmembrane pressure from 450 to 4200 kPa, in 350 kPa intervals. Flow rate samples were measured at each pressure for 10 to 15 minutes, and an average flux for each pressure was determined. The second type of experiment was done in much the same way as that described in Subsections 3.2.2.2 and 3.3.2.2. In this case however, the applied pressure was fixed at 1400 kPa rather than 4200 kPa.

3.4.3 Results

All of the experiments using the whey feed solution were conducted on the membrane head with the pitch of 90. A summary of these experiments is given in Table 3.12.

Experiment #	Membrane Module Orientation	Experiment Type
1	90,270,0	variable pressure
2	90,270,0	variable pressure
3	90,180,y (y = 0 & 90)	variable pressure
4	90,180,y (y = 0 & 90)	fixed pressure

Table 3.12 Whey solution fouling experimental conditions

3.4.3.1 Variable Pressure Results

This experiment examined if the CMDS process gives a flux-pressure response similar to that illustrated in Figure 3.26. The results of this experiment are illustrated in Figure 3.27. The shape of the curve indicated that there was a gel layer forming in both processes, but the onset of this was reached at a higher pressure in the case of the dynamic process (orientation 90,270,0). The graph also indicated that a higher flux was being achieved in the dynamic process. This same type of analysis was performed for the 90,180,y orientation (Figure 3.28), with similar results. The only difference in this case occurred with the onset of the gel layer formation. In this case, it seemed to occur at approximately the same pressure as the static process.

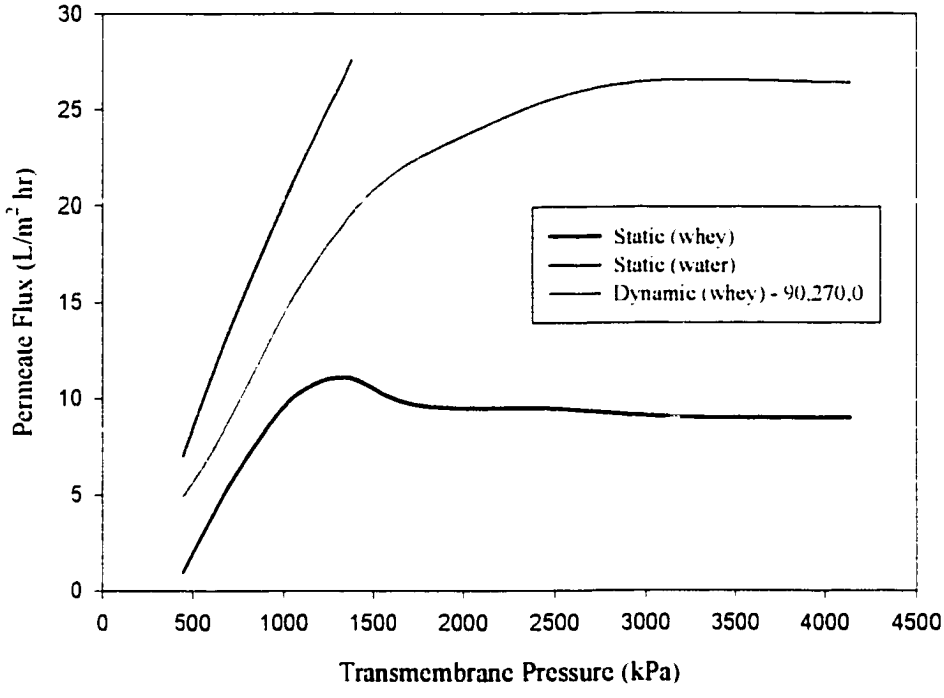

Figure 3.27 Whey experiment #1

Quantification of these results differed somewhat from that done for the humic acid and silica fouling results. The benefit of the dynamic process over the static process could be measured by examining the part of the curve where the flux is mass transfer controlled, or the portion where the gel layer forms. A modified offset factor (κ') and a "rollover" pressure term (p_r) are used for the variable pressure experiments. The κ' is based on the same idea as the κ term used in the previous two sections on fouling (refer to Equation 3.2), however this offset is based on the difference in absolute flux rather than relative flux. Because of this, the value of κ' will be considerably larger than that of κ, and therefore will not allow for direct comparison. The term p_r refers to the pressure at which the flux levels off, or where the gel layer forms. This is determined by visual inspection of the pressure flux plots. The results for the variable pressure experiments are presented

below in Table 3.13. These results indicate that the 90,270,0 dynamic orientation achieves the onset of the gel layer at a higher pressure and provides a higher flux relative to the static case.

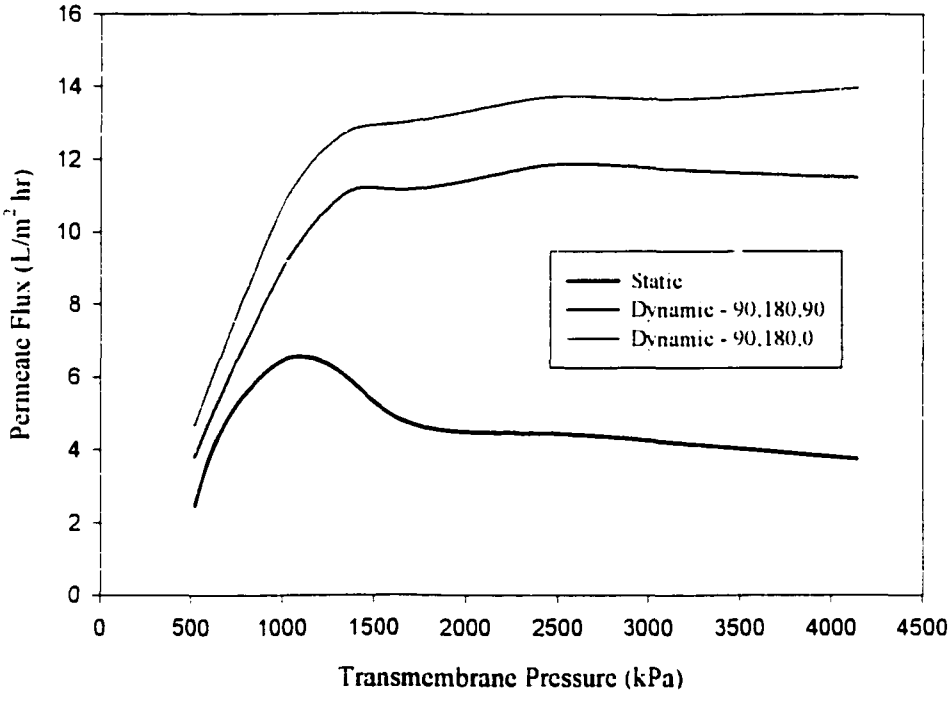

Figure 3.28 Whey experiment #3

Orientation & Experiment #		κ'	p_r (kPa)
Static	1	0.0	1200
	2	0.0	1300
	3	0.0	1100
90,270,0	1	17	2700
	2	10	2000
90,180,90	3	7.3	1400
90,180,0	3	9.6	1400

Table 3.13 κ' values and "rollover" pressures for variable pressure experiments

3.4.3.2 Fixed Pressure Results

This experiment involved an experimental approach similar to that presented in the sections of this chapter on humic acid and silica fouling. The results of this experiment (Figure 3.29) showed some different results relative to those given for the silica fouling stream (see Figure 3.19), but provided some similarity to the results obtained from the humic acid fouling experiments (see Figure 3.9). The similarity exists in the fact that there was a significant pattern of decay in relative flux for both the static and dynamic cases. This may be due to the rapid onset of the gel layer under the operating pressures used.

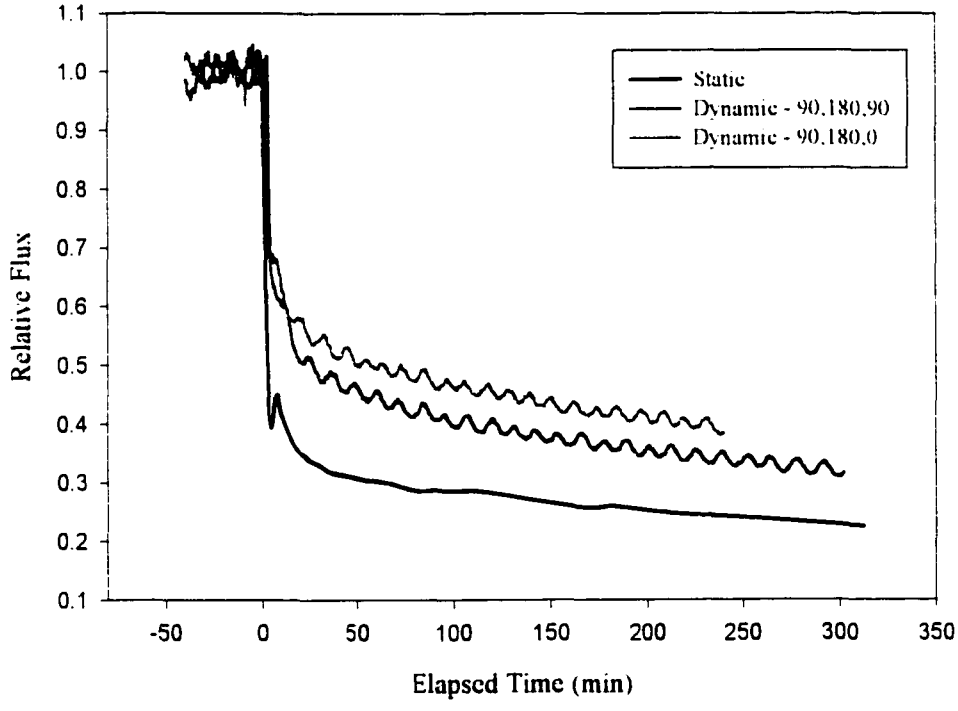

Figure 3.29 Whey fouling experiment #4

The results for the quantification of the flux over time plot are given in Table 3.14. As was the case for some of the results obtained for the silica fouling, the values of α for the whey were greater than one, indicating a more rapid decline in flux relative to the static

case. Unfortunately, the runs were limited in elapsed time; so this trend could not be examined further to determine if these α values would remain greater than one over a greater period of time. However the positive κ values illustrated a greater flux in the dynamic processes relative to the static case. The experiment also once again confirmed that the maximum Coriolis force orientation (90,180,0) produces an improved performance relative to that of the minimum Coriolis force orientation (90,180,90).

Orientation	α	κ
Static	1.0	0.00
90,180,0	1.6	0.17
90,180,90	1.9	0.11

Table 3.14 α and κ values for fixed pressure experiment (experiment #4)

3.4.4 Microscopic Analysis of Fouling Layer

Only an SEM analysis was undertaken, as the composition of the fouling layer did not allow for an effective EDX analysis. This is due to the fact that the fouling layer is composed primarily of organic material without a significant portion of inorganic material in its matrix (as was the case with humic acid fouling layers). The preparation of the samples for the SEM analysis was the same as that described in subsection 3.2.4 of this chapter.

The results of the surface SEM images (Figure 3.30) were not very conclusive, and surface material was difficult to differentiate from the membrane material. This may have occurred due to a possible decomposition of the protein fouling layer during the gold coating process. As mentioned in Subsection 3.2.4.1, the sputter coating process involves the use of desiccation and a vacuum environment to prepare a sample for coating. It is this process that may have damaged the fouling layer, thus making it difficult to observe under the microscope. Visual inspection of the membrane modules after a fouling experiment also gave little insight into the nature of the fouling layer. It appeared to be a fairly translucent layer, with a slimy, gelatinous texture.

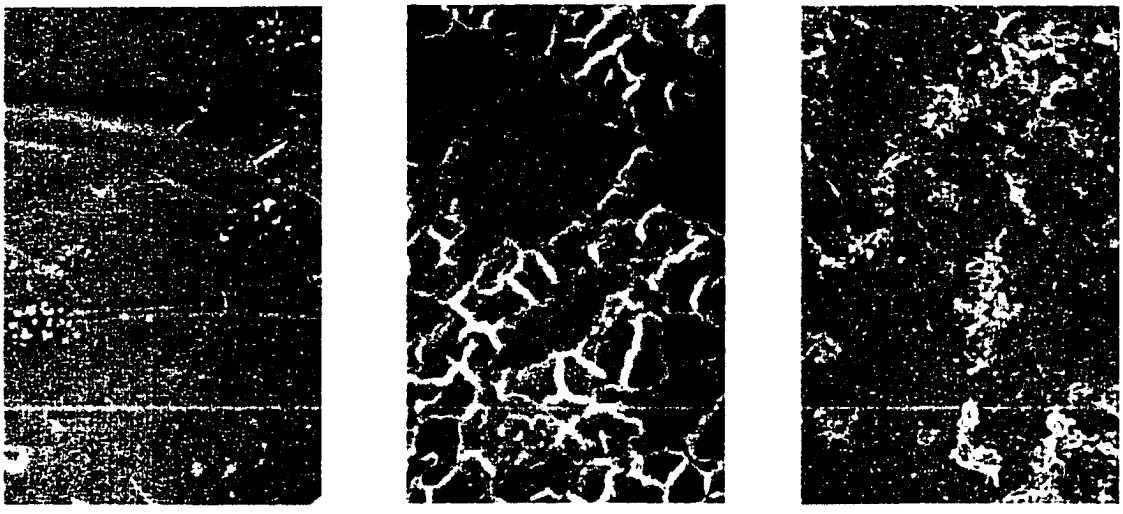

Figure 3.30 Surface electron micrographs (250x magnification) of: (a) unused membrane; (b) static protein fouled membrane; and (c) 90,180,90 orientation dynamic protein fouled membrane

The edge SEM images (Figures 3.31 and 3.32) provided even less information than that from the surface images. The identification of a fouling layer in Figures 3.31(b) and 3.32(b) cannot be established relative to the image of the unused membrane in Figures 3.31(a) and 3.32(a). As an EDX analysis of the fouling layer could not be undertaken, thus the presence of this fouling layer could not be confirmed. Once again, the culprit may have been the degradation of the layer during the gold coating process. It is interesting to note that the membrane itself did not show the same level of compaction as that for the experiments utilizing the reverse osmosis membrane material (refer to Figures 3.14, 3.15, and 3.23). This indicates that there may be a critical pressure were compaction occurs for a given membrane material, or that the level of permeation may play a role in this compaction. In either case, the apparent lack of compaction made it too difficult to identify the presence of a fouling layer.

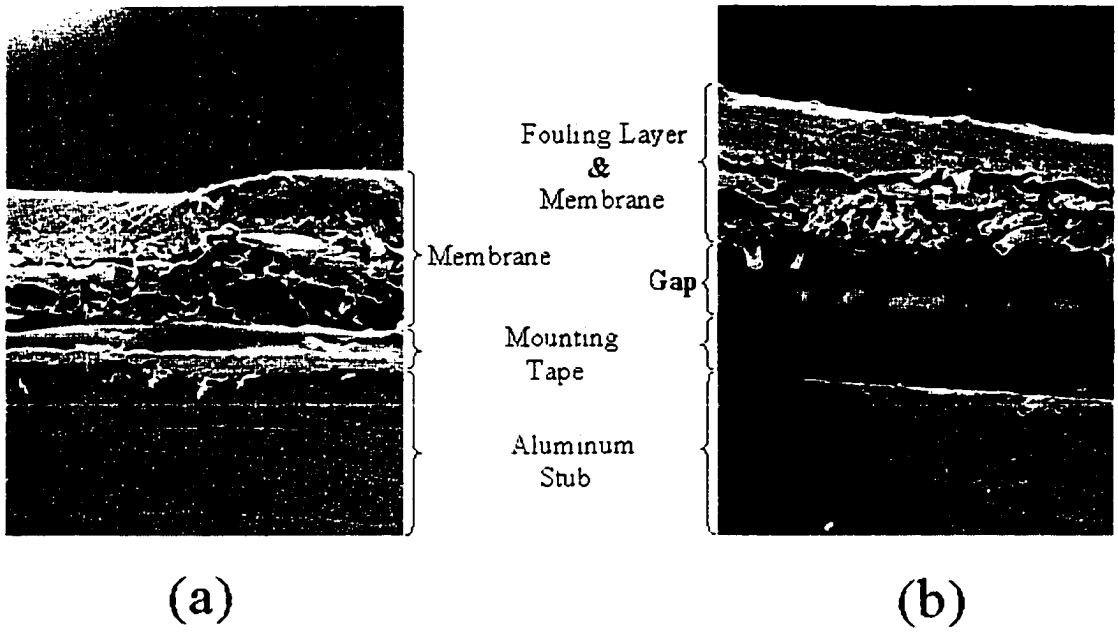

Figure 3.31 Edge electron micrographs (100x magnification) of: (a) unused membrane and (b) static protein fouled membrane

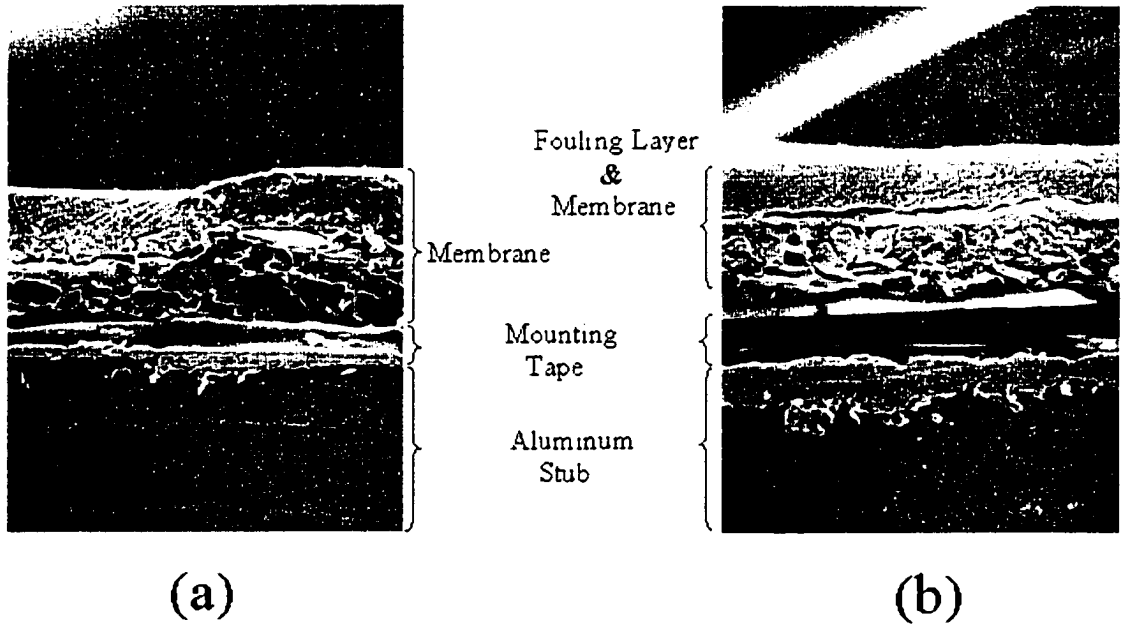

Figure 3.32 Edge electron micrographs (100x magnification) of: (a) unused membrane and (b) dynamic (90,180,90 orientation) protein fouled membrane

A different qualitative method was utilized to determine if a fouling layer was present on the surface of the membranes. This test was done with membranes that had just been used in a fouling experiment, as well as ones that had been rinsed to see if fouling layers adhered to the membrane (similar to that done for humic acid and silica in Subsections 3.2.4.2 and 3.3.4.2, respectively). This test used the same BioRad reagent that was used in the protein assay analysis. It was noted that when the diluted reagent was in the presence of protein, a resulting blue colour was established. Utilizing this observation, the membrane modules were covered in the diluted reagent and allowed to sit for 5 minutes. The greater the amount of protein on the membrane surface, the more prevalent the blue colour. From this analysis it was noted that the static fouled membranes showed bluer colour on the surface than the corresponding dynamic fouled membranes. This qualitative experiment appears to indicate more protein fouling on the surface of the static fouled membranes. Using this test on the rinsed membranes yielded little blue colouration, thus indicating protein was not present. This also identifies a loosely adhered fouling layer on both the static and dynamic fouled membranes.

4 Conclusions

4.1 CMDS Process Conclusions

The previous two chapters have outlined a variety of experiments utilizing the CMDS process. From this work, several conclusions with respect to both the performance of the CMDS process and fouling mechanisms can be drawn. By using different feed solutions, membrane materials and process conditions in the various experiments, a number of phenomena have been observed. However, underlying these conclusions is the main point of the research; when compared to a conventional membrane process, does the CMDS process work better with respect to fouling reduction and flux enhancement? The answer to these questions is yes. While the process does not eliminate fouling, it was found to minimize its deleterious effects. Table 4.1 provides an overall summary of the experiments completed (typical results illustrated), and how they relate to membrane orientation and the forces at work in the CMDS process. The significance of the various factors presented in Table 4.1 can be summarized as follows: (a) a value of β greater than one indicates flux enhancement relative to the static process; (b) a value of α less than one indicates that the flux is not declining at the same rate at it is for the static process; (c) a value of κ greater than zero indicates that there is a higher flux relative to the static case; and (d) a value of κ' greater than zero indicates that there is a higher absolute flux relative to the static case The subsequent subsections will summarize the observed phenomena of the previous two chapters that support the assertion that the CMDS process is a better means of membrane separation relative to a conventional system.

Membrane Orientation	Centrifugal Force	Coriolis Force	Brine		Humic Acid	Silica	Whey
			NaCl	$MgSO_4$			
0,0,0 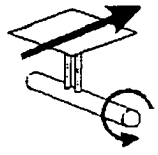	away from membrane surface (normally)	directed normally towards membrane surface	β=1.16	β=1.49	N/A	α=0.87 κ=0.21	N/A
0,180,0 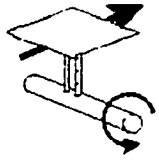	towards membrane surface (normally)	directed normally away membrane surface	β=0.88	β=0.91	N/A	α=3.7 κ=-0.26	N/A
90,90,0 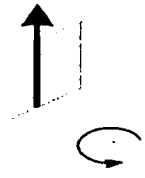	away from the membrane surface in plane with feed flow	directed tangentially away from membrane surface	β=1.27	N/A	α=1.1 κ=-0.01	α=5.9 κ=0.53	N/A
90,180,0 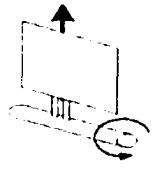	away from the membrane surface in plane with feed flow	directed normally away from membrane surface	β=1.54	N/A	α=0.61 κ=0.01	α=0.09 κ=0.42	κ'=9.6 α=1.6 κ=0.17
90,180,90 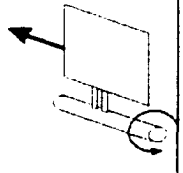	away from the membrane surface in plane at right angles with feed flow	minimum Coriolis force	β=1.12	N/A	α=0.69 κ=-0.03	α=0.14 κ=0.33	κ'=7.3 α=1.9 κ=0.11
90,180,180 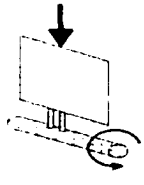	away from the membrane surface in plane against feed flow	directed normally towards membrane surface	β=1.22	N/A	N/A	N/A	N/A

90,180,270 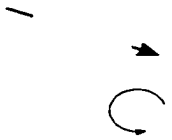	away from the membrane surface in plane at right angles with feed flow	minimum Coriolis force	β=1.12	N/A	N/A	N/A	N/A
90,270,0 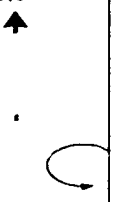	away from the membrane surface in plane with feed flow	directed tangentially away from membrane surface	N/A	N/A	α=0.39 κ=0.14	α=0.14 κ=0.59	κ'=17.5
90,270,90 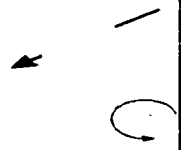	away from the membrane surface in plane at right angles with feed flow	directing particles away from the membrane surface (tangentially)	N/A	N/A	α=0.70 κ=0.04	N/A	N/A

Table 4.1 Summary of membrane orientation performance for flux enhancement

4.1.1 Membrane Orientation

The focus of this part of the research involves examining several orientations and observing their flux behaviour with respect to membrane orientation. The purpose is not to highlight any particular orientation, but rather to understand the influence of the rotating environment on a variety of fouling processes. When discussing membrane orientation, one is developing links between the direction in which the feed is passed over the membrane with respect to the Coriolis and centrifugal forces.

In the chapter on concentration polarization (Chapter 2) it was determined that the 90,180,0 orientation gave the greatest flux enhancement of the orientations tested, relative to the static case (higher β number). In this orientation (Figure 4.1), the centrifugal force is directed from the axis of rotation to the periphery, in the same manner as the feed flow (positive y direction). The Coriolis force is being directed away from the membrane in a direction that is normal to the surface (positive x direction). As suggested in the computational fluid dynamic work done by Pharoah [21,22], it is the combination of the Coriolis and centrifugal forces that create the flow instabilities, which then create

better mixing of the bulk fluid at the membrane surface. While this phenomenon occurs at most orientations in the CMDS process, it is the 90,180,0 orientation that gives the greatest magnitude of these forces acting upon the membrane surface creating flow instabilities. This is based only on the experiments conducted for the concentration polarization determination and the CFD simulations, both of which did not examine all orientations.

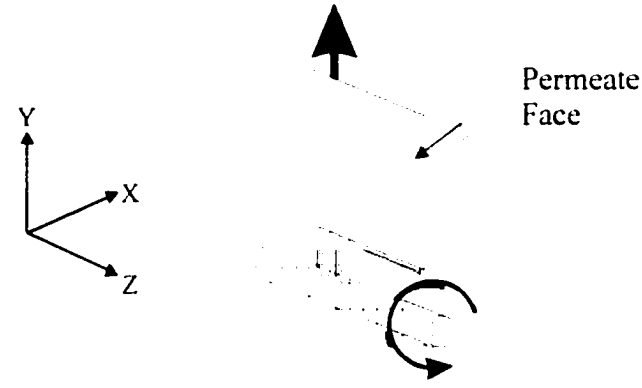

Figure 4.1 90,180,0 orientation with reference axis

The fouling experiments gave slightly different results with regard to which of the studied orientations created more fouling reduction and greater flux enhancement. For both the humic acid and silica results, the 90,270,0 orientations showed the most promise with respect to flux enhancement relative to the static process experiments. This was based on the analysis of the results using the derived terms α and κ. As mentioned in Subsection 3.2.3.1, a value of α less than one and a positive value of κ indicated that the particular dynamic orientation had a slower rate of flux decline and a greater flux relative to the static case. In this orientation (Figure 4.2), the centrifugal force is also directed from the axis of rotation to the periphery, in the same manner as the feed flow (positive y direction). The Coriolis force is directed in the plane of the membrane (positive x direction). There is no direct comparison with the results obtained for the concentration polarization experiments, as the 90,270,0 orientation was not studied in these experiments. However, in experiments done by Bergen [18] it was noted that the two orientations performed the same at 22500 ppm NaCl. For the silica and humic acid, the

results obtained for the 90,180,0 orientation in the fouling experiments were not as good as those obtained for the 90,270,0 orientation, but they were still quite reasonable. This suggests that the 90,180,0 orientation is also a suitable one with respect to flux enhancement for all types of feed solutions.

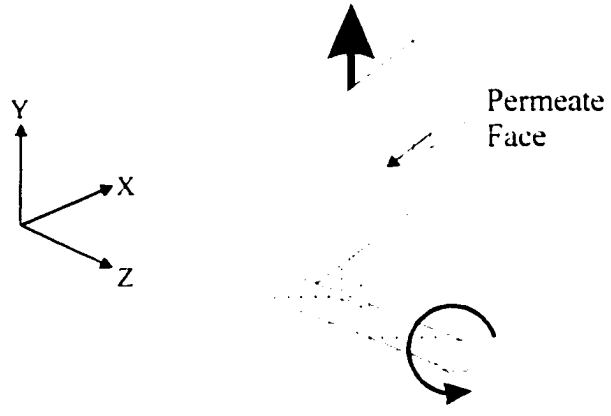

Figure 4.2 90,270,0 orientation with reference axis

With respect to membrane module orientation, certain configurations performed in a less satisfactory way. It was observed that the orientations where Coriolis and centrifugal forces are directed towards the face of the membrane, flux performance is poor. Examples of these orientations include 0,0,0, 0,180,0 and 90,180,180.

4.1.2 Fouling in CMDS and Conventional Membrane Processes

4.1.2.1 Fouling Feed Stream Differences

A significant difference was observed in the flux decline for the humic acid compared to the colloidal silica, with respect to the static fouling of the reverse osmosis membranes. This occurred due to a combination of factors. The first of these is the feed solution concentration, which was significantly higher for the silica than for the humic acid (21 g/L for silica compared to 0.3 g/L for humic acid). It is expected that a feed solution with a higher concentration will foul at a greater rate. On a general note, the feed solution concentrations that were used in the reverse osmosis fouling experiments were quite high compared to those used in experiments described in membrane fouling literature [42,39]. This further adds to the observations that indicate that the CMDS is capable of significant

flux enhancement relative to a conventional membrane process. However, the protein concentration of the whey feed solution that was used in the nanofiltration experiments is typical of that described in the literature [51].

Another factor involves the electokinetic properties of the two feed solutions realtive to that of the membrane material. As previously mentioned, the membrane material has an overall negative charge, while the humic acid and silica have a negative and a neutral charge, respectively. In terms of initial fouling layer deposition, the attraction of the neutrally charged silica particles to the negatively charged membrane material is favoured. For the subsequent build up of the fouling layer, the neutrally charged particles are not as likely to repel each other as are the negatively charged humic acid particles. One final difference between silica and humic acid that may account for the increase in the rate of fouling is their respective specific gravities. While humic acid has a specific gravity close to 1.0, that of silica is approximately 2.6. This density difference could account for a denser fouling layer for the silica feed solution, which in turn leads to a greater decline in flux compared to the humic acid feed solution (only in the conventional, static membrane process).

The density difference described above may also contribute to the greater flux enhancement of the silica relative to the humic acid in the CMDS process (for example, Figure 3.19 *vs.* Figure 3.3). As there are significant centrifugal forces at work, a denser particle is more likely to be drawn away from the surface of the membrane (except where the centrifugal force is acting toward the surface of the membrane, for example 0.180.0 orientation). This would reduce the solute concentration at the membrane surface, as well as create a scouring effect upon the fouling layer. As described previously, there is evidence that material is being sloughed off the surface of the membrane and is being deposited at the top of the flow channel (Figure 3.10), thus indicating a density separation.

4.1.2.2 Fouling Layer Permeability

One of the most significant observations was that the fouling layer thickness appeared to be the same in both the static and the dynamic process for the two feed streams that were examined (silica was excluded as an edge sample could not be prepared for the reasons mentioned in Subsection 3.3.4.1). Given that there was a flux enhancement in the dynamic process relative to the static process, it would appear that the fouling layer in the dynamic process has a higher permeability. This was probably caused by the unstable flow at the membrane surface causing the fouling layer to be deposited in an irregular way. In a large scale version of the CMDS process this would provide a significant benefit over a conventional membrane process in the reduction of membrane module cleaning frequency.

4.1.2.3 Adherence of Fouling Layer

Another significant observation was that the fouling layer tended to adhere better to the membrane modules that had been used in the CMDS apparatus compared to those used in the conventional static apparatus. It is an interesting contradiction given that the fouling layer in the CMDS membranes is more permeable than that in the static process membranes. This adhered material is likely a remnant of the initial fouling layer that is deposited on the membrane surface. This phenomenon occurs in the CMDS process because of the higher flux and its associated higher force due to the permeation. The higher permeation force, denoted as F_D in Figure 1.2, is causing the particles to be more strongly attached to the membrane surface and its pores. Subsequent layers might be more porous than the static case, but the initial layer is held firmly.

This phenomenon does not occur with the protein fouling of the nanofiltration membranes, as the foulant is poorly adhered to the membrane's surface in both processes. Unlike the reverse osmosis fouling, lower permeation forces are not the cause of poor fouling layer adherance. In the nanofiltration membranes, there is significant permeation, so by using the logic of the previous paragraph, the foulant should adhere quite well. It appears that the lack of adherence for both the static and dynamic processes is due to the

nature of the foulant itself. The protein is fairly soluble in the rinse water, therefore it is easily removed from the surface of the membrane, for both processes.

4.2 Toward Industrial Applications

As the CMDS process is a new approach to membrane separations, it is useful to identify where it may fit in the field of industrial process stream applications. While the benefits of membrane processes in general are known, the problems associated with fouling still remain as a barrier to universal industrial acceptance. In general, process streams that are difficult to treat in conventional membrane processes would benefit from the flux enhancing capabilities of this dynamic membrane process. Some of these process applications may include: (1) surface waters – with high humic material and silica content; (2) municipal wastewater – high suspended solids content, (3) brackish and sea water – significant dissolved solids, (4) various pulp and paper process streams – high fibre burden or paper fillers, and (5) food product dewatering – high solids content.

Future development of the CMDS process will involve going from a membrane area in the cm^2 scale to one in the m^2 scale. Development of this next step hinges upon the need for the benefits obtained from this process. For some process industries, stream value is significant, and thus recovery/purification may drive the need for a larger scale CMDS apparatus. In terms of a centrifugal membrane process with a larger membrane surface area, the Centrifugal Reverse Osmosis (CRO) process developed by Vickers and Wild [15,16] provides this. The fouling reduction potential of this process has yet to be examined, but its use of conventional spiral wound cartridges would create an attractive cost benefit. As the fouling research in this dissertation has illustrated the fact that there are several membrane orientations that can enhance flux, the multiple membrane orientations available in the spiral wound cartridges may suffice for some orientations. However, if a large flux enhancement is necessary, then a new module based on the preferred orientation would have to be developed. Bergen describes the potential of a module design with annular rings or axial vanes [18]. He mentions that the module would be functionally similar to the spiral wound modules used in the CRO design, but optimized for the dynamic environment, thus making it more attractive. The

development of such a membrane module for use in the CMDS apparatus would necessitate series of fouling experiments to evaluate the level of the benefits obtained. Once again, silica and humic acid experiments would help to quantify the benefits of this scaled up design.

References

[1] W.J. Koros, *et al*, Terminology for membrane and membrane processes, *Journal of Membrane Science*, 120 (1996) 149.

[2] S. Loeb and S. Sourirajan, Seawater demineralization by means of an osmotic membrane, *Advances in Chemistry Series*, 38 (1963) 117.

[3] G. Belfort and A. Zydney, Membrane Fouling, North American Membrane Society (NAMS) Workshop, Portland, OR (1995).

[4] G. Belfort, *et al.*, Diagnosis of membrane fouling using a rotating annular filter. 1. Cell culture media, *Journal of Membrane Science*, 77 (1993) 1.

[5] S.I. Graham, *et al.*, Improving reverse osmosis performance through periodic cleaning, *Desalination*, 74 (1989) 113.

[6] S. Ebrahim, Cleaning and regeneration of membranes in desalination and wastewater applications: State-of-the-art, *Desalination* 96 (1994) 225.

[7] G. Belfort, Pretreatment and cleaning of hyperfiltration (reverse osmosis) membranes in municipal wastewater renovation, *Desalination*, 21 (1977) 285.

[8] C. Clarotti, *et al.*, Plasma deposition of thin fluorocarbon films for increased membrane hemocompatibility, *Journal of Membrane Science*, 61 (1991) 289.

[9] D. Mukherjee, *et al.*, Flux enhancement of reverse osmosis membranes by chemical surface modification, *Journal of Membrane Science*, 97 (1994) 231.

[10] S. Akhtar, *et al.*, Coatings reduce the fouling of microfiltration membranes, *Journal of Membrane Science*, 107 (1995) 209.

[11] M.M. Dal-Cin, *et al.*, Ultrafiltration of waste waters with a centrifugally enhanced crossflow module, NAMS '95 Proceedings, Portland, Oregon, May 22-24 (1995).

[12] J.Y. Park, *et al.*, A study on dynamic separation of silica slurry using a rotating membrane filter: 1. Experiments and filtrate fluxes, *Journal of Membrane Science*, 97 (1994) 263.

[13] C.A. Grenci, Centrifugal reverse osmosis for desalination, U.S. Patent No. 3,400,074, 1968.

[14] B.G. Keefer, Rotary reverse osmosis apparatus and method, U.S. Patent No. 4,230,564, 1980.

[15] P.M. Wild and G.W. Vickers, The technical and economic benefits of centrifugal reverse osmosis desalination, *Desalination*, 89 (1992) 33.

[16] P.M. Wild et al., Centrifugal reverse osmosis desalination unit, U.S. Patent No. 4,886,597, 1989.

[17] Munir Cheryan, Ultrafiltration Handbook, Technomic Publishing Company, Inc., Lancaster, Pennsylvania (1986) 161.

[18] A. Bergen, M.A.Sc. Thesis, University of Victoria, 1999.

[19] A. Bergen, unpublished results.

[20] P.W.G. Byrnes, The CMDS Flow-Rate and Conductivity Transducer: Design, Manufacture and Testing, M.A.Sc. Thesis, University of Victoria, 1997.

[21] J.G. Pharoah, Computational modeling of centrifugal membrane and density separation, M.A.Sc. Thesis, University of Victoria, 1997.

[22] J. G. Pharoah and N. Djilali, Rotation induced secondary flows in centrifugal membrane and density separation, *7th Annual Conference of the Computational Fluid Dynamic Society of Canada Proceedings*, 1999.

[23] P.M. Wild, *et al.*, The fundamental principles and design considerations for implementation of centrifugal reverse osmosis desalination, J. Procee Mech. Eng. (Proc. Inst. Mech. Eng. E.), 211 (1997) 67.

[24] Zahid Amjad (Editor), Reverse Osmosis: Membrane Technology, Water Chemistry, and Industrial Applications, Chapman and Hall, New York (1993) 5.

[25] Munir Cheryan, Ultrafiltration Handbook, Technomic Publishing Company, Inc., Lancaster, Pennsylvania (1986) 84.

[26] E. Mattiasson and B. Sivik, Concentration Polarization and Fouling, *Desalination*, 35 (1980) 59.

[27] Osmonics, Inc. Web Page, www.osmonics.com/products/Page288.htm

[28] SigmaPlot for Windows Version 5.00, Copyright© 1986-1999 SPSS Inc.

[29] J. G. Pharoah and N. Djilali, Rotation induced secondary flows in centrifugal membrane and density separation, *7th Annual Conference of the Computational Fluid Dynamic Society of Canada Proceedings*,1999.

[30] J.G. Pharoah, unpublished results.

[31] Handbook of Physics and Chemistry. 62nd Ed. R.C. Weast and M.J. Astle (Eds.), C.R.C. Press, Boca Raton (1982) D200.

[32] W.H. Hamill, *et al.*, Principles of Physical Chemistry - Second Edition, Prentice-Hall Inc., New Jersey (1966) 57.

[33] R.D. Cohen and R.F. Probstein, Colloidal fouling of reverse osmosis membranes, *Journal of Colloid Interface Science* 114 (1986) 194.

[34] X. Zhu and M. Elimelech, Fouling of reverse osmosis membranes by aluminum oxide colloids, *Journal of Environmental Engineering*, December (1995) 884.

[35] V. Chen, *et al.*, Particle deposition during membrane filtration of colloids: transition between concentration polarization and cake formation, *Journal of Membrane Science* 125 (1997) 109.

[36] P.K. Cornel, *et al.*, Diffusion of humic acid in dilute aqueous solutions, *Journal of Colloid Interface Science* 110(1) (1986) 149.

[37] C. Combe, *et al.*, The effect of CA membrane properties on adsorptive fouling by humic acid, *Journal of Membrane Science* 154 (1999) 73.

[38] M. Elimelech, *et al.*, Role of membrane surface morphology in colloidal fouling of cellulose acetate and composite aromatic polyamide reverse osmosis membranes, *Journal of Membrane Science* 127 (1997) 101.

[39] C. Jucker and M.M. Clark, Adsorption of aquatic humic substances on hydrophobic ultrafiltration membranes, *Journal of Membrane Science* 97 (1994) 37.

[40] K. Ruohomäki, *et al.*, Characterization and removal of humic substances in ultra- and nanofiltration, *Desalination* 118 (1998) 273.

[41] M. Elimelech, *et al.*, Measuring the zeta (electrokinetic) potential of reverse osmosis membranes by a streaming potential analyzer, *Desalination* 95 (1994) 269.

[42] Private Communications, Dr. C. Singla, Department of Biology, University of Victoria (1999).

[43] S.G. Yiantsios and Y.J. Karabelas, The effect of colloid stability on membrane fouling, *Desalination* 118 (1998) 142.

[44] Osmonics, Inc. Web Page, www.osmonics.com/products/Page227.htm

[45] DuPont Product Database Web Page, www.dupont.com/corp/products/index.html.

[46] G.A. Collins, Colloidal fouling of a reverse osmosis membrane – comparison of conventional reverse osmosis systems and the centrifugal membrane and density separation (CMDS) apparatus, Chemistry 499 Report, University of Victoria, 1997.

[47] H.S. Alkhatim, *et al.*, Treatment of whey effluents from dairy industries by nanofiltration membranes, *Desalination* 119 (1998) 177.

[48] J.P.S.G. Crespo, *et al.*, Use of fluorescence labeling to monitor protein fractionation by ultrafiltration under controlled permeate flux, *Journal of Membrane Science* 155 (1999) 209.

[49] Munir Cheryan, Ultrafiltration Handbook, Technomic Publishing Company, Inc., Lancaster, Pennsylvania (1986) 82.

[50] A. Muller, *et al.*, Ultrafiltration modes of operation for the separation of α-lactalbumin from acid casein whey, *Journal of Membrane Science* 153 (1999) 9.

[51] Osmonics, Inc. Web Page, www.osmonics.com/products/Page232.htm

[52] Aldrich Online Product Information Web Page, www.sigma-aldrich.com /SAWS.nsf/Pages/Aldrich?EditDocument

[53] Private Communications, Dr. F. Brot, Research Technical Service, Sigma-Aldrich Company (1999).

[54] Osmonics, Inc. Web Page, www.osmonics.com/products/Page243.htm

[55] Bio-Rad Laboratories Product Information Web Page, www.bio- rad.com /apps/t3server/templates/tafs/searchBioRad.taf?division_id=corp